Local regulation of T-cell immunity in the intestinal mucosa

Lokale Regulation der T-Zell-Immunität in der Darmschleimhaut

Doctoral thesis for a doctoral degree
at the Graduate School of Life Sciences
Julius-Maximilians-Universität Würzburg,
Section Infection and Immunity

submitted by

María Josefina Peña Mosca

from

Montevideo, Uruguay

Würzburg, 2023

Submitted on:

Office stamp

Members of the thesis committee:

Chairperson:	Prof. Dr. Georg Gasteiger
Primary supervisor:	Prof. Dr. Dr. Andreas Beilhack
Second supervisor:	Prof. Dr. Manfred Lutz
Third supervisor:	Prof. Dr. Wolfgang Kastenmüller
Fourth supervisor:	Prof. Dr. Dirk Bumann

Date of public defense:

Date of receipt of certificates:

I. Summary

After priming in Peyer's patches (PPs) and mesenteric lymph nodes (mLN) T-cells infiltrate the intestine through lymphatic draining and homing through the bloodstream. However, we found that in mouse models of acute graft-versus-host disease (GvHD), a subset of alloreactive T-cells directly migrates from PPs to the adjacent intestinal *lamina propria* (*LP*), bypassing the normal lymphatic drainage and vascular trafficking routes. Notably, this direct migration occurred in irradiated and unirradiated GvHD models, indicating that irradiation is not a prerequisite for this observed behavior.

Next, we established a method termed serial intravascular staining (SIVS) in mouse models to systematically investigate the trafficking and migration of donor T-cells in the early stages of acute GvHD initiation. We found that the direct migration of T-cells from PPs to *LP* resulted in faster recruitment of cells after allogeneic hematopoietic cell transplantation (allo-HCT). These directly migrating T-cells were found to be in an activated and proliferative state, exhibiting a T_H1/T_H17-like phenotype and producing cytokines such as IFN-γ and TNF-α. Furthermore, we observed that the directly migrating alloreactive T-cells expressed specific integrins (α_4^+, α_E^+) and chemokine receptors ($CxCR3^+$, $CCR5^+$, and $CCR9^+$). Surprisingly, blocking these integrins and chemokine-coupled receptors did not hinder the direct migration of T-cells from PPs to *LP*, suggesting the involvement of alternative mechanisms. Previous experiments ruled out the involvement of S1PR1 and topographical features of macrophages, leading us to hypothesize that mediators of cytoskeleton reorganization, such as Coro1a, Dock2, or Cdc42, may play a role in this unique migration process.

Additionally, we observed that directly migrating T-cells created a local inflammatory microenvironment, which attracts circulating T-cells. Histological analysis confirmed that alloreactive PPs-derived T-cells and bloodborne T-cells colocalized. We employed two experimental approaches, including either photoconversion of T-cells in PPs or direct transfer of activated T-cells into the vasculature, to demonstrate this colocalization. We hypothesize that cytokines released by migrating T-cells, such as IFN-γ and TNF-α, may play a role in recruiting T-cells from the vasculature, as inhibiting chemokine-coupled receptors did not impair recruitment.

II. Zusammenfassung

Nach der Priming-Phase in den Peyer-Plaques (PPs) und mesenterialen Lymphknoten (mLN) migrieren T-Zellen über die lymphatische Drainage und den Blutkreislauf die Darmschleimhaut. Allerdings haben wir festgestellt, dass in Mausmodellen der akuten Graft-versus-Host Erkrankung (GvHD) eine Untergruppe alloreaktiver T-Zellen direkt von den Peyer-Plaques in das benachbarte intestinale *Lamina propria* (*LP*) migriert, ohne lymphatische Drainage- oder vaskuläre Transportwege zu nutzen. Bemerkenswert ist, dass diese direkte Migration sowohl in bestrahlten als auch in nicht bestrahlten GvHD-Modellen auftrat, was darauf hindeutet, dass Gewebeschaden durch ionisierende Strahlung keine Voraussetzung für dieses beobachtete T-Zell-Migrationsverhalten ist.

Anschließend haben wir die Methode der "serielle intravaskulären Zellmarkierung" (SIVS) für Mausmodelle etabliert, um systematisch das Migrationsverhalten von alloreaktiven Spender-T-Zellen in den frühen Stadien der akuten GvHD-Initiierung zu untersuchen. Wir beobachteten, dass die direkte Migration von T-Zellen von PPs zu *LP* zu einer schnelleren Rekrutierung von Zellen nach allogener hämatopoetischer Zelltransplantation (allo-HCT) führte. Diese direkt migrierenden T-Zellen befanden sich in einem aktivierten und proliferativen Zustand, wiesen einen T_H1-/T_H17- ähnlichen Phänotyp auf und produzierten Zytokine wie IFN-γ und TNF-α. Darüber hinaus beobachteten wir, dass die direkt migrierenden alloreaktiven T-Zellen spezifische Integrine (α_4^+, α_E^+) und Chemokinrezeptoren (CxCR3$^+$, CCR5$^+$ und CCR9$^+$) exprimierten. Überraschenderweise verhinderte die Blockierung dieser Integrine und Chemokinrezeptoren nicht die direkte Migration von T-Zellen aus PPs in *LP*, was auf die Beteiligung alternativer T-Zellmigrationsmechanismen schließen lässt. Vorangegangene Experimente schlossen die Beteiligung von S1PR1 und topografischer Merkmale gewebeständiger Makrophagen aus, was uns zu der Hypothese führte, dass Mediatoren der Zytoskelett-Reorganisation wie Coro1a, Dock2 oder Cdc42 eine Rolle in diesem einzigartigen Migrationsprozess spielen könnten.

Zusätzlich beobachteten wir, dass direkt migrierende T-Zellen in der Darmschleimhaut ein lokales entzündliches Mikromilieu schaffen, welches zirkulierende T-Zellen anzieht. Die histologische Analyse bestätigte die Kolokalisation von direkt aus PP stammenden T-Zellen und T Zellen, welche über die Blutbahn in die

Darmmukosa einwanderten. Um die direkte T-Zellmigration eindeutig zu bestätigen, wählten wir zwei experimentelle Ansätze: Die Photokonversion von T-Zellen in PPs während der Priming-Phase sowie den direkten Transfer aktivierter T-Zellen in das Gefäßsystem, um eine T-Zellkolokalisierung nachzuweisen. Aufbauend auf den Ergebnissen vermuten wir, dass Zytokine, die von migrierenden T-Zellen freigesetzt werden, wie zum Beispiel IFN-γ und TNF-α, möglicherweise eine Rolle bei der Rekrutierung von T-Zellen aus dem Gefäßsystem spielen, da die Hemmung von G-Protein-gekoppelter Rezeptoren (und somit aller Chemokinrezeptoren) die T-Zell-Rekrutierung nicht beeinträchtigte.

III. Table of contents

IV. List of figures

V. List of abbreviations

Abbreviation	Definition
aGvHD	acute GvHD
allo-HCT	allogeneic hematopoietic cell transplantation
APC	antigen-presenting cell
BSA	bovine serum albumin
CCL	C-C Motif Chemokine Ligand
CCR7	C-C Motif Chemokine Receptor
cGvHD	chronic GvHD
DAMP	damage-associated molecular patterns
DAPI	4′,6-diamidino-2-phenylindole
DC	dendritic cell
ECM	extracellular matrix
EDTA	ethylenediaminetetraacetic acid
FAE	follicle-associated epithelium (of the Peyer's patch)
FcRn	neonatal Fc receptor
FCS	fetal calf serum
FOV	field of view
FRC	fibroblastic reticular cells
G-CSF	granulocyte colony-stimulating factor
GAGs	glycosaminoglycans
GALT	gut-associated lymphoid tissue
GPCR	G-protein-coupled receptor
GvHD	graft-versus-host disease
GvL	graft-versus-leukemia
Gy	Gray
HBSS	Hank's balanced salt solution
HEV	high endothelial venule
HLA	human leukocyte antigen
i.p	intraperitoneally
i.v	intravascularly
ICAM	intercellular adhesion molecule-1
IFN-γ	interferon γ
ILC	innate lymphoid cell
iNKT	CD-1 restricted invariant NKT
IL	Interleukin
iLN	inguinal lymph nodes
IEL	intestinal epithelial cells
ISL	isolated lymphoid follicles
LFA-1	lymphocyte functional antigen 1
LN	lymph node
LP	*lamina propria*
LPAM	lymphocyte Peyer's patch adhesion molecule
LPS	lipopolysaccharides

LSFM	light sheet fluorescence microscopy
LSM	laser scanning microscopy
LTB4	leukotriene B4
Lti	lymphoid inducer cell
MAdCAM-1	mucosal addressin cell adhesion molecule-1
MAIT	mucosal associated invariant T-cell
MAMP	microbe-associated molecular pattern
MHC	major histocompatibility complex
miHAg	minor histocompatibility antigens
mLN	mesenteric lymph nodes
nT_{regs}	natural derived regulatory T-cells
nIEL	natural IEL
NK	natural killer
NRS	normal rat serum
PAMP	pathogen-associated molecular pattern
PBS	phosphate-buffered saline
PFA	paraformaldehyde
pIEL	peripheral IEL
PNAd	peripheral LN addressin
PP	Peyer's patch
PRR	pattern recognition receptor
PSGL-1	P-selectin glycoprotein ligand-1
pT_{reg}	peripheral regulatory T-cells
PTx	pertussis toxin
r.p.m	rotations per minute
RT	room temperature
S1P	sphingosine-1-phosphate
S1PR1	sphingosine-1-phosphate receptor 1
SD	standard deviation
SLOs	secondary lymphoid organs
SED	subepithelial dome (of the Peyer's patch)
SIVS	serial intravascular staining
T_H	T helper
TCR	T-cell receptor
T_{FH}	follicular T-cells
TLR	Toll-like receptors
TNF-α	tumor necrosis factor-alpha
T_{reg}	regulatory T-cells
T_{RM}	tissue resident memory T-cell
VCAM-1	vascular cell adhesion molecule 1
VLA-4	very late antigen 4

1. Introduction

1.1. Graft-versus-host disease

1.1.1. Hematopoietic cell transplantation

Hematopoietic cell transplantation (HCT) is a therapy consisting of the adoptive transfer of hematopoietic cells from the bone marrow, umbilical cord blood, or mobilized from peripheral blood (with granulocyte colony-stimulating factor (G-CSF), to reconstitute the hematopoietic system (Crees et al., 2023; Snowden et al., 2022). Based on cell source, HCTs are classified into autologous HCT when a patient´s hematopoietic cells are used as a rescue strategy (e.g., for recovery after administration of chemo-radiotherapy to eradicate a malignancy); or allogeneic HCT, when a patient receives hematopoietic cells from a donor to establish donor-derived hematopoiesis and immunity (Levin et al., 2022).

Allogeneic hematopoietic cell transplantation (allo-HCT) is a therapy against malignant (leukemias, lymphomas, multiple myeloma, or myelodysplastic syndromes) and non-malignant bloodborne diseases (anemias or other acquired or inherited hematological disorders. Many of these diseases have poor prognoses, and for some patients allo-HCT remains the only treatment to cure them (D'Souza et al., 2020).

Allo-HCT requires a pre-transplant myeloablative or conditioning treatment (with cytotoxic drugs, radiotherapy, monoclonal antibodies, or its combination), which creates space for donor hematopoietic engraftment, minimizes host-versus-graft-reaction and eradicates residual cancer cells in case of malignant disorders (Murphy and Weaver, 2022). The efficacy of allo-HCT for hematologic malignancies derives from intensive conditioning and desired graft-versus-leukemia (GvL) effect associated with the engraftment of the donor immune system, which recognizes allogeneic histocompatibility antigens and eradicates residual tumor cells (Malard et al., 2023). Mature donor T-cells in HCT preparations critically contribute to maintaining remission after transplant. However, alloreactive T-cells can also react to healthy patient tissues causing graft-versus-host disease (GvHD), one of the principal causes of non-recurrence-associated mortality after allo-HCT (Song et al., 2021).

T-cell depletion is an effective approach for preventing GvHD. It involves depleting mature alloreactive T-cells from the donor either before or after transplantation using techniques like antibody-based depletion or positive selection of $CD34^+$ stem cells. T-cell depletion efficiently prevents acute and chronic GvHD and was commonly used in the 1980s and 1990s (Holler et al., 2019). Unfortunately, the markedly decreased frequency of severe GvHD beneficial for the patient is also associated with a higher relapse rate of malignant hematological diseases (no GvL effect), an increased risk of graft failure, and infections (due to immunodeficiency) (Diaz et al., 2021). Unfortunately, no successful separation of GvL and GvHD effects has been achieved. Therefore, clinicians need to find a compromise between sufficient immunosuppression to stop GvHD from damaging healthy tissues and sufficient alloreactivity to prevent tumor relapse.

1.1.2. Allorecognition

The major histocompatibility complex (MHC), known in humans as human leukocyte antigen (HLA), encodes highly polymorphic cell surface molecules and is, therefore, the genetic locus primarily involved in allorecognition (Abbas et al., 2017). Peptide antigens are presented to T-cells by MHC molecules, with CD4 and CD8 serving as co-receptors. CD4 interacts with MHC class II molecules, while CD8 interacts with MHC class I molecules, facilitating T-cell receptor (TCR) recognition of the peptide-MHC complex. Peptides associated with MHC class I originate from cytosolic antigens, while peptides associated with MHC class II originate from extracellular and self-membrane proteins degraded in the endosomal pathway. Additionally, through a process known as cross-presentation, extracellular proteins can be presented on MHC class I molecules (Murphy and Weaver, 2022).

An HLA mismatch between patient and donor increases the risk for engraftment failure and acute graft-versus-host-disease (aGvHD) (Tiercy, 2016). HLA super-locus genes are closely linked in chromosomal position 6p21 and co-dominantly expressed in a Mendelian fashion. Six classical HLA transplantation genes play a crucial role in transplantation. Practically every cell in the body expresses MHC-I molecules, which are encoded by the HLA-A, -B, and -C genes. MHC II molecules are encoded for by the HLA- DQ, -DR, and -DP loci, which are expressed on antigen-presenting cells (APCs) such macrophages, B cells, and dendritic cells (DCs) (Abbas et al., 2017). Non-

classical HLA genes have limited polymorphism and play a less defined role in transplantation.

The level of HLA matching predicts the clinical outcome of a transplant. Particularly important are HLA-A, -B, -C, and -DR. Ideally, alleles at both loci are matched between donor and patients at high resolution (known as 8/8 and 10/10 matches when HLA-DQ is included) (Tiercy, 2016). Only 30% of patients have siblings that match their HLA, thus for patients without them, the solution is to identify an unrelated but HLA-matched donor (Singh and McGuirk, 2016; Zheng and Tian, 2021). Alternative sources, particularly haploidentical (half-matched) family relatives, are being used more frequently (Zheng and Tian, 2021). In a major MHC mismatch, 1 to 10% of donor T-cells can directly recognize the recipient's MHC molecules regardless of the presented peptide, which happens more often than the typical recognition of MHC-cognate peptides (Abdelsamed and Lakkis, 2021; Son et al., 2021).

After complete HLA-matched transplantation, donor T-cells can still recognize polymorphic peptides presented by cognate HLA molecules on the patient´s cell surface. Minor histocompatibility antigens (miHAg), are responsible for weaker graft versus host reactions and are encoded by genetic variations outside of HLA loci (Ferrara et al., 2009; Tak W et al., 2014). Some miHAg are encoded in the male Y chromosome (H-Y), generating a female anti-male immune response. However, most are autosomal genes whose identities are largely unknown (Murphy and Weaver, 2022). Single-nucleotide polymorphisms for chemokines, cytokines, co-stimulatory molecules, and micro-RNAs are also associated with a risk of aGVHD (Zeiser and Blazar, 2017). There are two separate but non-exclusive mechanisms via which alloantigen recognition can happen: direct and indirect. In direct recognition, intact MHC-peptide complexes on donor-derived APCs are recognized directly by recipient T-cells. In contrast, in indirect recognition, allo-peptides are processed and presented by recipient-derived APCs in self-MHC class II (Benichou and Thomson, 2009).

Over the past three decades, transplantation research has significantly advanced our understanding of histocompatibility, GvHD/GvL effects, and immune reconstitution after allo-HCT. These improvements have led to better transplant outcomes due to improvements in infection prophylaxis, immunosuppressive

treatments, and better supportive care with better donor selection with tailored conditioning regimens. However, despite these advances, one of the principal complications of allo-HCT, GvHD, often remains lethal and limits its application (Holtan et al., 2022).

1.1.3. Clinical relevance of graft-versus-host disease

Current standard prophylactic treatment consists of drugs that suppress T-cell proliferation and cytokine production, such as cyclosporine, calcineurin inhibitors, or tacrolimus (which impair transcription of interleukin 2 (IL-2)) for 6 months plus a short course of methotrexate (an antiproliferative agent) (Singh and McGuirk, 2016). Despite prophylactic treatment, GvHD causes morbidity in close to half of patients and contributes to 20 to 30% of deaths after allo-HCT for the treatment of malignancies (Gooley et al., 2010). Allo-HCT recipients would all develop GvHD if prophylactic treatments were absent (Ferrara et al., 2017).

GvHD risk factors include recipient age, high conditioning intensity, gender inequality, and the site of cell collection (cord blood and bone marrow transplants have a lower risk than peripheral blood cell transplants). Due to HLA complexity and variability, every tenth patient cannot find a suitable donor (DKMS, 2022). In addition, many patients are too elderly and morbid to deal with side effects and complications associated with allo-HCT.

Historically, the timing of symptom onset classified GvHD into acute and chronic forms, when symptoms appeared within the first 100 days after allo-HCT or later, respectively (Malard et al., 2023). The distinction between acute and chronic GvHD (cGvHD) is currently made based on pathophysiology and clinical manifestation after this categorization was improved by a National Institutes of Health consensus conference in 2005 (Jagasia et al., 2015). aGvHD is primarily a cell-mediated reaction driven by alloreactive T helper 1 (T_H1) and T_H17 cells infiltrating the target organs. In contrast, cGvHD is characterized by antibody-mediated mechanisms and fibrosis. Symptoms of aGvHD include skin rashes, nausea, constipation, lung obstruction, and liver disorders such as hyperbilirubinemia. cGvHD, additionally affects the eyes, salivary glands, vulva, vagina, mouth, and lungs more frequently (Dean and Sroussi, 2022; Machado et al., 2022). Additionally, aGvHD represents a risk factor for cGvHD

in allo-HCT patients. The clinical phenotype defines GvHD in mouse models, and the time onset of symptoms differs (Patel et al., 2022).

aGvHD is a complication in 30 to 60% of patients undergoing allo-HCT, with up to 14% experiencing a severe or very severe course (Zeiser and Blazar, 2017). In 1995, consensus guidelines for grading aGvHD severity were published (Przepiorka et al., 1995). According to the extent of the rash, the level of bilirubin, and the amount of diarrhea, respectively, the skin, liver, and gastrointestinal tract were first scored separately. Glucksberg criteria (staged from I-IV) (Glucksberg et al., 1974), or the international bone marrow transplant registry criteria (staged from A-D) can be then used to get an overall aGvHD score (Rowlings et al., 1997).

First-line therapy against GvHD involves adding methylprednisolone to the prophylactic treatment. Unfortunately, approximately half of the patients experience steroid-refractory GvHD, necessitating alternative therapies. However, these alternatives have limited success rates, leading to mortality rates ranging from 70 to 80% (Hill et al., 2018). Among the available options, the only FDA-approved treatment for steroid-refractory GvHD is Ruxolitinib, a Jak1/2 inhibitor (Zeiser et al., 2020). Other second and third-line therapies are primarily based on increased immunosuppression and lack consistently shown benefits (Jansen et al., 2022). The causes of GvHD mortality are opportunistic infections, renal and hepatic toxicity, secondary graft failure, cancer relapse, and GvHD itself. Therefore, GvHD continues to be a serious complication and a leading cause of death in patients receiving allo-HCT despite progress in understanding the disease (Bader et al., 2018).

1.1.4. Graft-versus-host disease pathophysiology

1.1.4.1. Graft-versus-host disease induction and conditioning tissue damage

The pathophysiology of aGvHD involves three phases: induction, activation, and effector phase (Ferrara et al., 2009). During the induction phase, underlying disease and conditioning induce massive tissue damage leading to the breakdown of epithelial barriers and local inflammation. The release of damage-associated molecular patterns (DAMPs) produces the endothelial secretion of high levels of tumor necrosis factor-alpha (TNF-α), IL-1, and IL-6, creating a highly inflammatory environment (Hill et al., 2021). Disruption of the gastrointestinal tract integrity by conditioning causes a further

increase in the inflammatory milieu through translocation of bacteria and lipopolysaccharides (LPS) and other pathogen-associated molecular patterns (PAMPs), causing activation of macrophages and monocytes via Toll-Like receptors (TLR) (Heidegger et al., 2014). Activated APCs secrete IL-12, inducing host type 1 innate lymphoid cells (ILC1s) and T-cells to release IFN-γ. IFN-γ upregulates MHC-II on nonprofessional APCs (epithelial and stromal cells) (Hill et al., 2021), and sensitizes macrophages to LPS stimulation and activates them to release IL-12 and TNF-α (Wang and Yang, 2014). Providing the ideal environment for alloreactive T-cell activation and T_H1 and T_H17 polarization, subsequently increasing tissue damage.

1.1.4.2. Activation of T-cells in acute graft-versus-host disease

The organs of the immune system can be classified into two main categories: lymphohematopoietic organs (which include the thymus and bone marrow), and secondary lymphoid organs (SLOs), where immunological responses occur. Transfused donor $CD4^+$ and $CD8^+$ T-cells quickly migrate into SLOs, such as lymph nodes (LNs), spleen, or Peyer's patches (PPs), with the help of specific adhesion molecules. As a result of their activation, APCs express more MHC, co-stimulatory (CD80/86), and adhesion molecules, allowing activated APCs to move toward SLO drainage (Murphy and Weaver, 2022).

Host hematopoietic APCs are critical drivers of aGvHD initiation. aGvHD can be initiated by host B-cells, macrophages, plasmacytoid DCs, or Langerhans cells (Hashimoto et al., 2011; Koyama et al., 2011; Li et al., 2012, 2011; MacDonald et al., 2010; Matte-Martone et al., 2010). Even though host hematopoietic APCs are most important in priming alloreactive T-cells, host non-hematopoietic APCs and donor APCs also play remarkable roles. For instance, Koyama and colleagues reported that MHC class II expressing intestinal epithelial cells (IECs) could initiate lethal gut GvHD, which in turn is influenced by microbiota and regulated by IL-12-IFN-γ cytokine axis (Koyama and Hill, 2019).

SLOs allow for interaction between alloreactive T-cells and activated APCs. Upon binding of the MHC-peptide complex to the TCR, proximal and distal signaling pathways are activated; however, complete T-cell activation requires a second co-stimulatory signal (Murphy and Weaver, 2022). Antigen recognition in the absence of

co-stimulation renders naïve T-cells anergic, a state of growth arrest, and inhibition of effector functions (Hill et al., 2021). Co-stimulatory molecules from the immunoglobulin superfamily, including CD28 and inducible costimulator (ICOS), as well as the TNF receptor superfamily, such as 4-1BB, CD27, CD40, and OX40, have been identified and extensively studied (Wang et al., 2022).

CD28 is constitutively expressed even on naïve T-cells, and it interacts with CD80/86 on APCs, playing a pivotal role in the activation of naïve T-cells (Murphy and Weaver, 2022). Upon interaction with CD80 or CD86, CD28 enhances multiple signaling pathways, including NFAT, NFκB, and mTOR. Activation of T-cells and the subsequent signaling events lead to cell proliferation, the production of IL-2, and the upregulation of CD25, which is the α subunit of the IL-2 receptor. These events play a crucial role in T-cell growth, differentiation, and survival (Murphy and Weaver, 2022). After several rounds of cell division, T-cells differentiate into various effector functions based on polarizing cytokines.

Co-stimulatory and co-inhibitory molecules finely regulate T-cell activation during immune responses. CD28 superfamily member ICOS is upregulated, amplifying CD28/B7 ligand responses and promoting the production of cytokines. Co-stimulatory molecules such as OX40 and CD40L provide later T-cell co-stimulation, proliferation, and apoptosis resistance (Hill et al., 2021). Upon T-cell activation, many coinhibitory pathways are upregulated and can attenuate TCR and costimulatory signals. One such example is the expression of cytotoxic T-lymphocyte-associated protein 4 (CTLA-4) on activated T-cells, which leads to inhibition by binding to CD80 and CD86 (Wang et al., 2022). Based on the polarizing cytokines produced, naive T-cells differentiate into various effector subtypes specialized for tissue destruction (Zeiser et al., 2016). The cytokines IL-12 and IL-6 direct the differentiation of T-cells into T_H1/Tc1 or T_H17/Tc17 cells, respectively (Hill et al., 2021).

1.1.4.3. Tissue damage and “cytokine storm” during the effector phase

Ultimately, primed T-cells egress through the lymphatic system into the systemic circulation and selectively target the recipient's tissues, particularly the epithelial cells of the skin, liver, and intestine. One factor that may contribute to alloimmune responses against the gut, liver, and skin is their high cell turnover rate, affecting the degree of

tissue damage during conditioning. Another contributing factor to the preferential attack of target organs in GvHD is their high exposure to microbiota. Microbiome antigens can activate the innate immune system and trigger inflammatory responses (Sporrer et al., 2015). Additionally, the three target organs are rich in resident immune cells, that partially survive the conditioning, providing a significant reservoir of cells capable of producing cytokines during the effector phase.

Cellular effectors of this phase include Tc1, which primarily leads to target destruction through Fas/FasL interactions or secretion of granzyme B/perforin granules and TNF-related apoptosis-inducing ligand (TRAIL). Apart from their direct killing ability, cytotoxic T-cells secrete TNF-α and IFN-γ, which have cytotoxic effects when released near target cells (Hill et al., 2021). Moreover, T_H17 and Tc17 cells are important mediators of GvHD, particularly in the gastrointestinal tract (Gartlan et al., 2015; Kappel et al., 2009). T_H17/Tc17 cells produce proinflammatory cytokines such as IL-17A, IL-22, GM-CSF, and IFN-γ, directly contributing to tissue damage (Gartlan et al., 2015). Additionally, T_H17/Tc17 cells recruit neutrophils to inflammatory sites through the secretion of CXCL8 (Hill et al., 2021). T_H17 donor T-cells can be categorized based on their co-expression of IFN-γ. The subset of T_H17 cells that produces both IL-17A and IFN-γ (IL-17A$^+$ IFN-γ$^+$ T_H17) exhibits a more proinflammatory phenotype and is highly pathogenic in preclinical models of GvHD (Gartlan et al., 2017). T_H17 cells exhibit plasticity and can transform into T_H1-like cells when exposed to IL-12 or IL-23. These T_H1-like T_H17 cells produce both IL-17A and IFN-γ and express RORγt and T-bet (Hirota et al., 2011; Lee et al., 2009).

In the effector phase, a cascade of inflammatory and cellular effectors act synergistically, ultimately resulting in inflammation, cytokine production, and immune cell-mediated organ destruction (Socie and Michonneau, 2022). Tissue damage and released cytokines not only cause direct tissue destruction but also promotes the induction of inflammatory chemokines and recruitment of effector cells to effector organs, further amplifying the process to more advanced stages of GvHD, which are extremely challenging to control (Ferrara et al., 2009; Hill et al., 2021; Yabe et al., 2016).

1.1.5. Gastrointestinal tract as an early graft-versus-host disease target organ

The relevance of the small intestine stands not only in being an aGvHD target organ but also as a site of amplification of systemic disease enhancing the cytokine storm (Hill and Ferrara, 2000). Classically, intestinal GvHD is induced in PPs (Murai et al., 2003) and mesenteric LNs (mLNs) (Masopust et al., 2010). Upon activation, T-cells increase the expression of intestinal-specific homing receptors, allowing them to enter and infiltrate the colon and small intestine. Notably, peripheral LNs and spleen might also contribute to intestinal T-cell homing (Beilhack et al., 2008).

Prophylactic antibiotics are often given to HCT patients to stop opportunistic infections while they are neutropenic. Van Bekkum and colleagues, in 1974, were the first to prove that mice treated with broad-spectrum antibiotics reduced intestinal inflammation and had better transplant outcomes (Bekkum et al., 1974). Subsequent clinical studies corroborated these findings and suggested a benefit from near-total bacterial decontamination (Storb et al., 1983; Vossen et al., 1990). However, later studies were contradictory and did not show a clear benefit (Petersen et al., 1987; Russell et al., 2000; Martin et al., 2004; Shono et al., 2016). Recently, studies using different antibiotic treatments highlight the pivotal role of intestinal microbiota composition and how this might influence and change allo-HCT outcomes. The high diversity of microbiota and the presence of *Lactobacillus,* or *Blautia* genus, have been associated with better GvHD outcomes. On the other hand, loss of microbial diversity and dominating *Enterococcus* and Enterobacteriaceae are linked to GvHD and a worse prognosis (Jenq et al., 2015, 2012; Mathewson et al., 2016).

Decreased bacterial diversity is generally linked with the loss of *Clostridium* species known to produce short-chain fatty acids (SCFAs), such as butyrate, from the fermentation of dietary fibers. Butyrate is not only the primary energy source for IECs but is also involved in wound reparation and impacts inflammatory signaling pathways. Depletion of butyrate-producing species contributes to epithelial defects and promotes the emergency of pathobionts (Fredricks, 2019). Expansion of mucus-degrading bacteria, such as *Akkermansia muciniphila*, in the absence of complex dietary carbohydrates, diminishes glycocalyx thickness, letting bacteria come into intimate contact with the epithelial surface, activating immune cells, and exacerbating GvHD (Shono et al., 2016). Effective treatment for GvHD may involve manipulating the

intestinal microbiota. This treatment's effectiveness appears to be dependent on the selective eradication of bacterial species. Other promising approaches are the transplantation of fecal microbiota or engineered microbial communities to allow the reformulation of microbiota in allo-HCT patients (Spindelboeck et al., 2017; Taur et al., 2018).

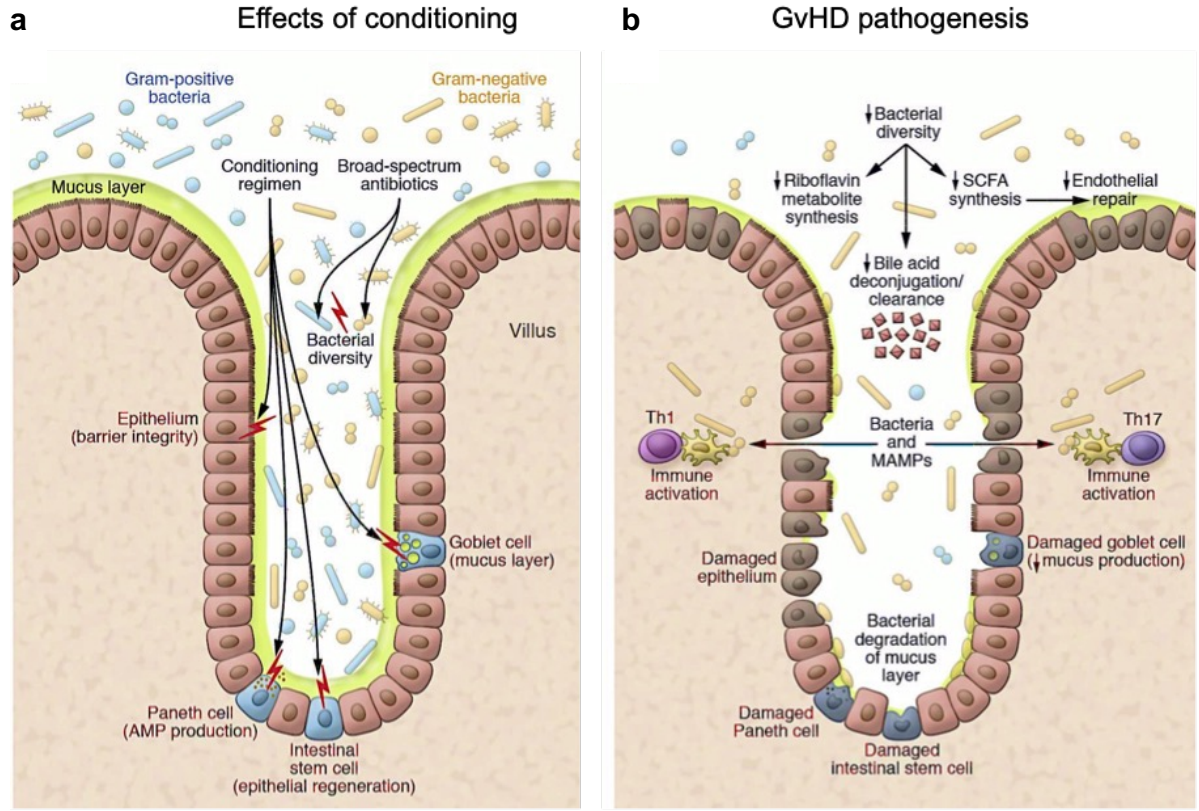

Fig. 1.1 Gastrointestinal tract as a site of amplification of systemic disease. a. The gut immune system's first line of defense is the gut epithelial barrier that divides the lumen from the underlying mucosa. One layer of IECs (linked by tight junctions) forms the barrier, which is covered in an extracellular layer of mucus made by Goblet cells that prevents direct contact with luminal content. Irradiation damages intestinal epithelial cells disrupting the intestinal barrier, and the loss of intestinal stem cells impairs their regeneration. Reduced Goblet cells and accompanying glycocalyx also allow for direct bacterial contact with the epithelial surface, activating immune cells in the process. Furthermore, damage to Paneth cells, specialized in producing different antimicrobial peptides, dysregulates the composition of intestinal flora. **b.** Upon intestinal barrier disruption, translocating PAMPs and DAMPs leak from the intestinal lumen and are detected by the immune system. Subsequent activation of immune cells and release of pro-inflammatory cytokines elicit T_H1 and T_H17 responses that enhance tissue damage. Adapted from (Fredricks, 2019).

Conditioning chemotherapy and irradiation harmed various cells in the small intestine, leading to disruption of the intestinal barrier with inflammation that worsens and maintains GvHD (**Fig. 1.1**). Noteworthy, IL-22-secreting ILC3s or exogenous IL-22 supplementation supports intestinal stem cell regeneration (Hanash et al., 2012). The damage causes the intestinal lining to become more permeable, allowing gut

bacteria to cross the intestinal barrier. As a result, bacterial LPS and other PAMPs and DAMPs leak from the lumen and are detected by pattern recognition receptors (PRRs). Consequently, the innate immune system is activated and responds producing pro-inflammatory cytokines (IL-1, TNF-α, and IL-6), providing the ideal environment for alloreactive T-cell activation and T_H1 and T_H17 polarization, subsequently increasing tissue damage.

The major mediator causing the apoptosis of intestinal stem cells and intestinal injury is IFN- γ, which is produced by alloreactive T-cells (Takashima et al., 2019). Moreover, IFN-γ induces expression of CXCL9-11, attracting $CXCR3^+$ alloreactive T-cells into target organs (Bouazzaoui et al., 2009). Nevertheless, IFN-γ may negatively regulate GvHD progression. IFN-γ amplifies the inhibitory pathways of indoleamine-2,3-dioxygenase (IDO) and PD-L1/PD-L2 (Hill et al., 2021). Additionally, IFN-γ limits alloreactive T-cell proliferation and promotes apoptosis of activated $CD8^+$ and $CD4^+$ T-cells (Asavaroengchai et al., 2007; Wang and Yang, 2014). If diarrhea results in excessive water loss and obstructs appropriate nutrient absorption, intestinal GvHD symptoms can become life-threatening.

The small intestine is infiltrated earlier than other target organs (Beilhack et al., 2008), and infiltration of alloreactive T-cells into the small intestine is linked to more severe GvHD stages. Thus, blocking T-cell infiltration into the small intestine is a promising prophylactic and therapeutic approach. CCR9 and $\alpha_4\beta_7$ are upregulated on donor T-cells primed in PP and mLN and mediate intestinal homing (Iwata et al., 2004). CCR9 binds C-C Motif Chemokine Ligand 25 (CCL25) produced by intestinal epithelial cells, and $\alpha4\beta7$ integrin binds MAdCAM-1 on intestinal endothelial cells (Beilhack et al., 2008; Hammerschmidt et al., 2008). CCR9 deletion did not ameliorate GvHD (Schreder et al., 2015), and its blocking with Vercirnon antagonist failed in phase III of clinical trials for Crohn's disease (Wendt and Keshav, 2015). Blockade or deletion of $\alpha_4\beta_7$ diminished GvHD severity (Gorfu et al., 2009; Schreder et al., 2015), and blocking of CCR5 resulted in lower aGvHD incidences (Moy et al., 2017). Since different and redundant homing molecules mediate the infiltration of allogeneic T-cells, completely blocking gut homing is extremely challenging (Beilhack et al., 2008). We hypothesize that direct access from PPs to the surrounding *LP* may be an unknown source of intestinal-infiltrating T-cells besides vascular recruitment.

1.2. Gut-associated lymphoid tissue

With a surface area of about 300 m^2, the intestinal mucosa serves as a significant point of contact between an organism and its surroundings (Helander and Fändriks, 2014). The intestinal mucosa is exposed to antigens derived from an estimated 10^{14} commensal microbes and 30 to 35 kg of food proteins each year, and it is only protected by a single layer of epithelial cells covered in an extracellular layer of mucus (Iweala and Nagler, 2019; Murphy and Weaver, 2022). To preserve tolerance to self-antigens and non-pathogenic non-self-antigens while still being able to react against pathogens, the intestinal immune system must be strictly controlled (Park et al., 2018).

Oral tolerance, an active immunologic process mediated by a variety of mechanisms, is a state of oral antigen-specific hyporesponsiveness (Commins, 2015). Tolerance induced by high doses of oral antigen is primarily mediated by clonal deletion and/or clonal anergy. Repeated low doses of oral antigen induce tolerance by generating $FoxP3^+$ peripheral regulatory T-cells (pTreg) (Weiner et al., 2011), which are central players in immune tolerance to food and commensal microbiota. pTregs can be differentiated from natural derived Tregs (nTregs) by the surface receptor neuropilin-1 and the absence of the Helios transcription factor. Moreover, the TCR repertoire of pTregs reflects their development in response to non-self-antigens and not to self-antigens expressed in the thymus, as in natural or thymic-derived Tregs (Murphy and Weaver, 2022).

The gut-associated lymphoid tissue (GALT) can be divided into inducer and effector areas (Misra and Shahiwala, 2020). Organized tissues, including PPs, mLNs, isolated lymphoid follicles (ILFs), and cryptopatches, are the sites where an immune response is initiated. Effector sites consist of lymphocytes distributed throughout the epithelium and *lamina propria* (*LP*), representing the body's largest reservoir of T-cells.

1.2.1. Peyer’s patches

PPs are macroscopic lymphoid aggregates irregularly distributed along the antimesenteric side of the small intestine. Adult PPs have a structure and organization like LNs and splenic white pulp, with T and B-cells segregating into well-defined and

organized regions dependent upon CXCL13 and CCL19/21, respectively (Suzuki et al., 2010). PPs consist of multiple B-cell follicles that contain germinal centers, separated by T-cell zones. As germinal centers form the core of each follicle, PPs have a curved appearance towards the luminal side of the small intestine. Lymphoid areas are separated from the lumen by a specialized epithelium known as the follicle-associated epithelium (FAE), and the associated subepithelial dome (SED), which contains B-cells, T-cells, macrophages, and DCs (Reboldi and Cyster, 2016) (**Fig. 1.2**).

In man, PPs may consist of over a hundred B-cell follicles (Murphy and Weaver, 2022). There are about 60 PPs in newborns, peaking at puberty with up to 240 and then declining with age (Cornes, 1965). From the duodenum to the ileum, they become more numerous and larger, and nearly half of the PPs accumulate in the distal 25 cm of the ileum forming a structure known as a lymphoid ring (Van Kruiningen et al., 2002). In mice, 5-12 PPs are dispersed in the intestine (Reboldi and Cyster, 2016).

In FAE, mucus production is weak, and membrane-bound digestive enzymes are lightly expressed. FAE's most notable feature is the presence of microfold or M cells, which lack apical microvilli and mediate transcytosis of intact luminal antigens across the epithelial barrier into PP. M cells express SIgA receptors facilitating receptor-mediated endocytosis of IgA-trapped antigens. Therefore, luminal IgA prevents mucosal pathogens' penetration and redirects them into M cells (Breedveld and van Egmond, 2019). M cells are highly invaginated at their basal side, forming pockets containing DCs and T and B-cells (Ohno, 2016). M cells transport intact antigens from the lumen to professional APCs within the epithelium or the underlying dome region of lymphoid areas. Alternatively, *LP* myeloid cells can directly sample lumen antigens with transepithelial dendrites and soluble antigens transported across the epithelial tight junctions (paracellular transport) (Murphy and Weaver, 2022). Notably, additional intestinal antigen sampling mechanisms rely on cells outside the FAE. For instance, enterocytes can capture and internalize antigen: antibody complexes using their neonatal Fc receptor (FcRn), which binds and transcytoses IgG bidirectionally across the epithelium. M cells in villus epithelia can transcytose antigens to DCs in the villous *LP*, and Goblet cells can transfer small soluble antigens to underlying $CD103^{+}$cDC2 in *LP* (Murphy and Weaver, 2022). Following antigen sampling, APCs relocate to T-cell regions and/or B-cell follicles where they can interact

with immature lymphocytes to stimulate T-cell differentiation and B-cell maturation into IgA-producing plasma cells, which is dependent on T-cells. These plasma cells home to *LP*, where they secrete dimeric IgA, which is transported into the intestinal lumen. Many follicular T-cells (T_{FH}) supporting IgA class switch derive from pTreg (Murphy and Weaver, 2022).

Compared to LNs, PPs integrate differently with the lymphatic network since they lack afferent lymphatics. M cell-dependent transcytosis is the strategy used to allow antigen sampling instead. Efferent lymphatics emerge from lymphatic sinuses on the serosal side and drain lymph and immune cells to mLN and then to the thoracic duct (Schmidt et al., 2013). This allows antigens taken up across FAE to stimulate local responses in PPs, ILFs, and mLNs. Furthermore, in response to antigens derived from the microbiome and food, PPs constitutively produce germinal centers while peripheral LNs exhibit no obvious germinal center responses under physiological settings (Murphy and Weaver, 2022). PPs are the site of the most intense activation of B-cells in the body (Reboldi et al., 2016; Reboldi and Cyster, 2016). PPs and larger ILFs extend from the epithelium to the submucosa, whereas smaller ILFs are fully contained within the mucosa (Murphy and Weaver, 2022). Thus, both are embedded inside the organ they immunosurvey, as opposed to LNs that drain mostly distant regions.

The lymphatic nodules group of non-encapsulated lymphatic tissues includes PPs, ILFs, tonsils, and lymphatic tissue of the appendix. Fibrous capsules of LN are required to sustain the pressure to drain the lymphatic vessels (Browse et al., 1984). In the intestine, this pressure can be produced by muscle layers that produce frequent peristaltic movements. Additionally, laminin staining (an integral part of basement membranes) revealed no basement membrane encapsulating PPs (Jarick, 2020 Ph.D. thesis). Consequently, in contrast to LNs, a continuous migration space from PPs to *LP* offers an alternative route for immune cells to use as they go from activation to the effector site (see section **1.4**).

1.2.2. Isolated lymphoid follicles

ILFs are lymphoid structures in the small intestine that resemble PPs. Like PPs, ILFs are covered by a FAE, which contains M cells. However, unlike PPs, ILFs do not have distinct T-cell zones, and are thus involved in T-cell-independent antibody

responses (Gommerman, 2020; Tsuji et al., 2008). ILFs develop after birth in response to antigen stimulation from commensal microorganisms (Murphy and Weaver, 2022) (**Fig. 1.2**).

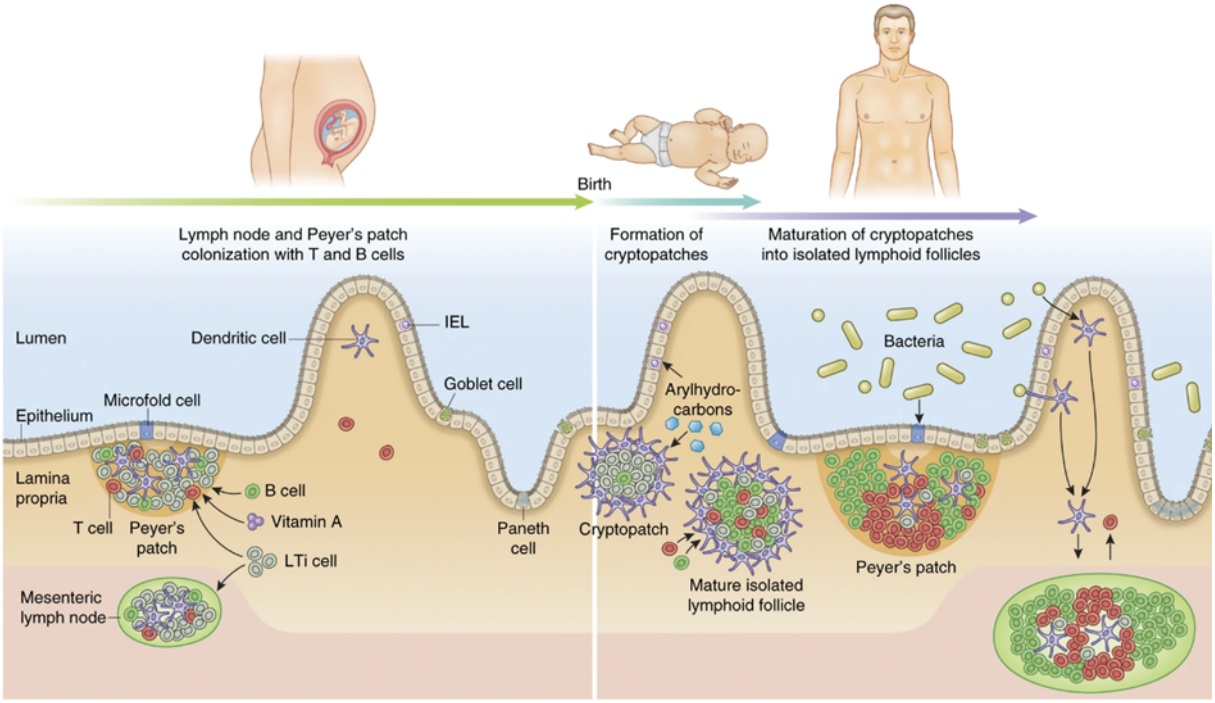

Fig. 1.2 Development of the intestinal mucosal immune system. Only warm-blooded vertebrates have LNs and PPs, which are dependent on lymphotoxin-α1β2 (LTα1β2), produced by a subset of type 3 innate lymphoid cell (ILC-3) termed lymphoid inducer cells (LTi), for their development (Cherrier et al., 2012). As lymphatic vessels form, LTi cells arise in the fetal liver and traffic to sites of prospective LNs and PPs. LTi cells interact with stromal cells inducing the production of cytokines and chemokines, which stimulate the recruitment of DCs, B, and T-cells. At birth, the gut develops small lymphoid clusters called cryptopatches. Cryptopatches mature into ILFs as a result of the recruitment of more B-cells and T-cells stimulated by microbe-associated molecular patterns (MAMPs) recognized by PRR on intestinal epithelial cells and DCs near cryptopatches. In contrast, PPs are already present in the fetal gut, albeit they do not fully develop until the intestinal microbiota colonizes them after birth. Modified from (Veldhoen and Ferreira, 2015).

1.2.3. Intraepithelial lymphocytes

IELs are highly motile cells representing 10 to 15% of the cells in the intestinal epithelium. IELs are early sensors of changes and, thus, rapid responders that destroy malfunctioning enterocytes maintaining barrier integrity (Murphy and Weaver, 2022). Typical properties of IELs are CD69 surface expression, cytolytic capacities (reflected in their expression of perforin and granzyme B), and expression of type I cytokines. Critical to epithelium homing is the expression of CD8αα homodimer and α_E integrin (CD103), which pairs with β_7 to form $\alpha_E\beta_7$, which in turn binds to E-cadherin on intestinal epithelial cells (Cheroutre et al., 2011).

IEL includes conventional T-cells but consists mainly of unconventional T-cells, also called thymic-derived or natural IELs (nIELs). nIELs originate directly from the thymus and can be of two types: αβTCR T-cells and invariant γδTCR T-cells. These cells may exhibit different characteristics, such as lacking a co-receptor or expressing the CD8αα homodimer. Invariant γδ T-cells constitute the largest fraction of IEL in the intestines and are not activated by classical peptide: MHC recognition. In mice, $CD4^-$ $CD8^-$ double-negative γδ precursors leave the thymus expressing invariant Vγ7 (most common) or Vγ4 (Murphy and Weaver, 2022). Due to their location, nIELs play a significant role in mucosal monitoring and tolerance. As opposed to γδ T-cells, nIEL αβ T-cells undergo positive selection in the thymus, requiring recognition of MHC molecules. However, unlike conventional TCR αβ, nIELs αβ T-cells are responsive to a diversity of MHC molecules, including MHC I and MHC II, as well as non-classical MHC I molecules (Murphy and Weaver, 2022).

In contrast, conventional αβ T-cells have diverse TCR repertoires and migrate into intestinal epithelium only after their activation in GALT, recognizing peptide antigens presented in the MHC context. Thus, they can be referred to as pIELs (peripheral IELs) in analogy to Tregs nomenclature. pIELs maintain expression of their naïve co-receptor and therefore acquire $CD4^+CD8αα^+$ and $CD8^+CD8αα^+$ phenotypes. Moreover, few ILC-1 can also be found (Murphy and Weaver, 2022).

1.2.4. Lymphocytes in the *lamina propria*

Under the intestinal epithelium is a layer of loose connective tissue and interstitial matrix known as *LP*. Here, many types of lymphoid and myeloid cells (macrophages, DCs, eosinophils, and mast cells) can be found (Mowat and Agace, 2014). The majority of *LP* B-cells are IgA-secreting plasma cells that are located below the epithelial basement membrane. In a healthy human intestine, hundreds of millions of IgA-producing plasma cells produce 3 to 4 g of IgA per day. Produced IgA is transported through the epithelium by transcytosis, which is mediated by polymeric Ig receptor (pIgR) and diffuses over the basement membrane. Once secreted into the lumen, the IgA and antimicrobial peptides adhered to mucus-coating epithelial surfaces. There, secretory IgA enhances uptake by M cells and local DC, and

aggregates commensal bacteria, making them less able to penetrate the glycocalyx and neutralize pathogens and their toxins. IgA is also capable of neutralizing viruses and bacterial LPS in the endosomes of epithelial cells (Murphy and Weaver, 2022).

Most of the T-cells in healthy *LP* are effector cells that express an αβ TCR with a 3:1 CD4:CD8 ratio (Murphy and Weaver, 2022). αβ T-cells in *LP* are considered to develop from conventional T-cells stimulated in SLOs (Mowat and Agace, 2014). T-cell subset composition mainly depends on the specific microbial exposure and in industrialized countries, where parasite infections are rare, T_H1 and T_H17 $CD4^+$ T-cells predominate. T_H17 cells (involved in recognizing extracellular antigens) is the dominant subtype reflecting constant immune recognition of microbiota (Murphy and Weaver, 2022).The abundance of T_H1 cells, T_H17 cells, and cytotoxic effector T-cells in *LP* is balanced by IL-10-producing T-cells. Intestinal *LP* is additionally populated before birth by tissue resident ILCs, which play a central role in early response to pathogens. As in conventional T-cells, the composition of ILCs depends on microbial exposure, and similarly to T_H17 cells, with which they share many properties, ILC3 are dominant.

Moreover, 23% of *LP* T-cells express an invariant TCR consisting of a highly conserved α chain paired with a limited repertoire of β chains. CD-1 restricted invariant NKT (iNKT) cells recognize lipids and glycolipids complexed with CD1d, whereas mucosal-associated invariant T-cells (MAIT) recognize metabolites of vitamin B complex with MR1 (Murphy and Weaver, 2022). MAIT cells play a protective role in the maintenance of gut integrity by secreting IL-17A and IL-22 cytokines (Hill et al., 2021). Additionally to the dominant αβ TCR T-cells, the presence of γδ T-cells is also reported (Kadivar et al., 2016).

1.3. T-cell motility

1.3.1. T-cell trafficking through blood and lymph vessels

Leukocyte trafficking to specific sites is regulated by the expression of tissue-specific integrins and selectins, as well as by the local release of chemokines. These regulatory mechanisms ensure that leukocytes are directed to appropriate locations, contributing to the maintenance of tissue homeostasis and the effective functioning of immune responses.

Selectins, (including L-, E-, and P-selectin) are a family of transmembrane adhesion molecules with different lectin- likedomains that bind carbohydrates and mediate leucocyte rolling, which is the first adhesive step in transendothelial extravasation. L-selectin is expressed on naïve T-cells, whereas P-selectin is expressed on the surface of activated platelets. On the other hand, E-selectin and P-selectin are both expressed by activated endothelial cells (McEver, 2015).

Chemokines are chemotactic cytokines that regulate the movement of immune cells by interacting with G-protein coupled receptors (GPCRs), which activate integrins and regulate the remodeling of the actin cytoskeleton (Lämmermann and Kastenmüller, 2019). Chemokines can be classified into four subfamilies; (C, CC, CXC, and CX3C chemokines) according to the position and number of cysteine residues within the NH_2-terminal (Moser et al., 2004). Chemokine gradients, which direct transendothelial migration, are created by binding to glycosaminoglycans (GAGs), like heparan sulfate, found on endothelial cell surfaces and in the ECM (Shulman et al., 2011).

Integrins are heterodimeric transmembrane proteins that mediate interactions between cells and the ECM by pairing a long α chain non-covalently with a smaller β chain (Pang et al., 2023). Most integrins bind to ECM components such as laminins, collagens, and fibronectin. Arg-Gly-Asp (RGD), an integrin-binding motif, is shared in many ECM proteins. The specificity of integrins is determined by the pairing of their α- and β-subunits. When integrins bind chemokines, they undergo a conformational change from a closed, bending form to an open, extended form that has a stronger binding activity. This binding activity can also be improved by clustering induced by the ligand (Sun et al., 2019).

1.3.2. T-cell migration inside tissues

To move forward during T-cell migration, internal force must be generated to give traction against the extracellular environment. Mechanisms of cell propulsion in adhesion-dependent migration (usually integrin-based) have been long known and extensively described. More recently, it has been discovered that non-adhesive cell migration occurs when cells pass over a friction contact produced by confinement and surface topography or texture (Bergert et al., 2015; Lämmermann et al., 2008; Liu et al., 2015; Reversat et al., 2020). Non-adhesive migration is characterized by few adhesive interactions and pronounced cellular deformability (Paluch et al., 2016). Fully mechanisms of cell propulsion in non-adhesion-dependent migration are still poorly understood (Jankowiak et al., 2020). Noteworthy, migratory T-cells can adapt their migration mode according to cell-intrinsic, and cell-extrinsic cues arising from their environments, a property known as plasticity (Lämmermann and Sixt, 2009) (**Fig. 1.3**).

Lamellipodia-based or adhesion-dependent cell migration initiates with the binding of plasma membrane receptors located at the leading edge to an extracellular substrate. Such as cell integrins binding to components of extracellular matrix (ECM) (collagen or fibronectin); and cell chemokine-coupled receptors binding to chemokines adhered to extracellular GAGs (Woolf et al., 2007). During lamellipodia-based migration, cells typically adopt an elongated, spindle-like shape and adhere to its substrate forming focal contacts at the leading cell pole. Actin nucleation and polymerization at the leading cell pole form a plasma protuberance known as *lamellipodium*. As a result, the generation of pushing forces occurs, and the tension of the plasma membrane actively opposes the expansion of the actin network, thereby pushing actin filaments back towards the cell body. Focal contact dissolution and actin-mediated contraction at the cell's posterior pole cause the protrusion of the cell, which creates the traction force needed to advance. The described mechanisms depend on cell polarity and are regulated by factors such as cell membrane rigidity, nucleus rigidity, and the inherent actin polymerization rates specific to each cell type (DeSimone and Horwitz, 2014; Krummel et al., 2016).

In ***bleb*-based migration,** plasma membrane protrusions, referred to as *blebs,* that lack actin cortex are preferentially pushed through the path of least resistance in the ECM. *Blebs* form due to hydrostatic forces caused by intracellular actin

contractions and a local loosening of the interaction between the actin cortex and plasma membrane (Lämmermann et al., 2008). The loss of cortical actin initiates the formation of membrane *blebs*, which expand until a new actin cortex is formed inside. These *blebs* then contract, facilitating cell movement and migration (Lim et al., 2013). *Bleb*-based migration is characterized by rounded or irregular cell morphology.

Lobopoidal- based migration can be seen as a hybrid of Lamellipodia-based and bleb-based migration and is observed only in a 3D-constrained environment. Actin-mediated intracellular pressure leads to the formation of blunt-ended cylindrical membrane protrusions, known as *lobopodia*. The cell forms focal adhesions at these protrusions, while the nucleus is pulled forward like a piston to generate anterior pressure (Yamada and Sixt, 2019). Although not fully described, the mechanism by which the nucleus is pushed forward to pressurize the anterior region of the cell appears to be myosin II connected to vimentin intermediate filaments, which are then anchored to the nucleus (DeSimone and Horwitz, 2014).

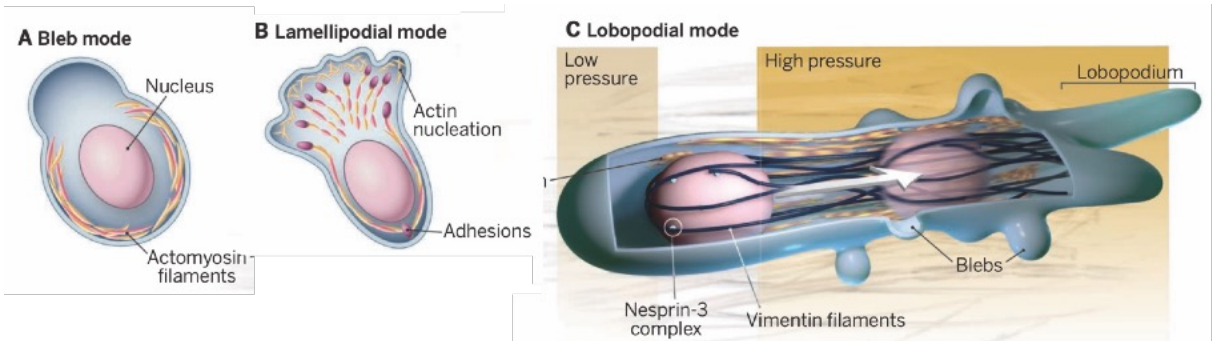

Fig. 1.3 Mechanisms of cell migration. a. During *bleb*-based migration, contractile actomyosin filaments generate higher intracellular hydrostatic pressure, allowing the cell membrane to protrude through areas of minimal resistance. **b.** Lamellipodial-based migration involves the transmission of intracellular pulling forces from specific adhesion points to the substrate, facilitating cell movement. **c.** During lobopodial-based migration, actomyosin filaments exert pulling forces to propel the nucleus forward, leading to cell compartmentalization and an increase in intracellular pressure at the leading edge. Extracted from (DeSimone and Horwitz, 2014).

T-cells migrate quickly (10 to 15 m/min) and frequently randomly through tissues. In comparison, fibroblasts migrate below 1 µm/min (Lo et al., 2000), DCs of 2 to 6 µm/min (Lindquist et al., 2004), and B-cells of 6 to 11 µm/min (Coelho et al., 2013). T-cell migration is distinct from other cell types in that its rate fluctuates often, reaching a maximum of up to 25 µm/min (Katakai et al., 2013). If the interaction between peptides and TCR is weak, T-cells tend to move slowly and change direction frequently

in an exploratory manner. This behavior may allow them to incorporate signals from other APCs while looking for cognate antigens. Cognate antigen recognition on MHC-peptide complexes in APCs surface represents a strong arrest signal (Egen et al., 2011; Shakhar et al., 2005). As a result, the frequency and duration of T-cell pauses in tissue to engage in cell-to-cell interactions also affect overall cell speed. The percentage of time when T-cells travel more slowly than 2 to 3 μm/min can be used to measure the arrest rate (Boissonnas et al., 2007). Therefore, T-cell migration in inflamed tissues is controlled by the interaction of migratory and arrest signals (Krummel et al., 2016; Sarris and Sixt, 2015).

The **extracellular matrix** provides a physical scaffold for presenting chemotactic cues and growth factors (Sorokin, 2010). T-cell migration through tissue may be guided by ECM ultrastructure, and intravital imaging has shown that T-cells frequently follow the collagen's fibrillar structure (Overstreet et al., 2013; Wilson et al., 2009). Leukocytes and other fast-migrating cells rarely cause permanent rearrangements or proteolysis of ECM components. Consequently, their trajectory depends on the size of natural channels within the ECM scaffold and the relative deformability of the ECM and the migrating cells (van Helvert et al., 2018). Compared to other cell types, T-cells are overall soft; its nucleus is the largest and stiffest cell organelle, becoming the rate-limiting step of cell migration. The size of pores in ECM, and hence the degree of cellular confinement, can influence speed, direction, and mechanisms used for 3D migration. Pore size has a linear relationship with T-cell speed. For instance, T-cells in tumors are highly confined and migrate slowly (5 to 8 μm/min) (Boissonnas et al., 2007). In contrast, inflammation promotes the loosening of collagen fibers facilitating cell movement (Nicolas-Boluda and Donnadieu, 2019). According to studies, T-cells migrate preferentially along the path of least resistance while distinguishing the size of pores in the ECM (Renkawitz et al., 2019), which might explain the random migration of effector T-cells in inflamed tissues (Harris et al., 2012; Lämmermann and Germain, 2014; Overstreet et al., 2013). T-cells possess the ability to sense mechanical forces during migration, a process known as mechanosensing, and tend to migrate from soft to stiff environments, driven by increased traction forces (Trichet et al., 2012; Zhu et al., 2019). The stiffness of the ECM depends on tissue-specific structure and inflammatory mediators.

Inside tissues, secreted **chemokines** are either free or bound to GAGs; only soluble chemokines can direct the migration of leukocytes (Graham et al., 2019). GAGs bind to components of ECM (Thompson et al., 2017). During inflammation, GAGs can be released from ECM, altering the bound to free chemokine ratio (Schumann et al., 2010). Regulation of sensitivity to the chemokine gradient occurs at the chemokine and chemokine receptor levels. Chemokine bioavailability can be controlled by proteolytic degradation and by atypical chemokine receptors on immune endothelial and cells that bind chemokines but do not activate GPCR signaling for cell migration (Majumdar et al., 2014). Clustering chemokine receptors on the cell membrane enhances chemoattractant sensitivity (García-Cuesta et al., 2022). Additionally, post-translation modifications on chemokines or their receptors (including proteolytic truncation, nitration, citrullination, and glycosylation) can alter their function (Vanheule et al., 2018). While chemokines are frequently thought to encourage cell migration, excessive concentrations of chemokines can cause cellular arrest because they can cause the internalization of chemokine receptors or loss of gradient sensing (desensitization) (Sarris and Sixt, 2015). Although chemokines can enhance the speed of migration, chemokines alone are not sufficient to drive locomotion (Hons et al., 2018).

The production of diffusible **lipid chemoattractant**, which further regulates T-cell migration, can take only a few minutes. For instance, as described in **1.3.5**, T-cells expressing S1PR1 migrate towards S1P gradients. Leukotrienes like leukotriene B4 (LTB4), which are produced during inflammation, are strong leukocyte chemoattractants. A high-affinity LTB4 receptor (BLT1) upregulated in effector T-cells mediates their early recruitment to inflamed tissues (Sadik and Luster, 2012).

Especially in a constrained 3D environment, immune cells, typically migrate without integrin binding via amoeboid migration and do not have excessively high adhesion to the substrate (Lämmermann et al., 2008). Recently, an *in-vitro* study found that in confined spaces, T-cell migration can be supported by the microenvironment´s topography without receptor-mediated adhesion. Without integrins, T-cells in confinement could not migrate on smooth surfaces, but when serrations were added to the surface, T-cell locomotion was successfully supported. The substrate's texture was followed by the retrograde flow of actin, which generated enough shear forces to move the cell forward (Reversat et al., 2020). Furthermore, a recent *in-vivo* study of

tissue-resident memory T-cells (T_{RM}) in salivary glands confirms that friction-based movement is possible without the intervention of integrins or chemokines, with macrophages providing the topographical surface required for tissue surveillance (Stolp et al., 2020).

Integrin-independent migration can be faster because firm substrate adherence slows down cells (Liu et al., 2015). Still, integrins provide additional traction forces in settings with few contact points. For instance, LFA-1/ ICAM-1 regulated high-velocity and relatively straight movements of T-cells migration in LNs, and in many circumstances, blocking integrin interactions slows down T-cell migratory rates (Katakai et al., 2013; Katakai and Kinashi, 2016). T-cells are likely to migrate rapidly due to highly dynamic micro-adhesive contacts that provide sufficient frictional force to allow cells to rapidly switch between integrin-mediated and non-integrin-mediated cell migration modes to maximize speed and tissue coverage (Renkawitz et al., 2009).

1.3.3. Access of circulating naïve T-cells to priming sites

T-cells derive from bone marrow lymphoid progenitors that migrate to the thymus. Inside the thymus, $CD4^+$ and $CD8^+$ T-cell progenitors get educated to ensure adaptive immunity and self-tolerance. During thymic development, progenitors lose one of the two coreceptors CD4 or CD8 and become restricted to the $CD4^+$ T helper cells or the $CD8^+$ cytotoxic lymphocytes lineage (Murphy and Weaver, 2022). Once T-cell progenitors mature into naïve T-cells, they exit the thymus and recirculate through SLOs searching for their cognate antigen (Abbas et al., 2017). The entry of circulating naïve T-cells to priming sites occurs through high endothelial venules (HEVs) in distinct stages, including rolling along the endothelial surface, activation of integrins, firm adhesion, and transmigration or diapedesis through the endothelium layer (**Fig. 1.4**).

T-cell-associated L-selectin, also known as CD62-L, on naïve T-cells makes weak on-and-off adhesive interactions with vascular addressins and is responsible for the initial contact between circulating naïve T-cells and the endothelial monolayer and mediates lymphocyte tethering and rolling on the endothelium (Takeda et al., 2017). Mucosal addressin cell adhesion molecule-1 (MAdCAM-1) is the most critical addressin expressed by HEVs in PPs or *LP* venules, whereas HEVs within mLNs also express peripheral LN addressin (PNAd) (Rich et al., 2012). In mLN, L-selectin binding

to MAdCAM-1/PNAd is sufficient to maintain rolling along HEVs, whereas, in PPs, binding of $\alpha_4\beta_7$ integrin to MAdCAM-1 is also necessary, adding additional tethering capacity.

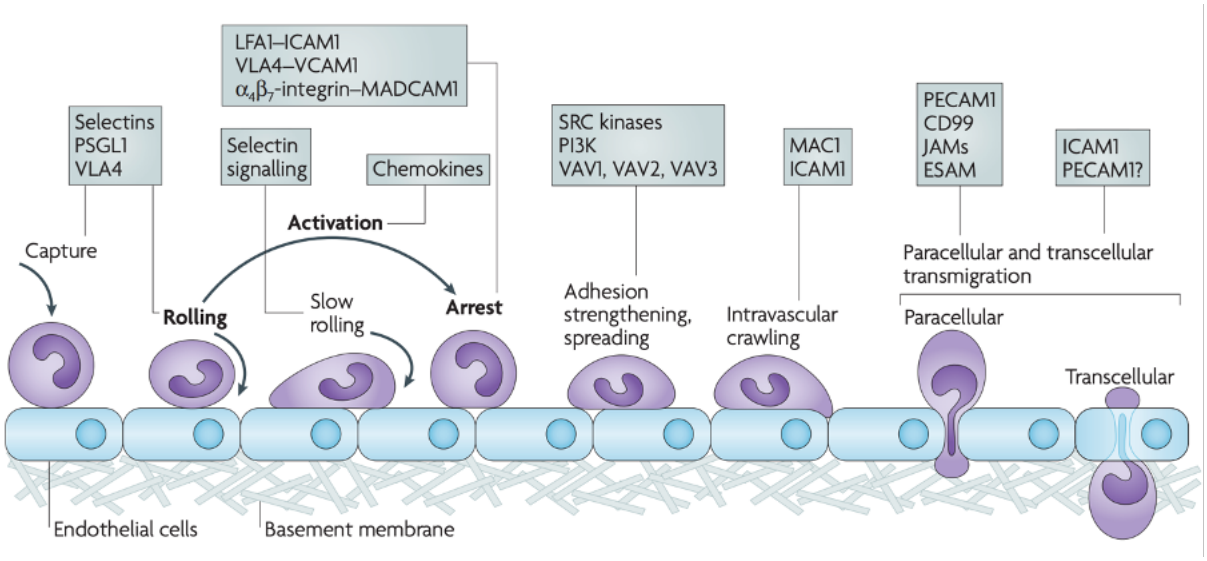

Fig. 1.4 Leukocyte extravasation. Selectins are used to capture leukocytes at the vascular surface as they roll along the endothelium. Chemokines help integrins achieve their high-affinity conformation, which leads the cell to get immobilized on the endothelium. Leukocytes can then enter tissue through a transcellular pathway or between two endothelial cells. Extracted from (Ley et al., 2007).

After lymphocytes roll along the endothelium, chemokine receptor signaling creates conformational changes in integrins, from resting into active conformations that induce firm cell arrest and enable transmigration (Abram and Lowell, 2009). CCL19 and CCL21 present on the endothelium of T-cell zones bind to the T-cell-associated chemokine receptor C-C motif chemokine receptor type 7 (CCR7) (Hong et al., 2022) and activate integrin $\alpha_L\beta_2$ (CD11a: CD18), better known as lymphocyte functional antigen-1 (LFA-1) and integrin $\alpha_4\beta_7$ on the naïve T-cells to bind to the intercellular adhesion molecule-1 (ICAM-1) and MAdCAM-1, respectively. CCR7 represents the primary homing receptor for the recruitment of T-cells into LNs (Hong et al., 2022). Finally, firm adhesion and arrest of lymphocytes are produced, triggering T-cell extravasation into PPs and mLNs at the junction between adjacent endothelial cells (paracellular route) or across the endothelial cell body (transcellular route) (Sage and Carman, 2009) (**Fig. 1.4**). In summary, naïve T-cells express CD62-L, LFA-1, and CCR7, allowing them access to SLOs (Fu et al., 2016).

1.3.4. Naïve T-cells priming in secondary lymphoid organs

Once across the HEV barrier, naïve T-cells move along a spatial network of fibroblastic reticular cells (FRC) that expands throughout the T-cell zone, expressing CCL19 and CCL21 and carrying immobilized CCL21 on its surface. CCR7 is expressed on activated DCs and naïve T-cells, increasing the probability of cognate antigen recognition on the FRC network (Bajénoff et al., 2006; Katakai et al., 2004; Sixt et al., 2005). Naïve T-cells typically exhibit a mean free path of movement spanning 20 to 30 µm. Their trajectory is frequently altered by directional changes occurring every 2 to 3 minutes. As a result, their migratory pattern closely resembles a "random walk" (Brownian motion) (Azarov et al., 2019). Naïve T-cells typically establish brief and transient contacts with DCs, with an average duration of several minutes (Bousso and Robey, 2003; Miller et al., 2004b, 2004a). During these interactions, the engagement of molecules such as LFA-1, ICAM-3, and CD3 on the T-cell with ICAM-1, ICAM-2, DC-SIGN, and CD58 on the APC facilitates effective binding between naïve T-cells and APCs (Murphy and Weaver, 2022). Following antigen encounter, LFA-1 undergoes a conformational change that significantly enhances its binding affinity to ICAM-1 and ICAM-2, allowing prolonged association between naïve T-cells and APCs, facilitating T-cell proliferation and differentiation (Murphy and Weaver, 2022).

After antigen recognition, and co-stimulation, naïve $CD4^+$ T-cells undergo extensive proliferation and develop into different T_H effector subsets according to the cytokine environment experienced during priming (Knochelmann et al., 2018) (**Fig. 1.5**). Notably, T_H17 cells and Tregs exhibit functional plasticity and, under certain cytokines, can acquire characteristics of other helper subsets (Knochelmann et al., 2018). During the priming process, T-cells undergo specific differentiation states that are associated with the induction of distinct homing receptors. For instance, T_H1 cells express homing receptors like CXCR3, which recognizes CXCL9-11, CXCR6, which recognizes CXCL16, and CCR5, which recognizes CCL3-5. On the other hand, T_H2 cells express CCR3, CCR4, and CCR8. CCR4 and CCR6, which exclusively bind to CCL20 in the case of T_H17 cells, are expressed in these cells (Fu et al., 2016).

Similarly, after TCR signaling and co-stimulation, naïve $CD8^+$ T-cells may also adopt phenotypes analogous to their $CD4^+$ T-cell counterparts. One well-studied $CD8^+$ T-cell effector subset is cytotoxic T lymphocytes or Tc1 cells, which mediate target cell killing through multiple mechanisms. Under specific cytokine polarization conditions, which promote the differentiation of $CD4^+$ T-cells into T_H1, T_H2, T_H9, T_H17 and Treg populations, similar polarization can occur in naïve $CD8^+$ T-cells, giving rise to Tc1, Tc2, Tc9, Tc17, and regulatory $CD8^+$ T-cell populations (Bensussen et al., 2022).

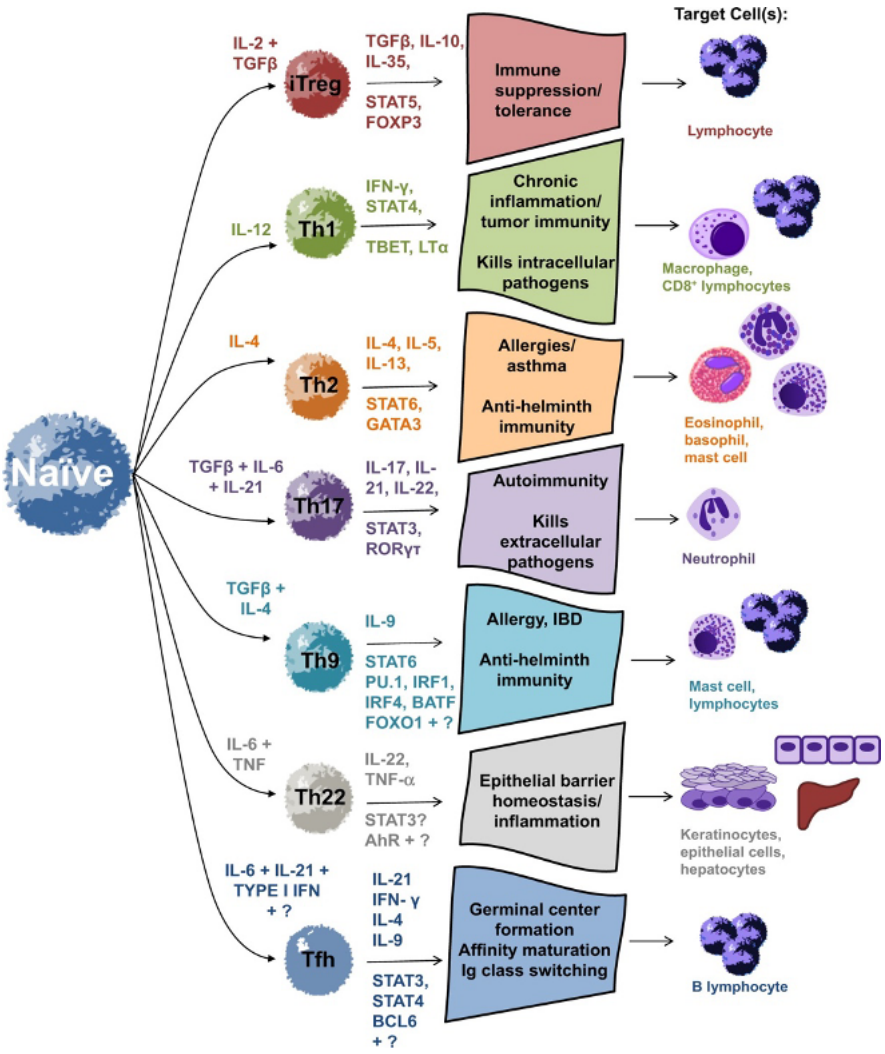

Fig. 1.5 $CD4^+$ T-cell differentiates into multiple T helper subsets. After being exposed to their cognate antigens, $CD4^+$ T-cells can differentiate into several T helper subsets based on the cytokines present during activation. Expression of master transcription factors, often known as lineage markers, and lineage-specific cytokine profiles serve to identify each subset. Extracted from (Knochelmann et al., 2018).

After cognate antigen recognition, T-cell search strategies differ. Chemotaxis or "informed motion" of activated T-cells, is made possible by the upregulation of chemokine receptors and integrins rendering them responsive to migratory cues present in their immediate surroundings (Krummel et al., 2016). Chemotaxis improves

T-cell ability to recognize APCs, enables T-cells to exit SLOs following a few rounds of proliferation and equips them with the necessary receptors to efficiently infiltrate target organs. For instance, the activation of $CD8^+$ T-cells relies on the production of CCL3/4 by APC that have interacted with $CD4^+$ T-cells (Castellino et al., 2006). Upon activation, $CD8^+$ T-cells upregulate CCR5 and are subsequently attracted to CCL3/4-producing APCs (Kastenmüller et al., 2013). Furthermore, after activation, $CD4^+$ T-cells release XCL1, which attracts DCs and helps $CD8^+$ T-cells (Eickhoff et al., 2015).

1.3.5. T-cells egress from secondary lymphoid organs

Although some PP-primed T-cells directly migrate to adjacent *LP* (section **1.4**), most T-cells must leave the PPs, returning to the bloodstream via efferent lymphatic vessels. To egress from SLOs, effector T-cells downregulate L-selectin and CCR7 and start to express homing receptors that allow access to target locations. Upregulation of sphingosine-1-phosphate receptor 1 (S1PR1) during the proliferation of activated T-cells mediates LN egress (Cyster and Schwab, 2012). S1PR1 recognizes sphingosine-1-phosphate (S1P), which is present in high concentrations in lymph and blood and promotes cell migration to lymphatic vessels lining the T-cell zone. The S1P gradient inside lymph nodes attracts T-cells to the cortical lymphatic vessels, which spread through the T-cell zone (Fang et al., 2017).

Whether a T-cell leaves LN is determined by the fine balance between the exit-promoting effect of S1PR1 and the retention effect of CCR7 (Pham et al., 2008). Constant binding of S1P to S1PR1 of T-cells in the bloodstream promotes internalization and desensitization of S1PR1. Upon re-entry into a LN in the absence of S1P exposure, S1PR1 is gradually recycled to the T-cell surface (Tomura et al., 2008). In the absence of cognate antigen recognition, naïve T-cells typically exit a LN within a time frame of 6 to 12 hours (h) (Tomura et al., 2008), whereas the presence of IFN-γ leads to the upregulation of CD69, which sequesters and degrades S1PR1 (Shiow et al., 2006), thereby prolonging T-cell retention within LNs during ongoing immune responses; additionally, cognate antigen recognition suppresses S1PR1 transcription for up to 3 days (Matloubian et al., 2004, p. 1), allowing for the expansion and selection of highly specific T-cell clones (Tomura et al., 2008). One crucial aspect is the activation requirement of T-cells, as once they differentiate into effector cells, specific antigen recognition alone is sufficient to trigger an immune response without

the need for co-stimulation. After several days of proliferation, CD69 expression declines, and S1PR1 is re-expressed, allowing effector T-cells to migrate out of LNs following S1P gradients (Murphy and Weaver, 2022).

1.3.6. Homing of effector T-cells

Activated T-cells upregulate tissue-specific integrins and selectins for homing. DCs in mLNs and PPs produce retinoic acid, enhancing $\alpha_4\beta_7$ and CCR9 expression on T-cells (Beilhack et al., 2008; Iwata et al., 2004). $CD103^+$ DCs are the predominant migratory DC population in intestinal *LP*, which express more vitamin A metabolism enzymes than $CD103^-$ DCs and are anticipated to be the most potent at imprinting gut homing (Fu et al., 2016, p. 200). Gut homing of antigen-stimulated T-cells depends on $\alpha4\beta7$ integrin, which binds MAdCAM-1 on the intestinal endothelial cells, and CCR9 that binds CCL25 produced by intestinal epithelial cells (Beilhack et al., 2008; Hammerschmidt et al., 2008). Nonetheless, interactions of lymphocyte-associated (PSGL-1, LFA-1, CD44, and $\alpha_4\beta_1$ with venular P/E-selectin, ICAM-1 (and ICAM-2), hyaluronate, and vascular cell adhesion molecule 1 (VCAM-1), respectively, play an important role, too (Fu et al., 2016).

The binding of P-selectin glycoprotein-1 (PSGL-1) to P- and E-selectins, which are upregulated on inflamed endothelium, leads to the tethering and rolling of effector T-cells on postcapillary venular endothelial cells in the intestine. The interaction between very late antigen-4 (VLA-4; $\alpha_4\beta_1$) also promotes the rolling of effector cells. T-cells can then use their receptors to find chemokines that have been presented on endothelium. Effector T-cells in the gut express CCR9, allowing them to recognize homeostatic CCL25 produced by epithelial cells (Habtezion et al., 2016). The conformational activation of LFA-1 and $\alpha_4\beta_7$ integrin is induced by GPCR signaling, enhancing the binding of effector cells to ICAM-1 (or ICAM-2) and MAdCAM-1, respectively. In contrast, T-cells stimulated in colon-draining lymph LNs express CCR10 and $\alpha_4\beta_7$. This expression pattern enables colon infiltration, as the colon epithelial cells express CCL28, chemokine recognized by CCR10 (Murphy and Weaver, 2022). Effector T-cells can transmigrate into the intestinal *LP* on the basolateral side of the endothelium or through endothelial cells (**Fig. 1.4**).

1.4. Direct alloreactive T-cell migration from Peyer's patches to intestinal *lamina propria*

An adaptive intestinal immune response is classically induced PPs or mLNs. Typically, effector T-cells return to the systemic circulation via efferent nodal lymphatics and home to the mucosa of the intestinal tract (section **1.3**). Since it is impossible to properly duplicate the complexity of GvHD in-vitro, pre-clinical animal models have been instrumental to explore donor T-cell trafficking and migration during aGvHD. Several well-established murine models are essential for testing new therapeutic strategies, examining novel molecular processes, and understanding pathophysiological mechanisms in aGvHD (Patel et al., 2022). To induce aGvHD, allogeneic T-cells are co-transplanted with bone marrow into a recipient mouse pre-conditioned by chemotherapy or irradiation.

Unpublished results from our group indicate that after activation, a subset of alloreactive T-cells can migrate directly from T-cell zones of PPs to adjacent *LP* of the small intestine early after GvHD initiation. These results proved a previously unknown migration shortcut bypassing T-cell lymphatic drainage and vascular trafficking. In these experiments we had used total body irradiation for myeloablative conditioning of the recipient's bone marrow. To induce aGvHD, we transplanted bone marrow cells and T-cells from a B6 (H-2b) donor into a myeloablative irradiated BALB/c (H-2d) recipient. In this model mice developed aGvHD within one week following allo-HCT, with $CD4^+$ and $CD8^+$ T-cells contributing to GvHD pathology (Patel et al., 2022).

This pre-clinical murine model provided a valuable platform for studying the infiltration of activated T-cells into target organs following synchronized proliferation in SLOs. The time course of T-cell infiltration after allo-HCT had previously been well characterized (Jarick, 2020). The strong and organized T-cell infiltration wave observed in this model facilitated to study the different infiltration steps efficiently and reproducibly. Consequently, we believed that former characteristics made this murine model adequate to study the direct migration of T-cells from PP to *LP*.

1.4.1. T-cells form a gradient around Peyer's patch

Early after allo-HCT (day +2 to +3,5), donor T-cells created a gradient surrounding PPs, visualized with light-sheet fluorescence microscopy (LSFM). The gradient of T-cells suggested that T-cells originated from PPs and spread laterally into nearby *LP*, as we would not expect if they came from vasculature (**Fig. 1.6**). T-cell infiltration grew on day +4 when the first activated T-cells began circulating in the blood, close to PP and farther away. On day +4, some samples still showed a visible gradient. On day +6, alloreactive T-cells heavily infiltrated throughout the gut, and the gradient had evened out.

To confirm the location of the quantified T-cells in the *LP*, we co-stained intestinal tissue samples with Lyve-1 (a lymphatic vasculature marker) and MAdCAM-1 (an HEV marker) to rule out their presence within lymphatic or blood vessels surrounding PPs. We found that T-cells located outside lymphatic or blood vessels, confirming their presence within the mucosal tissue.

1.4.2. T-cells directly egress from Peyer's patch to *lamina propria* in a random pattern

To rule out that the gradient of extravasated donor T-cells around PPs is solely due to increased vascular T-cell trafficking to this area, we established a technique to photoconvert fluorescent donor T-cells residing in PPs. After 12 h, T-cells photoconverted in PPs migrated into the nearby *LP*. Photoconversion utilizes light to induce irreversible fluorescence changes in cells expressing photoconvertible proteins. As previously described (Jarick et al., 2018), we illuminated donor Dendra2 T-cells located in PPs with UV light, resulting in the irreversible switch of Dendra2 fluorescence from green to red. These photoconverted cells were not observed near unconverted PPs or in locations farther away from the PPs. The absence of converted T-cells around unconverted PPs provided evidence that the photoconverted cells close to PPs did not originate via vascular trafficking (**Fig. 1.6**).

Around the photoconverted PPs, approximately 50% of the donor cells were unconverted T-cells. These cells may have been activated in SLOs other than the converted PPs and entered the tissue trough extravasation. Alternatively, these cells might have been activated within partially photoconverted PPs, and the red fluorescence from the Dendra2 marker was diluted due to cell proliferation. The first hypothesis seems more plausible, given the efficacy of photoconversion.

We visualized allogeneic T-cells directly egressing from PPs into the adjacent *LP* with intravital two-photon microscopy. Confinement ratio, rotation angle, and speed of migrating T-cells were examined inside PP and in adjacent *LP* on days +3 and +4 after allo-HCT. T-cells migrated faster in *LP* than within PP and overall faster on day +3 than on day +4 after allo-HCT. Directionality on day +3 after allo-HCT was lower in *LP* (0,44) than in PP (0,47), indicating random mobility, as determined by the confinement ratio (ratio between the linear displacement of a cell and its actual trajectory). Higher measurements of turning angles (87,6° vs. 91,5°) on day +3 showed that *LP* cells turned less abruptly. In quest of antigens, naïve T-cell movement in LNs and PPs generally seems random (**Fig. 1.6 e-f**). This is due to T-cells in these lymphoid organs migrating across a 3D network of FRC and constantly crossing paths with other cells, which causes them to frequently vary their motion, as previously mentioned (section **1.3.4**). On day +3, the PP-like confinement ratio of T-cells in *LP* suggests they also migrate randomly. We cannot rule out the possibility that irregularly distributed stimuli support directional migration inside the tissue. External barriers, including other immune cells, ECM, and blood vessels, can cause T-cells to migrate seemingly randomly despite following one or more directed migration cues (Beltman et al., 2007).

T-cell migration patterns around PPs differ more between days +3 to +4 than between PP and *LP*. Donor T-cells showed more directionality by day +4 after allo-HCT, as indicated by a higher confinement rate inside and outside PPs. On day +3, the T-cells may still be in the early stages of activation and had not undergone substantial proliferation. By day +4, most donor T-cells in PP are expected to be activated (Beilhack et al., 2005). Recent T-cell activation results in informed-based motion, and chemokine gradients are presumably less evident on day +3 as opposed to day +4 after allogeneic.

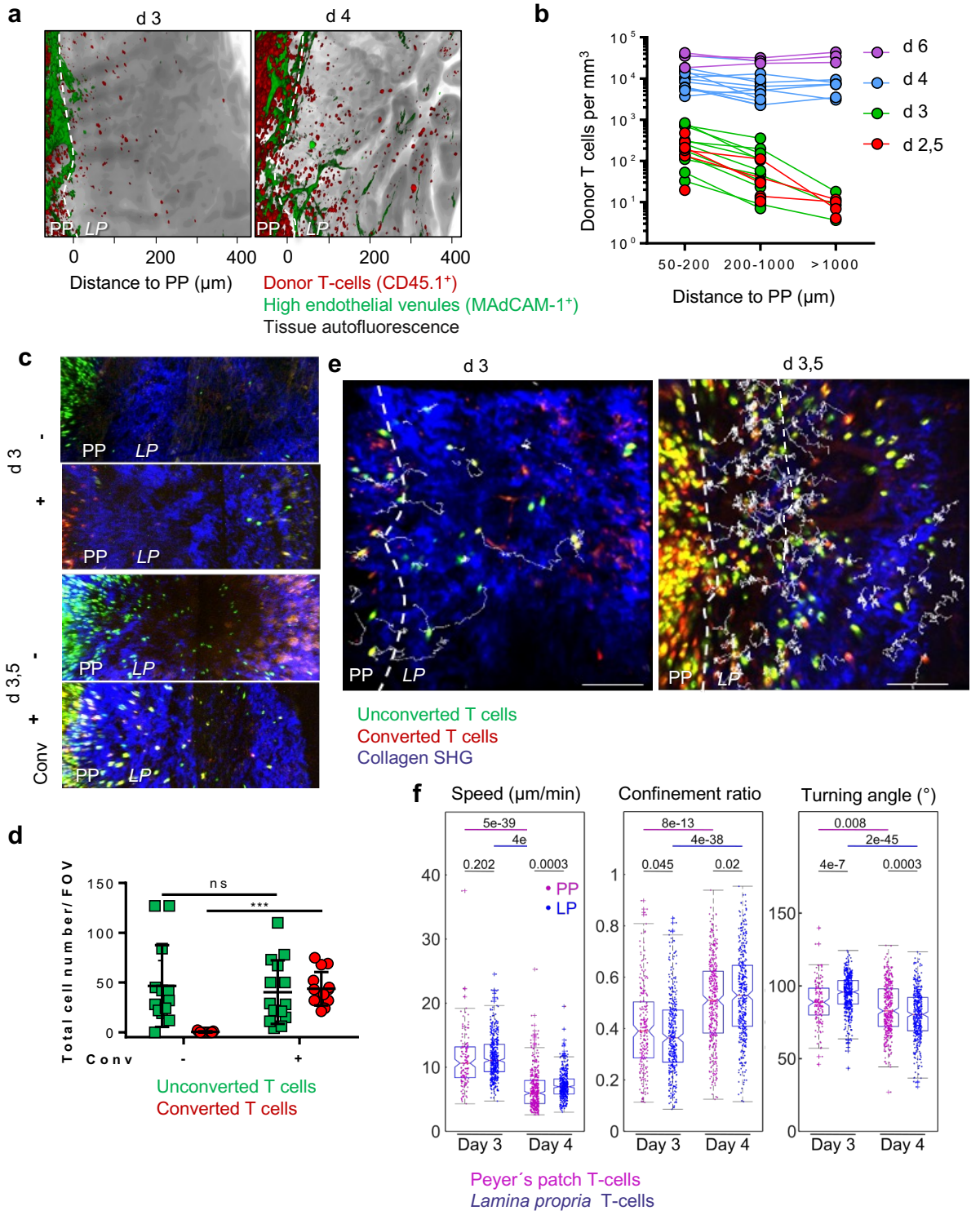

Fig. 1.6 T-cells migrate directly from Peyer´s patch to the adjacent *lamina propria*. **a.** Edge of PP was imaged in whole mount LSFM on days +3 and +4 following the transplantation of allogeneic CD45.1$^+$ T-cells from B6 to BALB/c, alongside B6 bone marrow. Scale bar 100 µm. Images are representative of 12 mice per day. **b.** Quantification of T-cell gradient from LFSM data. One triplet of connected dots represents one PP, *n* =12 (day +2 to 4), and 3 (day +6) mice. **c-d**. Dendra2 allogeneic T-cells were transplanted from B6 to BALB/c. **c.** Stitched two-photon image of explanted photoconverted PPs on day +3,5. Ileal PPs were photoconverted on day +3 12 h before imaging the PP border. Scale bar 200 µm. **d.** Quantification of donor T-cells in the *LP* around the PPs. One FOV represented by one dot, n =4 mice per group. Unpaired non-parametric Kruskal-Walli's test. **e.** Intravital two-photon microscopy tracks of allogeneic photoconverted T-cells crossing the PP border (dashed line) and migrating in *LP*. Scale bar

100 µm. Images are representative of at least 5 mice per day. Scale bar 100 µm. **f.** Migration analysis of photoconverted Dendra2 T-cells in PP (magenta) and *LP* (blue). One cell track represented by one dot. The analysis includes 5 and 13 mice in PP and *LP,* respectively (day +3) or 2 mice (day +4). Modified from (Jarick, 2020 Ph.D. thesis).

In contrast to amoeboid migration on day +3, most T-cells in *LP* followed the collagen network on day +4 and traveled slower, which may indicate an integrin-mediated motion. A combination of haptic and soluble cues may promote migration on collagen networks, as has been extensively studied for DCs (Schumann et al., 2010; Schwarz et al., 2017). The reduced speed rate is consistent with previous observations of activated T-cells (section **1.3.4**). In summary, there was no overall directionality within the T-cell population egress to *LP* (**Fig. 1.6 e-f**).

1.4.3. T-cell egress to tissue does not depend on S1PR1

S1PR1-mediated egress plays a role in LNs, PPs, spleen, and thymus (section **1.3.5)**. We blocked S1PR1 with fingolimod, a substance that mimics S1P, to determine if this common mechanism also contributes to the direct migration of T-cells to the nearby *LP*. Subsequent down-modulation of S1PR1 inhibits lymphocyte egress through the lymphatic system. In fingolimod-treated animals, donor T-cells were unable to exit SLOs and disappeared from the systemic circulation, confirming the successful blockade of lymphatic egress. Based on this observation, we analyzed whether T-cells could still leave PP into *LP* despite a block of lymphatic egress with photoconversion experiments. Both fingolimod-treated and untreated mice exhibited a similar number of unconverted T-cells around PPs, regardless of whether they were converted or not. Around unconverted PPs, there were no converted T-cells. Still, in both untreated and fingolimod-treated animals, converted T-cells were found, indicating that despite fingolimod treatment, T-cells can still migrate from PP to *LP* and that S1PR1 does not play an important role in this process (**Fig. 1.7**).

1.4.4. T-cell egress to tissue does not depend on CD11c$^+$ host macrophages

Topographic features of macrophages are used as substrates to migrate on by T_{RM} cells in salivary glands (Stolp et al., 2020). A purely friction-based movement without the intervention of integrins or chemokines. We used a mouse model of inducible depletion of host macrophages. Diphtheria toxin administration eliminates CD11c$^+$ cells, highly expressed by intestinal macrophages (Grainger et al., 2017), in

transgenic CD11cDOG mice. After the diphtheria toxin injection, the *LP* myeloid cells were reduced by 91,8%. (**Fig. 1.7**). Based on this finding, we investigated if T-cells could still migrate from PPs into *LP* in mice with macrophage depletion. Around unconverted PPs, there were no converted T-cells, converted T-cells were found in *LP* of converted PPs in mice with and without macrophage depletion implying that macrophages are not necessary for direct migration of T-cells from PPs to *LP* (**Fig. 1.7**).

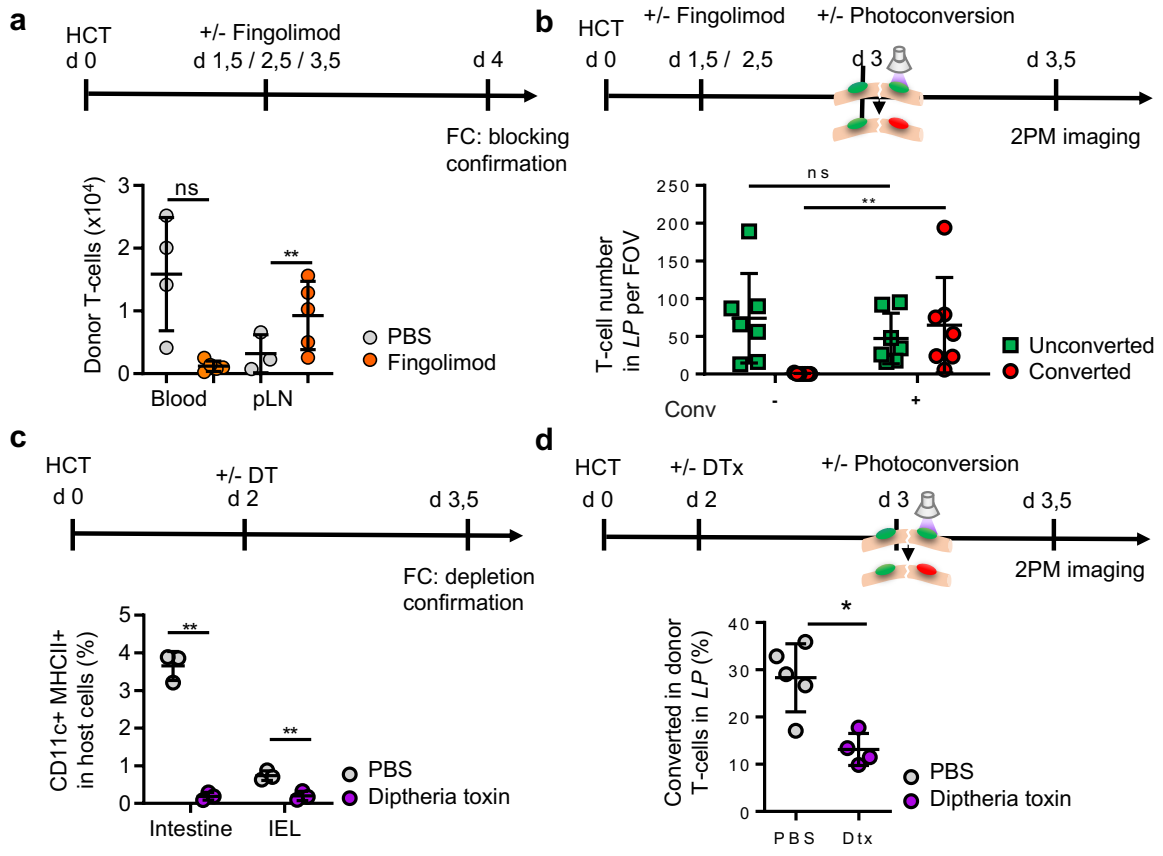

Fig. 1.7 T-cell egress directly from Peyer´s patch to the *lamina* independently from S1P gradient sensing or CD11c⁺ host macrophages. a. Myeloablative conditioned BALB/c recipients were transplanted with CD90.1⁺ T-cells. Fingolimod was administered to one group of mice on days +1,5, +2,5, and +3 after allo-HCT. Flow cytometric quantification of donor T-cells on day +4 after allo-HCT. **b.** Mice were transplanted with Dendra2 T-cells. Fingolimod was administered to one group of mice on days +1,5, +2,5 after allo-HCT. PPs were photoconverted on day +3 after allo-HCT. Quantification using two-photon microscopy imaging on days +3,5, and the Kruskal-Walli test. Modified from (Jarick, 2020 Ph.D. thesis). **c-d.** B6a.CD11cDOG x BALB/c F1 mice were transplanted with CD45.1 or Dendra2 T-cells. PPs were photoconverted three days later. One group of mice received a diphtheria toxin injection on day +2,5 after allo-HCT. **c.** We calculated the percentage of myeloid cells (CD11c⁺ MHCII⁺) in the population of alive host cells using flow cytometry plots, confirming the depletion of macrophages. Unpaired non-parametric Mann-Whitney test (*n* =6, ** P < 0,01). **d.** The percentage of photoconverted cells in *LP* of macrophage-depleted and non-depleted mice with aGvHD was quantified. Unpaired non-parametric Mann-Whitney test (*n* =5, *P <0,05).

1.5. Knowledge gap

A subset of alloreactive T-cells migrates directly from the T-cell zones of PPs to the adjacent *LP* of the small intestine early after GvHD initiation. This previously unknown T-cell migration route provides a shortcut bypassing lymphatic drainage and vascular trafficking. Direct T-cell migration was only observed in GvHD-developing mice conditioned with total body irradiation. As ionizing irradiation can damage stromal cells in PP´s border (macrophages, FRCs, or other stromal cells) we hypothesized that this event may create new migration spaces for highly proliferative allogeneic T-cells. Therefore, we asked whether allogeneic T-cells would also directly migrate from PP into the adjacent *LP* if recipient mice would not be exposed to myeloablative whole body irradiation.

The function of direct PP-to-*LP* migrating T-cells remains elusive. We hypothesized that direct PP-to-*LP* T-cell migration may help to initiate a faster local immune response. Furthermore we asked whether they may also act as seeder cells attracting other circulating T-cells to early sites of inflammation, e.g. through the secretion of chemoattractants, defensins, or other soluble mediators. For instance, $CD8^+$ can be recruited via the production of $CCL4^+$ (Cook et al., 1999). We speculated that this effect, already described for other GvHD target organs (Serody et al., 2000), could also a key driver for attracting T-cells from the PPs to the *LP*. Therefore, we investigated whether these early PP-to-*LP* T-cell emigrants could act as seeder cells to attract additional bloodborne antigen-specific or -nonspecific donor T-cells.

In previous experiments, we had confirmed that neither S1PR1 nor topographical features of macrophages would mediate the direct T-cell egress from PPs to the *LP*. As other molecular candidates could facilitate this process, we explored the role of integrins and chemokine receptors. Therefore, we tested which molecular interactions would allow for the direct T-cell egress from PPs to *LP*.

2. Specific aims

This project aims to understand further early mucosal events of T-cell activation in Peyer's patches and understand the molecular mechanism and biological relevance of direct migration of freshly activated effector T-cells from Peyer's patches (PP) into the adjacent intestinal *lamina propria* (*LP*) in contrast to conventional vascular homing. The specific aims of this thesis were to:

1. Investigate the role of pre-transplantation conditioning in direct T-cell migration from PP to *LP.*
2. Determine whether direct PP-to-*LP* T-cell migration leads to faster recruitment of antigen-specific T-cells.
3. Determine whether direct PP-to-*LP* T-cell migration triggers the secondary recruitment of further bloodborne lymphocytes.
4. Study how direct T-cell migration from PP to *LP* is regulated on a molecular level.

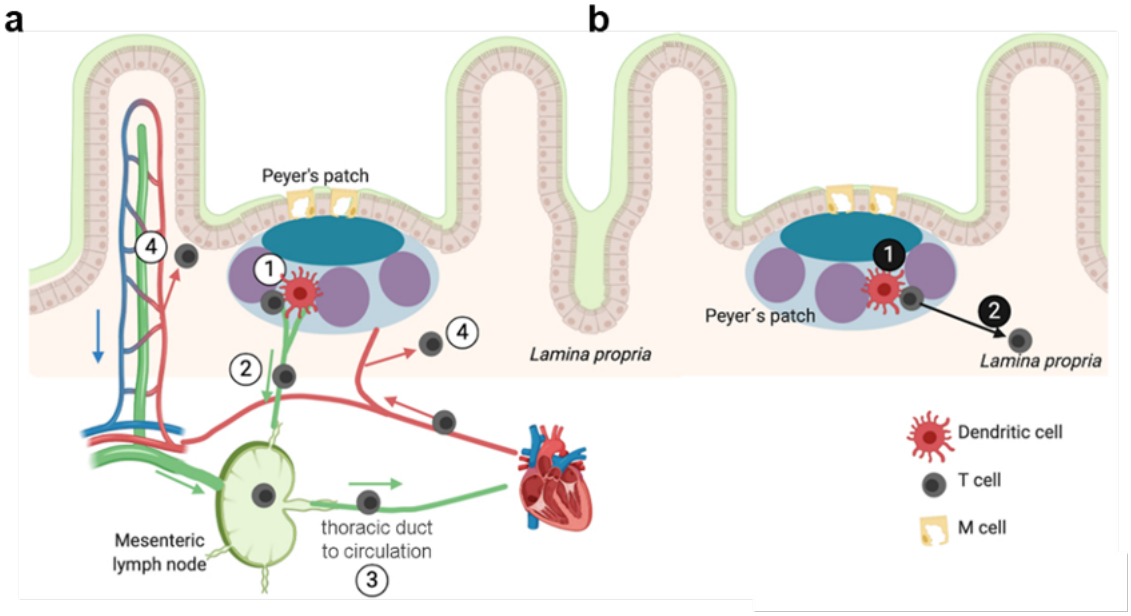

Fig. 2.1 Alternative route of T-cell trafficking from Peyer's patches to the adjacent *lamina propria.* **a. 1.** An intestinal immune response is classically induced in PPs or gut-draining mLNs. **2.** Conventionally, effector T-cells primed in the PPs exit lymphoid tissue via efferent nodal lymphatics, **3.** return to the systemic circulation, and **4.** home to gut using specific homing receptors. **b. 1-2**. Recent unpublished results from our lab indicate that a subset of alloreactive T-cells can migrate directly from T-cell zones of PPs to the adjacent intestinal *LP* early after GvHD initiation. Created with Biorender.

3. Materials and methods

3.1. Materials

3.1.1. Chemical reagents

Material	Catalog #	Company
Acetone	32201	Sigma-Aldrich
Ammonium chloride (NH_4Cl)	P726	Carl Roth
Baytril 10% (enrofloxacin 0,05%)	A5581	Bayer
Benzyl alcohol	4478.2	Carl Roth
Benzyl benzoate	B6630	Sigma-Aldrich
Bovine serum albumin (BSA)	8076.5	Carl Roth
Collagenase A from *Clostridium histolyticum*	10103586001	Roche
Collagenase D from *Clostridium histolyticum*	11088866001	Roche
CXCL11 from *Escherichia coli*	574904	BioLegend
DNase I	11284932001	Roche
Phosphate buffer saline (PBS) without Ca^{2+}/Mg^{2+}	P04-36500	Pan Biotech
Dithiothreitol (DTT)	6908.2	Carl Roth
Entellan®	1.07961	Merck
Ethanol absolute	2246	Chemsolute®
Ethanol (70%)	T913.3	Carl Roth
Ethylenediaminetetraacetic acid (EDTA)	X986.2	Carl Roth
Eye ointment (Bepanthen®)	6029009.00.00	Bayer
Fetal calf serum (FCS)	10270-106	Gibco®
L-glutamine	25030081	Gibco®
Hank's balanced salt solution (HBSS), Ca^{2+}/Mg^{2+}	24020117	Gibco®
HBSS, without Ca^{2+}/Mg^{2+} phenol red	14175095	Gibco®
HEPES	HN77.4	Carl Roth
n-Hexane	1.04367	Merck
L-Lysin	L5626-500G	Sigma-Aldrich
2-Mercaptoethanol	21985-023	Gibco®
Metamizol (Novalgin®)	00731672	Sanofi
Normal rat serum (NRS)	31888	Invitrogen
O.C.T™ tissue tek	4583	Sakura
OneComp eBeads	01-111-42	Invitrogen
Paraformaldehyde	158127	Sigma Aldrich
Paraformaldehyde 4% in PBS	J19943.K2	Thermo Fisher
PBS tablets	18912-014	Gibco®
Percoll™	17089101	Cytiva
Pertussis toxin from *Bordetella pertussis*	180	List Biological laboratories
Pertussis toxin mutant from *Bordetella pertussis*	184	List Biological laboratories

Penicillin, streptomycin	15140-122	Gibco®
Povidone iodine (Braunol® 7.5% solution)	3864219	BRAUN GmbH
Potassium bicarbonate ($KHCO_3$)	P748	Carl Roth
Recombinant IL-2	589106	BioLegend
Recombinant IL-7	577804	BioLegend
RPMI medium 1640	21875-034	Gibco®
Sodium chloride (NaCl) 0,9%		Fresenius
Sodium phosphate monobasic (NaH_2PO_4)	S8282-500G	Sigma-Aldrich
Sodium phosphate dibasic (Na_2HPO_4)	1.06586.0500	Merck
Sodium periodate ($NaIO_4$)	311448-5G	Sigma-Aldrich
Sucrose	S0389	Sigma-Aldrich
Triton® X 100	2051.3	Carl Roth
Trypan blue	A0668,0025	Applichem
Trypan blue solution	11413D	Thermo Fisher
Ursotamin® (ketamine 100 mg/ml)	12727581	Serumwerk
VECTASHIELD® mounting medium with DAPI	H-1200	Vector Laboratories
Xylavet® (xylazine 20 mg/ml)	401510.00.00	CP-Pharma

3.1.2. Buffers and solutions

Anesthetic: ketamine and xylazine were dissolved in PBS to a concentration of 8 mg/ml and 1,6 mg/ml, respectively. To achieve *in-vivo* concentrations of xylazine 16 mg/kg and ketamine 80 mg/kg, µl/g body weight was intraperitoneally (i.p.) injected.

Analgetic: Novalgin® was introduced into drinking water at a metamizole 1,33 mg/ml concentration. Metamizole was dissolved 1:25 in NaCl 0,9%. Then, 10 µl/g body weight was injected subcutaneously at recovery from anesthesia to reach *in-vivo* concentrations of metamizole 200 mg/kg.

Clearing solution: benzyl alcohol: benzyl benzoate mixed in a 1:2 ratio.

Enrichment buffer: BSA 0,1%, EDTA 2 mM in PBS, and sterile filtered.

Erythrocyte lysis buffer: NH_4Cl 1,68 M, $KHCO_3$ 0,1 M, and EDTA 1 mM were dissolved in deionized water to make a 10× stock that was diluted at 1:10 to generate a working solution.

Flow cytometry buffer: FCS 2%, EDTA 5 mM in PBS.

Intestinal dissociation buffer: HEPES 10 mM, EDTA 2 mM, DTT 1 mM, and FCS 5% in HBSS without Ca^{2+} or Mg^{2+}

Migration medium: penicillin-streptomycin solution 1%, L-glutamine 2mM, and BSA 0,1% in RPMI medium1640.

Periodate- lysine- paraformaldehyde (PLP) fixation buffer: L-lysine 0,075 M, $NaIO_4$ 2 mg/ml, and PFA 1% in $NaPO_4$ buffer 0,05 M pH 7,4.

Trypan blue solution: Trypan blue 1% (w/v) in PBS stock solution.

3.1.3. Antibodies and secondary reagents

Reactivity		Conjugation	Clone	Isotype	Company
CCR5	flow cytometry	PE	C34-3448	559923	Biolegend
CCR9	flow cytometry	PE/Cy7	CW-1.2	25-1991-82	eBioscience
CD25	flow cytometry	AF488	PC61.5	53-0251-82	Invitrogen
CD28	cell culture	purified	37.51	102101	Biolegend
CD3ε	flow cytometry	BV711	17A2	100241	Biolegend
CD3ε	cell culture	purified	145-2C11	553058	BD Pharmingen
CD4	flow cytometry	PerCP/Cy5.5	RM4-5	100540	Biolegend
CD4	flow cytometry	APC/Cy7	GK1.5	100414	Biolegend
CD44	flow cytometry	PE	IM7	103008	Biolegend
CD45	flow cytometry	pacific blue	30-F11	MCD4528	Invitrogen
CD45	flow cytometry	AF647	30-F11	103124	Biolegend
CD45	flow cytometry	APC/Cy7	30-F11	103116	Biolegend
CD45.1	histology	AF647	A20	110720	Biolegend
CD62-L	flow cytometry	AF488	MEL-14	104420	Biolegend
CD62-L	flow cytometry	PE/Cy7	MEL-14	25-0621-82	Biolegend
CD8a	flow cytometry	PE/Cy7	53-6.7	100722	Biolegend
CD8a	flow cytometry	AF488	53-6.7	100723	Invitrogen
CD90.1	flow cytometry	APC-eF780	HIS51	47-0900-82	Invitrogen
CXCR3	flow cytometry	PerCP/Cy5.5	CXCR3-173	45-1831-82	Invitrogen
IFN-γ	flow cytometry	BV421	XMG1.2	505829	Biolegend
IL-17A	flow cytometry	APC	TC11-18H10.1	506916	Biolegend
Ki67	flow cytometry	AF647	16A8	652408	Biolegend
MAdCAM-1	histology	Biotin	MECA-367	120706	Biolegend
RORyt	flow cytometry	PE	AFKJS-9	12-6988-82	BD Biosciences
RORyt	flow cytometry	AF647	Q31-378	562682	BD Pharmingen
Streptavidin	histology	AF546		S11225	Invitrogen
T-bet	flow cytometry	FITC	4B10	644812	Biolegend
T-bet	flow cytometry	PE	eBio4B10	12-5825-82	Biolegend
TNF-α	flow cytometry	PE	MP6-XT22	506306	BD Pharmingen
α4 (CD49d)	flow cytometry	FITC	PS/2	104901H0	Biolegend
α4 (CD49d)	blocking mAb	purified	PS/2	BE0071	Bio X cell
αE (CD103)	flow cytometry	PE	M290	557495	BD Pharmingen
αE (CD103)	blocking mAb	purified	M290	BE0026	Bio X cell
αL (CD11a)	flow cytometry	APC	FD441.8	E-AB-F1033UE	Elabscience
αL (CD11a)	blocking mAb	purified	FD441.8	BE0005	Bio X cell

3.1.4. Commercial kits

Material	Catalog #	Company
Avidin/biotin blocking kit	SP-2001	Vector Laboratories
Brefeldin A	420601	BioLegend
Cell activation cocktail (without Brefeldin A)	423302	BioLegend
Dynabeads™ untouched™ mouse T-cells kit	11413D	Thermo Fisher
Dynabeads™ mouse T activator CD3/CD28 for T-cell expansion and activation	11452D	Thermo Fisher
Mouse inflammation panel LEGENDplex™	740150	BioLegend
LIVE/DEAD™ fixable violet dead cell stain kit	L34955	Thermo Fisher
Precellys lysing kit	P000912-LYSK0-A	Precellys
Transcription factor staining buffer set	00-5523-00	Thermo Fisher
Zombie Aqua™ fixable viability Kit	423101	BioLegend

3.1.5. Consumables

Material	Catalog #	Company
1 ml insulin syringe 30G × ½ Omnican®100	9151141	Braun
1 ml syringe 26G × 3/8 BD plastipack™	300025	Becton Dickinson
5 ml syringe BD Discardit™ II	2023-04	Becton Dickinson
26-gauge needles	4665457	Stericon
6-well plates	83.3920.500	SARSTEDT
24-well plates Nunclon™ delta surface	142475	Thermo Fisher
96-well plates U-Bottom	351177	Corning
Cell strainer, 100 µm (MACS® smart strainers)	130-110-917	Miltenyi Biotec
Cell strainer, 70 µm EASY strainer™	542070	Greiner Bio-one
Coverslips (21 × 25 mm)	01 010 092	Marienfeld
Cryomolds (25 × 20 × 5 mm)	4557	Sakura
Microtubes 1,5 ml	72.706	SARSTEDT
Flat-bottom glass containers (Rollrandgläser)	RR02	Hartenstein
Falcon tubes (15, 50 ml)	188271, 227261	Greiner Bio-one
Gentle MACS™ tubes	130-093-236	Miltenyi Biotec
Lancets for capillary blood collection	6182003	BRAUN
Lithium Heparin tubes for plasma collection	078004	Kabe Labortechnik
Operation towel	800430	Mölnlicke Healthcare
Pasteur pipettes	2600111	NeoLab
Pippete tips (10, 200, 1000 µl)	70.1130, 70.3030, 70.3050	SARSTEDT
Razors	704028	Relax Pharma u. Kosmetik GmbH

Serological pipettes (5, 10, 25 ml)	606180, 607180, 760180	Greiner Bio-one
Shandon coverplate assemblies	72110017	Thermo Fisher
Shandon cuvette slide rack	73310017	Thermo Fisher
µ-slide chemotaxis collagen IV surface	80322	Ibidi
Sterile cotton swab	EH12.1	Carl Roth
Sterile dissecting swab	12780	Lohmann & Rauscher
Sterile gauze swab	13695	Lohmann& Rauscher
Sterile surgical blades	BB510	BRAUN
SuperFrost® Plus glass microscope slides	03-0060	R. Lagenbrinck GmBH
Suture, 6-0 with beveled needle	V301G	Ethicon
Tissue adhesive	149SB	3M VetBond™

3.1.6. Equipment

Equipment	Company
Accu-jet® pro (26300)	Brandt
Attune™ NxT flow cytometer (with 405, 488, 561, and 633 nm lasers, and a high throughput autosampler)	Thermo Fisher
Cell incubator HERA cell 150i	Thermo Fisher
Centrifuge (megafuge 40R)	Thermo Fisher
Cryomicrotome (CM1950)	Leica
Collimator for 405 nm, NA=0,6, f= 4,02 mm, fiber collimation F671SMA	THORLABS
Confocal scanning microscope (LSM 780)	ZEISS
Gentle MACS™ octo dissociator	Miltenyi Biotec
Heating mats (76085)	TRIXIE Heimtierbedarf
Heating and incubation insert P-Set 2000	Pecon
High-Power 405nm lamp coupled to a glass fiber (1500 µm, NA=0,5)	Prizmatrix
Hot bead sterilizer FST 250 (18000-45)	Fine Science Tools
Inverted routine microscope (eclipse TS100)	Nikon
Irradiation source (CP-160)	Faxitron
Laminar flow hood HERAsafe (KS18)	Thermo Fisher
Light sheet fluorescence microscopes	Home-built in Rudolf Virchow Center, Würzburg
Micropipettes (042760930, 642752433, 942741768, 342733754, 042720454, 942711302)	VWR
Neubauer cell counting chamber Cell (ZK03)	Hartenstein
Tissue homogenizer Precellys 24 (P000669-PR240-A)	Bertin instruments
Orbital Shaker (PSU-10i)	Grant Instruments

Mouse pie cage for total body mice irradiation (MPC-1)	Braintree Scientific
Tubing tygon	Cole-Parmer GmbH
Tubing pump (ISM795C)	Cole-Parmer GmbH
Two photon microscope (SP8) DM6000 CFS with HC Fluotar L 25x/1,0 IMM motCORR objective, two Hamamatsu R 9624 photomultiplier tubes, two HyD-RLD2 detectors, chameleon vision II TiSa laser, and beam splitters (RSP 620 + BP440/20 + 675/50, RSP 455, RSP 560 + 525/50 + 585/40, RSP 495 + BP 440/20).	Leica
UV protection glasses (F18P1L051001)	Laservision
Vortex mixer	Neolab
Water bath (WNB 14)	Memmert

3.1.7. Mice

Strain	Code #	Company
C57BL/6 (C57BL/6NCrl)	027	Charles River
BALB/c (BALB/cAnNCrl)	028	Charles River
CB6F1	176	Charles River
B6. Cg-Tg(CAGDsRed*MST)1Nagy/J	006051	Jackson Laboratories
B6; 129S-Gt(ROSA)26Sor$^{tm1.1(CAG-COX8A/Dendra2)Dcc}$/J	018397	Jackson Laboratories
C57BL/6. Tg(CAG-luc,-GFP)L2G85Chco Thy1a/J		Bred at Beilhack´ laboratory
C57BL/6. Tg(CAG-luc,-GFP)L2G85Chco Ptprca/J		Bred at Beilhack laboratory

Transgenic mice were genotyped with an end-point polymerase chain reaction with an agarose-gel electrophoresis readout. The mice were housed in a specific pathogen-free environment at ZEMM, Würzburg, and all animal experiments were approved by local authorities and adhered to the regulations outlined in the German animal protection law.

3.1.8. Software

Software	Version	Company
AxioVision	4.9.1	ZEISS
BioRender		BioRender
FlowJo	10.7	TreeStar
GraphPad Prism	7	GraphPad Software
IMARIS®	9.8.0	Bitplane
LEGENDplex™ data analysis software		BioLegend
Leica Application Suite X	3.1.5.16308	Leica
Office	Microsoft 365 (16.66)	Microsoft
ZEN	2012 SP1 (8.16484)	Zeiss
ZEN lite	2.3	Zeiss

3.2. Methods

3.2.1. Isolation of primary cells

3.2.1.1. Peripheral blood collection

Peripheral blood was sampled from the *vena facialis* with sterile lancets or from the caudal vein making a small incision. Blood was kept in lithium-heparin tubes until further processing. For 10 min, erythrocytes were lysed in 4 ml of lysis buffer. Cells were pelleted (330×g for 5 min at 4°C) and washed in 4 ml of PBS. Cell suspension was pelleted (330×g for 5 min at 4°C) and resuspended in PBS.

3.2.1.2. Bone marrow isolation

The *femur* and *tibiae* in the hind legs of 8 to 12-week-old mice were used to isolate bone marrow cells. Hind legs were obtained after hip joint dislocation, and skin and muscles were removed using a sterile surgical blade. At the knee side of the bones, a 26-gauge needle connected to a 5 ml syringe filled with PBS was inserted to flush bone marrow into a well on a 6-well plate. The bones were flushed until their color changed from red to white, implying that all the marrow had been removed. Cells were transferred onto a fresh tube thought a 70 µm cell strainer and rinsed with 5 ml of PBS. A normal bone marrow cell yield per mouse was 1 to 1,5 × 10^8 cells. Bone marrow preparations were kept at 4°C for up to two h prior to transplantation.

3.2.1.3. Single-cell suspension from spleen

Spleens were isolated from 8 to 12-week-old mice and kept in PBS on ice until they were further processed. On a 50 ml falcon, a 70 m strainer was positioned and pre-wetted with 2 ml of erythrocyte lysis buffer. The spleen was minced through the strainer after being cut several times crosswise. 4 ml of erythrocyte lysis buffer was used to rinse the strainer twice. Splenocytes were incubated for 2 min with 10 ml of erythrocyte lysis buffer at room temperature (RT). 10 ml of PBS added through the strainer stopped the lysis process. Splenocytes were pelleted (330×g for 5 min at 4°C) and resuspended in PBS.

3.2.1.4. T-cell enrichment from splenocytes

The Dynabeads® untouched™ mouse T-cells kit was used to enrich the splenocyte suspensions for T-cells in accordance with manufacturer's instructions. A

mixture of IgG rat monoclonal antibodies against CD11b$^-$, CD16/32$^-$, CD45R$^-$, and Ter-119$^-$ is first added to the sample. Then, cells are washed to remove excess antibodies and mouse depletion Dynabeads® are added. Superparamagnetic beads are coated with a secondary polyclonal antibody that binds rat IgG enabling the isolation of bead-bound cells by a magnet leaving purified target mouse T-cells in the supernatant. T-cell enrichment process yields 30% of the splenocyte input with a 95% T-cell purity.

3.2.1.5. Single-cell suspension from Peyer´s patches

PPs were precisely excised from the intestine using a scalpel and stored in 500 µl of RPMI 1640 on ice until further processing. PPs were generously trimmed using small scissors and digested at 37°C with horizontal rotation (200 r.p.m) in 1 ml DNase I 400 µg/ml in RPMI-1640. Digested PPs were minced through a pre-moistened 70 µm strainer. The filter was washed with 4 ml PBS and the cell suspension pelleted (330×g for 5 min at 4°C) and resuspended in PBS.

3.2.1.6. Single-cell suspension from mesenteric lymph nodes

mLNs were isolated from euthanized mice, and fat tissue and vessels were carefully removed and stored in 500 µl of RPMI 1640 on ice until further processing. mLNs were generously trimmed using small scissors and digested at 37°C with horizontal rotation (200 r.p.m) in collagenase A 1 mg/ml, collagenase D 1 mg/ml, and DNase I 400 µg/ml in RPMI-1640. Digested mLNs were minced through a pre-moistened 70 µm strainer. The filter was washed with 4 ml PBS and the cell suspension pelleted (330×g for 5 min at 4°C) and resuspended in PBS.

3.2.1.7. Single-cell suspension of the small intestine

Mice were euthanized, and small intestines from the stomach to the *caecum* were excised. Fat and mesenteric tissue was removed, and PPs were excised. Intestines were cut open longitudinally and vigorously cleared of fecal contents and mucus in ice-cold PBS. Small intestines were cut laterally into 1,5 cm pieces and transferred into a 50 ml tube containing 10 ml of ice-cold HBSS with 5% FCS until further processing.

Intestine pieces were transferred to a small plastic weighing boat and were quickly minced into 1 mm pieces using scissors. Intestine pieces were then transferred

to a 50 ml tube containing 20 ml of pre-warmed intestinal dissociation buffer and incubated for 15 min at 37°C with gentle horizontal rotation (100 r.p.m). Supernatants were filtered through a 100 µm cell strainer into a 50 ml tube and stored on ice. The remaining gut pieces were transferred back into the tube with 20 ml of fresh intestinal dissociation buffer and incubated and filtered as previously described. Flow-through of dissociation steps were united, centrifuged at 330×g for 5 min at 4°C, and resuspended in 7 ml of 44% Percoll™ in RPMI 1640 at RT lymphocyte enrichment or in ice-cold flow cytometry buffer and placed on ice.

3.2.1.8. Lymphocyte enrichment from the small intestine with Percoll™

Small intestine cell suspensions were resuspended in 7 ml of 44% Percoll™ in RPMI 1640 at 20°C as described in **3.2.1.7**. 15 ml tubes were pre-treated with FCS to prevent cells from sticking to tube walls, and 5 ml of 67% Percoll™ in RPMI 1640 at 20°C were transferred into tubes. Using a Pasteur pipette, 44% Percoll™ cell suspension was carefully overlaid on top of 67% Percoll™ in RPMI 1640 at RT. Gradient separation was performed by centrifuging at 600×g for 20 min at 20°C without acceleration or brakes. After gradient centrifugation, contaminated erythrocytes were visible in a red ring below the interphase. At the top lay a layer of epithelial cells and a pellet of debris and dead cells at the bottom. The top layer was removed, and the white ring between 44/67 Percoll™ phases was carefully isolated with a Pasteur pipette and transferred to a fresh 15 ml tube containing 3 ml of flow cytometry buffer and top it up to 5 ml. The cell suspension was centrifuged at 500×g for 10 min at 4°C and resuspended in 2 ml of flow cytometry buffer.

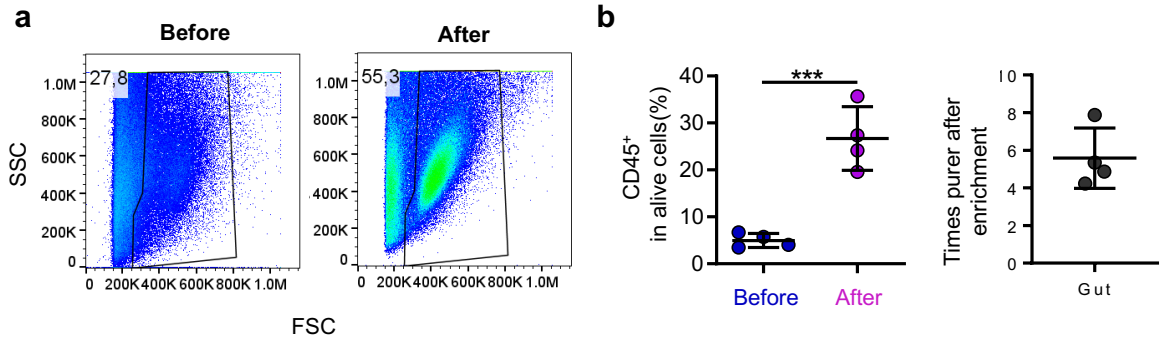

Fig. 3. 1 Percoll™ 44/67 is efficient for the density separation of small intestine lymphocytes. a. flow cytometry of small intestine of aGvHD mice on day +3 after allo-HCT, before and after Percoll™ enrichment. **b.** Percentage of $CD45^+$ single alive cells before and after enrichment.

3.2.2. Cell culture

3.2.2.1. T-cell or splenocytes culture

Enriched T-cells or splenocytes were cultured at 37°C in a humidified atmosphere containing 5% CO_2 with RPMI-1640 media supplemented with penicillin streptomycin solution 1%, L-glutamine 1%, FCS 10%.

3.2.2.2. *In-vitro* T-cell stimulation

24-well plates were coated for 2 h with CD3 (3 µg/ml) and CD28 (1 µg/ml) in a humidified cell culture incubator. Enriched T-cells from splenocytes at a 1×10^6 cell/ml in cell medium described in **3.2.2.1** supplemented with 2-mercaptoethanol 1%, 1 mM retinoic acid, and IL-2 100 U/ml were transferred to the coated wells and incubated for 2 days. On day +2, cells were pelleted and resuspended in the fresh medium described in **3.2.2.1** supplemented with 2-mercaptoethanol 1%, IL-2 100 U/ml, and IL-7 110 ng/ml and incubated for 2 additional days.

3.2.2.3. *Ex-vivo* intracellular cytokine staining

Splenocytes or enriched lymphocytes from the small intestine were *ex-vivo* restimulated with PMA (Phorbol-12-myristate-13-acetate) and ionomycin for 4 h at 37°C using a cell activation cocktail kit with Brefeldin A according to manufacturer's protocol.

3.2.3. Inhibition of Gi-coupled receptors

3.2.3.1. *In-vitro* inhibition

Cells were cultured as described in **3.2.2.1** with 200 ng/ml pertussis toxin (PTx) for 2 h. Control cells were incubated with a PTx inactive mutant in similar conditions.

3.2.3.2. *In-vivo* inhibition

To inhibit chemokine-coupled receptors, mice were i.p injected with 12,5 µg PTx. Control mice were injected with a PTx inactive mutant in similar conditions.

3.2.4. Intravascular infusion of blocking or fluorescent monoclonal antibodies

For the blocking of integrins, a mix of blocking monoclonal antibodies against lymphocyte integrin α_L, α_E, and α_4, 100 µg of each, were i.v injected into healthy or

GvHD developing mice. Monoclonal fluorescently labeled antibodies were i.v injected to allow the intravascular staining of cells of interest.

3.2.5. Chemotactic response of activated T-cells

PT_X inhibition was studied by comparing the chemotactic response of activated T-cells exposed to a CXCL11 gradient. µ-Slide Chemotaxis was used according to the manufacturer's protocol. The µ-Slide is composed of two large reservoirs connected by a small observation gap where cells are seeded. T-cells at 10×10^6 concentration were seeded into the observation gap, and loaded slides were incubated for 45 min at 37°C and 5% CO_2 for proper cell attachment to the surface of the observation gap. After attachment, one reservoir was filled with migration medium and the other with CXCL11 400 ng/ml in migration medium. In a steady state, concentration inside reservoirs is homogenous. Therefore, T-cells placed in the observation gap were exposed to a linear gradient of chemokines. Non-inhibited T-cells exposed to a chemokine gradient, or no gradient were used as a positive and negative control, respectively. Chemotaxis was examined at 5% CO_2 and 37°C in a laser scanning microscope (LSM) 780 confocal microscope equipped with a Pecon P-set 2000 incubation system. Time-lapse images of the observation gap were acquired every 60 s for 3 h. Cells were tracked with IMARIS®. MATLAB was used to evaluate migrating cells' directionality and quantify migration properties. For each condition, 90 cells were followed for at least 30 min.

3.2.6. Hematopoietic cell transplantation

To study aGvHD, inbred mouse strains with dissimilar MHC were used as donor and recipient animals. After transplantation, mice were monitored daily. Clinical evaluations for GvHD was performed according to a cumulative scoring system that considered changes in nine clinical characteristics, including weight loss, hunching posture, behavior, fur texture, skin integrity, licking/scratching of inflamed skin regions, feces, and anemia.

3.2.6.1. Total body irradiated GvHD model

Recipient mice 10-14 weeks of age were placed in a pie irradiation cage with a sterile filter and underwent single total body irradiation as conditioning for

transplantation. The irradiation dose was 8 Gray (Gy) in BALB/c mice and 9 Gy in B6 and CB6F1 mice. Allogeneic donor T-cells and 5×10^6 bone marrow cells were intravenously injected into anesthetized mice four h after irradiation in 200 µl of PBS. To prevent infections after transplantation, drinking water containing Baytril was provided for a period of 7 days. To ensure that myeloablative treatment was effective, an irradiation control group were only irradiated and anticipated to die from anemia 8 to 15 days after irradiation, demonstrating the efficacy of the myeloablative therapy. To evaluate donor bone marrow engraftment following myeloablative therapy, control bone marrow group was transplanted with 5×10^6 BM in 100 µl (without T-cells). These mice were put to a 30-day survival study, and it was anticipated that they would live without exhibiting any symptoms of illness.

3.2.6.2. Sub-lethally irradiated and unirradiated GvHD model

Recipient CB6F1 mice aged 10 to 14 weeks were either sub-lethally X-ray irradiated (2 Gy) or unirradiated. Within 4 h after irradiation, mice were anesthetized, and 3×10^7 allogeneic B6 T-cells or 8×10^7 splenocytes were intravenously injected in 200 µl PBS.

3.2.7. Flow cytometry

3.2.7.1. Surface staining

Up to 1×10^6 cells on single-cell suspensions were transferred into each well of a 96 U-bottom plate. Unspecific binding sites were blocked with 100 µl NRS 1:20 in PBS for 5 min at 4°C. Cells were stained by adding 100 µl of a mixture of fluorescently labeled antibodies for 30 min at 4°C. Cells were stained simultaneously using a fixable viability kit to screen out dead cells from the analysis (LIVE/DEAD™ or Zombie Aqua). Cells were pelleted (330 g for 5 min at 4°C) and resuspended in 200 µl of PBS. When maintained at 4°C in a dark, protected environment, stained cells could be measured up to 6 h after staining.

3.2.7.2. Intracellular staining

For staining intracellular antigens, cells were fixed 30 min at 4°C with a transcription factor staining kit and stained overnight (ON) at 4°C in permeabilizing buffer according to the manufacturer's protocol.

3.2.7.3. Measurement

The cells were centrifuged at 330×g for 5 min at 4°C, and then resuspended in 200 µl of PBS. Measurements were acquired using an Attune™ NxT flow cytometer at a rate of 1000 to 3000 events/s. Single-stained oneComp eBeads™ compensation beads were used as compensation controls, and fluorescence minus one method was used for gating controls. Acquired cytometry data were analyzed with FlowJo.

3.2.8. Cytokine bead array

Segments of 10 cm from small intestine at different distances to PPs were homogenized (2x 20 s each) at 55000 r.p.m in 500 µl of PBS in Precellys 24 tissue homogenizer. The supernatant was then stored at -80°C until further processing. According to the manufacturer's protocol, cytokine concentrations were determined using the LEGENDplex™ mouse inflammation panel kit. Data were analyzed with LEGENDplex™ online software.

3.2.9. Multicolor light sheet microscopy

Mice were anesthetized and perfused though the heart with 40 ml of PBS to eliminate blood from tissues, followed by 40 ml 4% PFA in PBS (pH 7,2) to fix tissues. Following perfusion, segments of the small intestine of 1,5 to 2 cm containing selected PPs were harvested and stored in PFA 4% in PBS (pH 7,2) for 2 h at 4°C. Intestinal segments were washed 3 times with PBS at 4°C. Segments were blocked and permeabilized in PBS containing 2% FCS and 0,01% Triton X-100 at 4°C ON, and then stained in 800 µl of PBS at a 1:100 dilution with primary antibodies for 24 h at 4°C on an orbital shaker. After a second wash in PBS for 30 min at 4°C (3 times), samples were stained with secondary antibodies in 800 µl of PBS at a 1:400 dilution for 24 h at 4°C on an orbital shaker. A series of ethanol-water solutions with increasing ethanol concentrations (30%, 50%, 70%, 80%, and 90%) were used to dehydrate samples for 90 min each at RT. The samples were then kept at 4°C ON in 100% ethanol. A final dehydration step with n-hexane for 2 h at RT, was followed by gradual replacement with clearing solution, ensuring that the samples were not exposed to air. The tissue specimens became optically transparent after a 2-hour incubation at RT, enabling them to be used for subsequent LSFM imaging. The cleared tissue samples were stored and imaged in the clearing solution.

Image acquisition was performed in a home-built LSFM equipped with 20× or 5× lenses (Stegner et al., 2017). The samples were positioned within a custom-made cover glass chamber, which enabled imaging of the cleared samples while immersed in the clearing solution. Laser light sheets of varying wavelengths were then used to illuminate the samples and, optical z-stacks were generated by moving the samples incrementally through the light sheet in 1 to 5 µm steps. LSFM optical z stacks were assembled, allowing a computational 3D reconstruction with IMARIS®.

3.2.10. Immunofluorescence microscopy of histological sections

3.2.10.1. Sample preparation of non-fluorescent tissues

Organs of interest were isolated and embedded in O.C.T™ using plastic cryomolds within 10 min of mice euthanasia. Embedded cryomolds were frozen on dry ice and stored at -20°C.

3.2.10.2. Sample preparation of fluorescent tissues

Anesthetized mice were perfused through the heart with 40 ml of PBS to wash out blood, followed by 40 ml of PLP buffer. Following perfusion, organs of interest were harvested and fixed in PLP buffer for 3 h at RT. Tissues were washed in PBS at 4°C and cryopreserved in ascending concentrations of sucrose in PBS (10% ON followed by 20% 4 h and 30% 2 h). Organs of interest were subsequently embedded in O.C.T™ using plastic cryomolds and were directly frozen on dry ice and stored at -20°C.

3.2.10.3. Cryosectioning

Cryosections of the small intestine of 5 to 15 µm thickness were obtained using Leica CM1950 cryomicrotome. The chamber temperature on the cryostat was set between -20°C and -25°C. Sections were collected onto SuperFrost® Plus glass microscope slides and inspected visually that at least two or three PPs were cut using a standard low-power light microscope. Cryosections were stored at -20°C until they were used.

3.2.10.4. Immunostaining for confocal microscopy

Immunostaining steps were done using the Thermo Scientific Shandon system at RT. Sections were thawed (5 min), fixed with acetone (7 min), air-dried (5 min), re-hydrated, and washed in PBS (3× 5 min). Then, each section was placed in a Shandon cuvette slide rack with a Shandon coverplate™ assembly. Nonspecific binding sites were blocked with FCS (fetal calf serum) 2% in PBS for 15 min, and when required, with an avidin-biotin blocking kit. Samples were stained with primary antibodies for 1 h and washed in PBS (3× 5 min). Staining with streptavidin and/or secondary antibodies for 30 min and washing in PBS (3× 5 min). Samples were coated with VECTASHIELD® mounting medium with 4′,6 Diamidin 2 phenyl indol (DAPI), covered with coverslips, sealed with Entellan®, allowed to air dry for 1 h, and kept at -20°C until imaging.

3.2.10.5. Imaging

Confocal images were acquired using the 10× and 20× objectives, which have numerical apertures of 0,25 and 0,8, respectively. To capture large areas with high resolution, a tiling function, and a zoom of 0,6 were frequently employed. Images were processed using AxioVision or IMARIS®.

3.2.11. Photoconversion

Donor Dendra2 T-cells located in PPs were photoconverted, as previously described (Jarick et al., 2018). Mice were anesthetized and placed on a heating mat with a sterile OP towel. Animal eyes were treated with eye ointment to avoid ocular dehydration. Using a dissecting swab and 70% EtOH, the fur in the abdominopelvic region was moistened and then shaved. The skin was then povidone-iodine disinfected in a circular motion outward. A 1,5 cm median incision through the *linea alba* was used to access the abdomen. *Cecum* was exteriorized, and the small intestine was gently pulled out using cotton swabs dipped in PBS. PPs were placed upwards, and distances to the cecum were registered. Sterile aluminum foils with a small hole with a 2 mm diameter exposing PPs and protecting surrounding *LP* from UV light were used. On a lab stand, a collimator was mounted, with a glass fiber connecting it to the UV lamp. Desired PPs were illuminated for 2 min at maximum power at 3 to 5 mm over PPs, irreversibly switching Dendra2 fluorescence from green to red. We were protected from scattered UV rays using protection glasses whenever the lamp was on. Organs were then carefully reinserted into the peritoneum, and the peritoneum and skin were closed

using non-consecutive stitches. Finally, analgesics were provided subcutaneously and in drinking water.

3.2.12. *Ex-vivo* two-photon microscopy

Mice were euthanized 12 to 24 h after photoconversion, and segments of the small intestine of 1,5 to 2 cm containing converted and unconverted PPs were taken. Intestinal content was removed at the edges, and intestinal tissue was glued with tissue adhesive, with PPs facing diagonally upwards, into a 5 cm diameter petri dish. The petri dish was filled with PBS and placed into the two-photon laser scanning microscope stage.

Ex-vivo two-photon microscopy of converted and unconverted PP and surrounding *LP* was performed using a Leica SP8 with a water dipping objective. Fluorophores were excited with a pulsed Ti-Sapphire laser at 840 nm. The intensity of the excitation light was adjusted proportionally to the square of the penetration depth, ranging from 5 to 30% of the maximum laser power. Three reflected light detectors detected emitted fluorescent signals of Dendra2 green, Dendra2 red, and collagen's second harmonic generation signal. All image processing was performed using IMARIS®, and noise-induced outliers were removed with an Image J plugin.

3.2.13. Image analysis

3.2.13.1. Cell concentrations at defined distances from Peyer´s patches

Light sheet fluorescence 3D reconstruction of PPs and surrounding *LP* of the small intestine were obtained in a LSFM microscope with a 20x objective lens immunostained for donor T-cells (CD45.1) in red and MAdCAM-1 in green. First, the background was subtracted from CD45.1 and MAdCAM-1 to obtain specific staining. PPs were defined using intensity values of CD45.1. The surface of PPs was masked on the CD45.1 channel to only get donor T-cells located in *LP.* A distance transformation map was generated from the PP surface. Donor T-cells in *LP* were classified according to their distance to the PP surface and quantified. Surfaces produced by the autofluorescence channel were used to calculate the volume of the tissue that contained donor T-cells at defined intervals, then cell concentrations at defined distances were calculated (**Fig. 3.2**).

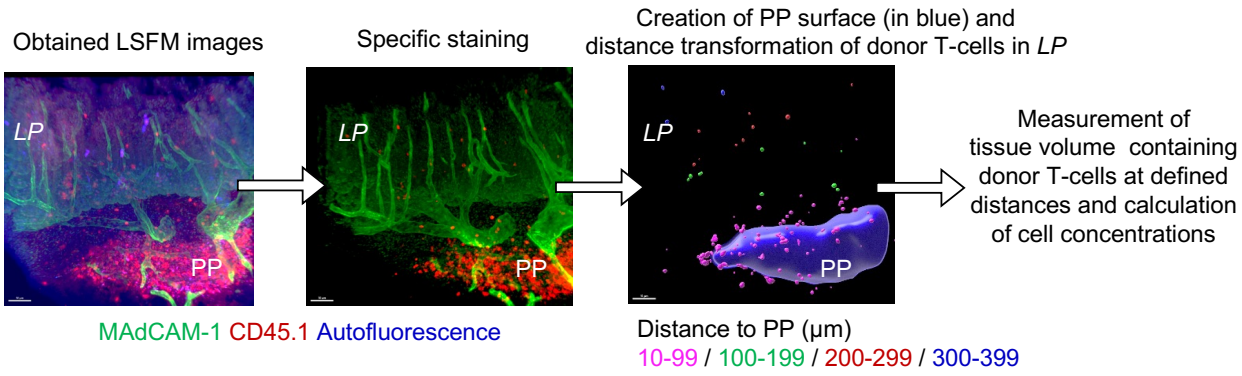

Fig. 3.2 Calculation of cell concentrations at defined distances from Peyer´s patches. Scale bar 50 µm.

3.2.14. Statistical analyses

GraphPad Prism 7 was used to analyze experimental data using unpaired, two-sided Student's t-tests. *P*-values under 0,05 were thought to represent a significant difference.

4. Results

4.1. Direct alloreactive T-cells migration from Peyer´s patches to *lamina propria* regardless of pre-transplantation conditioning

Classical inductive sites of an intestinal immune response are PPs and gut-draining mLNs. Conventionally, effector T-cells exit lymphoid tissue via efferent nodal lymphatics, return to the systemic circulation, and home to the gut. However, previously we demonstrated that a subset of T-cells can directly migrate from PPs to adjacent *LP* of the small intestine in early GvHD, as described in **1.4.2**.

To determine the contribution of irradiation to the observed direct T-cell migration, we compared irradiated and unirradiated allo-HCT recipients. We harvested small intestine sections from sub-lethally irradiated or unirradiated mice on day +3,5 after allo-HCT. In both cases, we observed donor T-cells in the intestinal *LP* adjacent to PPs (**Fig. 4.1 a**). Eliminating the pre-transplantation irradiation reduced the magnitude of T-cell infiltration but did not prevent direct T-cell migration from PP to *LP*.

We used LSFM to investigate the distribution of T-cells around PPs in more detail, confirming that irradiation was not necessary for direct PP-to-*LP* T-cell migration (**Fig. 4.1 b**). We quantified T-cell densities around PP on day +3,5 after allo-HCT in irradiated and unirradiated allo-HCT recipients (**Fig. 4.1 c**). In both irradiated and unirradiated GvHD models, donor T-cells infiltrating *LP* were predominantly located within 100 µm from PPs. Beyond 100 µm PPs, the number of infiltrating donor T-cells into *LP* showed a significant decrease (from 0-100 to 100-200 µm). However, there was no significant difference in the frequency of donor T-cells at greater distances from PPs, and the distribution patterns remained comparable between irradiated and unirradiated GvHD models across all distances analyzed. Donor T-cells formed a cell gradient from PPs to *LP* in irradiated and unirradiated allo-HCT recipients, providing evidence that activated T-cells moved directly from PPs to adjacent *LP* independently of host conditioning. By day +6 after allo-HCT, there was a huge infiltration of alloreactive T-cells throughout the bowel and the gradient disappeared.

To further demonstrate that irradiation is unnecessary to trigger direct PP-to-*LP* T-cell migration, we assessed the presence of PPs-derived T-cells in *LP* half a day

later. We transferred donor T-cells expressing Dendra2 to unirradiated F1 recipients. On day +3 after allo-HCT, we photoconverted donor T-cells in selected PPs. We acquired images on day +3,5 using *ex-vivo* two-photon microscopy. We found photoconverted T-cells in the intestinal *LP* of unirradiated recipients implying that irradiation was not necessary for the direct migration of T-cells from PPs to intestinal *LP* (**Fig. 4.1 d**).

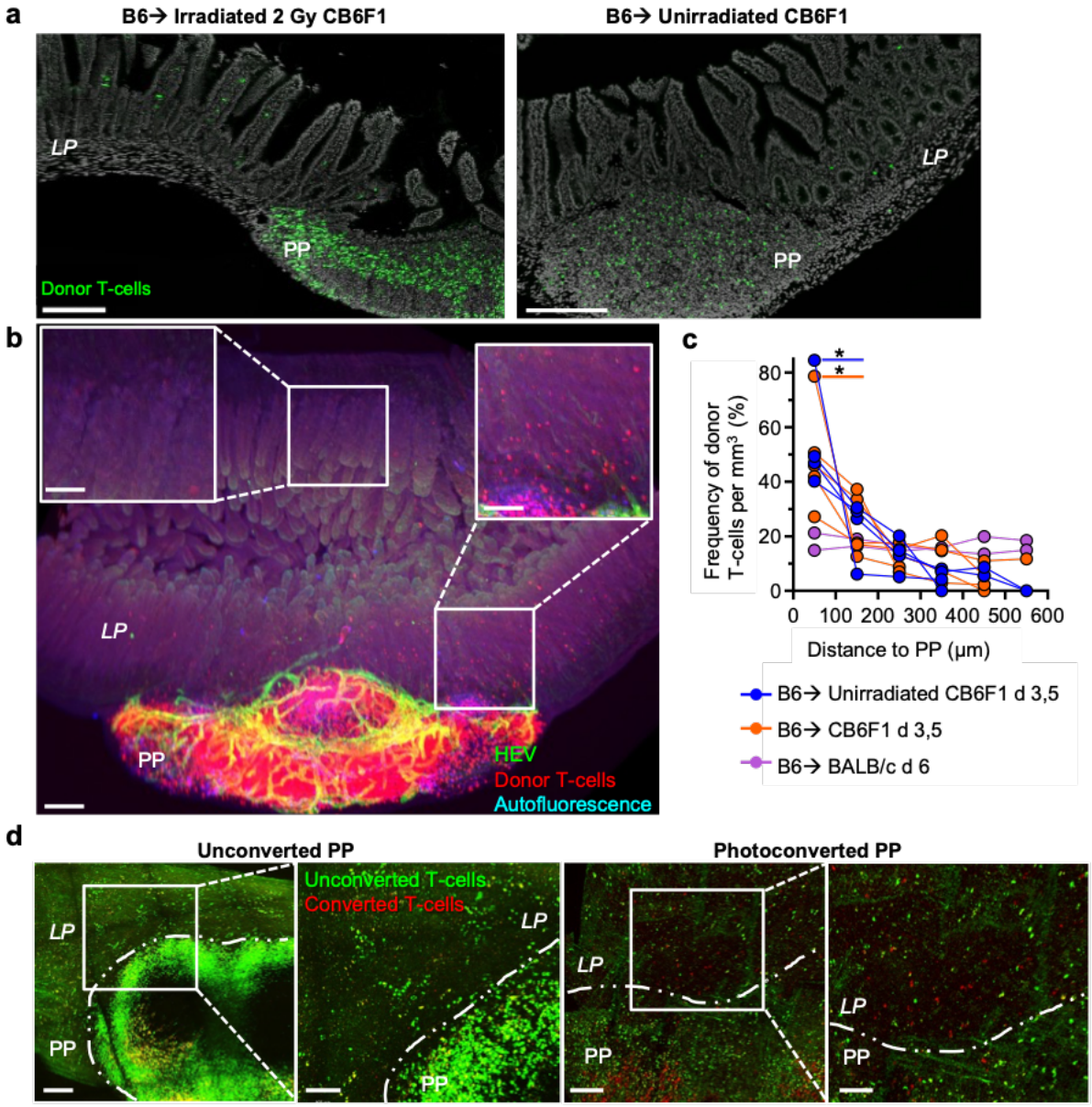

Fig. 4.1 Whole body irradiation did not trigger direct T-cell migration from Peyer's patch to adjacent *lamina propria*. We transferred parental strain T-cells into haploidentical irradiated, sub-lethally irradiated, or unirradiated F1 recipients. **a.** We harvested sections of the small intestine from sub-lethally irradiated or unirradiated mice on day +3,5 after allo-HCT. Representative Immunofluorescence microscopy co-staining shows donor T-cells (Dendra2) in green and cell nuclei stained by DAPI in grey. The scale bar is 200 µm and 100 µm for inserts. **b.** We performed LSFM 3D reconstruction of PPs and the surrounding *LP* of the small intestine from unirradiated mice on day +3,5

after allo-HCT, showing donor T-cells (CD45.1) in red and MAdCAM-1 in green. The scale bar is 200 µm. **c.** We calculated donor T-cell concentrations at defined distances from PP, obtained from irradiated or unirradiated mice on day +3,5 after allo-HCT. We quantified donor T-cell concentrations from LSFM data, as described in Fig. 3.2. Katja Jarick kindly provided the data from B6→BALB/c on day +6 after allo-HCT. Each data point corresponds to a PP of an independent mouse. We conducted statistical analyses for the different distances to PP within the same transplant group using paired t-tests and between groups at the same distances using unpaired t-tests. Asterisks indicate statistical significance (* $p \leq 0{,}05$, ** $p \leq 0{,}01$, *** $p \leq 0{,}001$, and **** for $p \leq 0{,}0001$). **d.** We transferred Dendra2 T-cells to unirradiated F1 recipients. On day +3 after allo-HCT, we photoconverted T-cells in selected PPs. Stitched two-photon images of explanted PP on day +3,5 after allo-HCT show regions adjacent to converted and unconverted PP, with unconverted donor T-cells in green and converted donor T-cells in red. Scale bar is 200 µm and 100 µm for inserts.

4.2. Direct Peyer´s patches-to- *lamina propria*- T-cell migration precedes infiltration of bloodborne donor T-cells

4.2.1. Leukocyte trafficking kinetics in mice tracked through serial intravascular staining

An anti-CD45 antibody infused intravenously selectively labeled circulating blood cells while leaving cells residing in tissue unmarked (Anderson et al., 2014). Therefore, infusion of an anti-CD45 labeled antibody allowed discrimination between vascular and tissue-localized cells at the time of antibody infusion. Thus, by sequentially infusing anti-CD45 antibodies labeled with distinct fluorophores for each time point allowed us to obtain positional histories of T-cells to infer trafficking dynamics (Potter et al., 2021; Tkachev et al., 2021). To enable staining by repeated infusions, serial intravascular staining (SIVS) required sub-saturating concentrations of monoclonal CD45 antibodies.

Consequently, we carried out trial experiments to determine the optimal concentration using a limited number of mice. We titrated each antibody to find a bright but sub-saturating dosage of CD45 antibodies appropriate for SIVS (**Fig. 4.2**). We infused different dosages of CD45-AF647 (0,1 to 8 g/ 20 g mouse), CD45-AF488 (0,05 to 4 g/ 20 g mouse), and CD45-PB (0,2 to 6,4 g/ 20 g mouse) into healthy BALB/c mice. We sampled peripheral blood, spleen, and mLN 5 min later. We measured saturation counterstaining with an anti-CD45-APC-Cy7 antibody (**Fig. 4.2 a**). However, because the number of healthy mice in the concentrations analyzed was less than three, we refrained from conducting statistical tests.

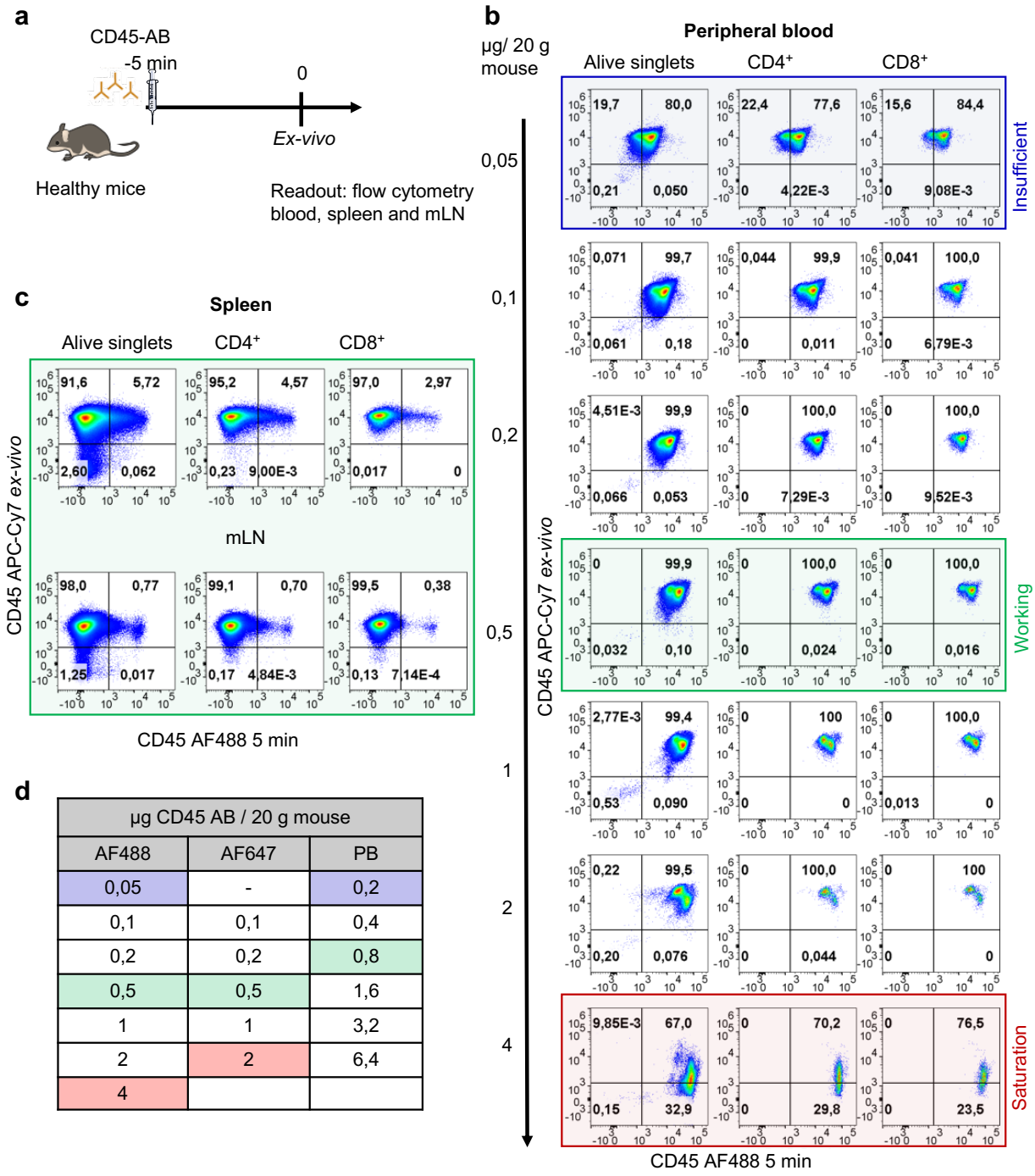

µg CD45 AB / 20 g mouse		
AF488	AF647	PB
0,05	-	0,2
0,1	0,1	0,4
0,2	0,2	0,8
0,5	0,5	1,6
1	1	3,2
2	2	6,4
4		

Fig. 4.2 Serial intravascular staining to track leukocyte trafficking kinetics using timed infusions of fluorescently labeled antibodies to stain circulating leukocytes. a. We infused different dosages of three different CD45 antibodies into healthy BALB/c mice and measured saturation in peripheral blood, spleen, and mLN after 5 min after infusion. **b.** Representative flow cytometry plots pre-gated on live cells, displaying anti-CD45-APC-Cy7 antibody counterstaining in peripheral blood after infusion of different dosages of a CD45-AF488 antibody (0,05 to 4 g/ 20 g mice). **c.** Representative flow cytometry plots pre-gated on live cells, displaying anti-CD45-APC-Cy7 antibody counterstaining in spleen and mLN after infusion of 0,5 µg/20 g, working SIVS dosage, of CD45-AF488 antibody ($n < 3$; no statistical tests conducted). **d.** The table summarizes titration results to determine the ideal concentration of a CD45 antibody for SIVS using different fluorescent dyes. Each column represents different fluorophores, while rows correspond to different concentrations of CD45 antibody (measured in µg per 20 g mice). Red color within a cell indicates saturation, blue indicates insufficient staining, and green represents the optimal working concentration of CD45 antibody, yielding optimal staining outcomes.

For example, in the case of the CD45-AF488 antibody, we found that a dose of 0,2 g/20 g mouse sufficed for bright vascular staining. We achieved staining of all vascular cells with a dose of 0,1 µg/20 g mouse, although we observed fewer differences between stained and unstained cells compared to higher doses. A 2 g/20 g mouse dose led to saturation (**Fig. 4.2 b**). We selected a working dose of 0,08 g/20 g mouse for SIVS with the CD45-PB antibody and 0,5 µg/20 g mouse for CD45-AF488 and CD45-AF647 antibodies (**Fig. 4.2 d**).

As SIVS, with multiparameter flow cytometry, provides a method to quantify and time cell trafficking, we collected blood samples before and after injections and stained them *ex-vivo* with CD45-APC-Cy7. As proof of principle, we demonstrated that we could stain peripheral blood lymphocytes intravascularly within 5 min. We also confirmed that two sequential infusions over 90 min could label intravascular cells, offering us a potential method to study the spatiotemporal distribution of lymphocytes in healthy mice.

Using this technique, we classified lymphocytes into four different compartments based on their spatiotemporal location in various tissues: continuous circulation, current circulation, recent infiltration, and tissue-localized (**Fig. 4.3 a**). Cells that were truly localized within the tissue as well as cells that migrated through tissue with a transit time longer than the experimental time frame were both incorporated into the tissue-localized compartment.

All $CD4^+$ and $CD8^+$ T-cells in peripheral blood were stained with the 5-minute CD45 PB or CD45 488 antibody, rendering the percentage of T-cells classified as recently migrated and tissue-localized negligible. Notably, $CD8^+$ T-cells (25%) exhibited a significant increase in continuous circulation over 90 minutes compared to $CD4^+$ T-cells (15%), which was associated with a decrease in currently circulating cells (**Fig. 4.3 b**).

For spleen, we observed no significant difference in the spatiotemporal compartmentation between $CD4^+$ and $CD8^+$ T-cells. Despite the spleen being a highly vascularized organ, 90% of T-cells were found to be tissue-localized, a percentage significantly higher compared to the recently migrated, currently circulating, and

continuously circulating counterparts. This suggests that, although spleen is highly vascularized, most cells reside in the white pulp. In the red pulp of the spleen, 7% of lymphocytes were continuously circulating, and 3% of cells extravasated from the blood within 90 minutes.

In mLN, nearly 99% of CD4⁺ and CD8⁺ T-cells localized in the tissue within 90 minutes of analysis. The remaining percentage included recently migrated, currently circulating, and continuously circulating cells. We found no significant difference in the spatiotemporal compartmentation between CD4⁺ and CD8⁺ T-cells on healthy mice (**Fig. 4.3 c**).

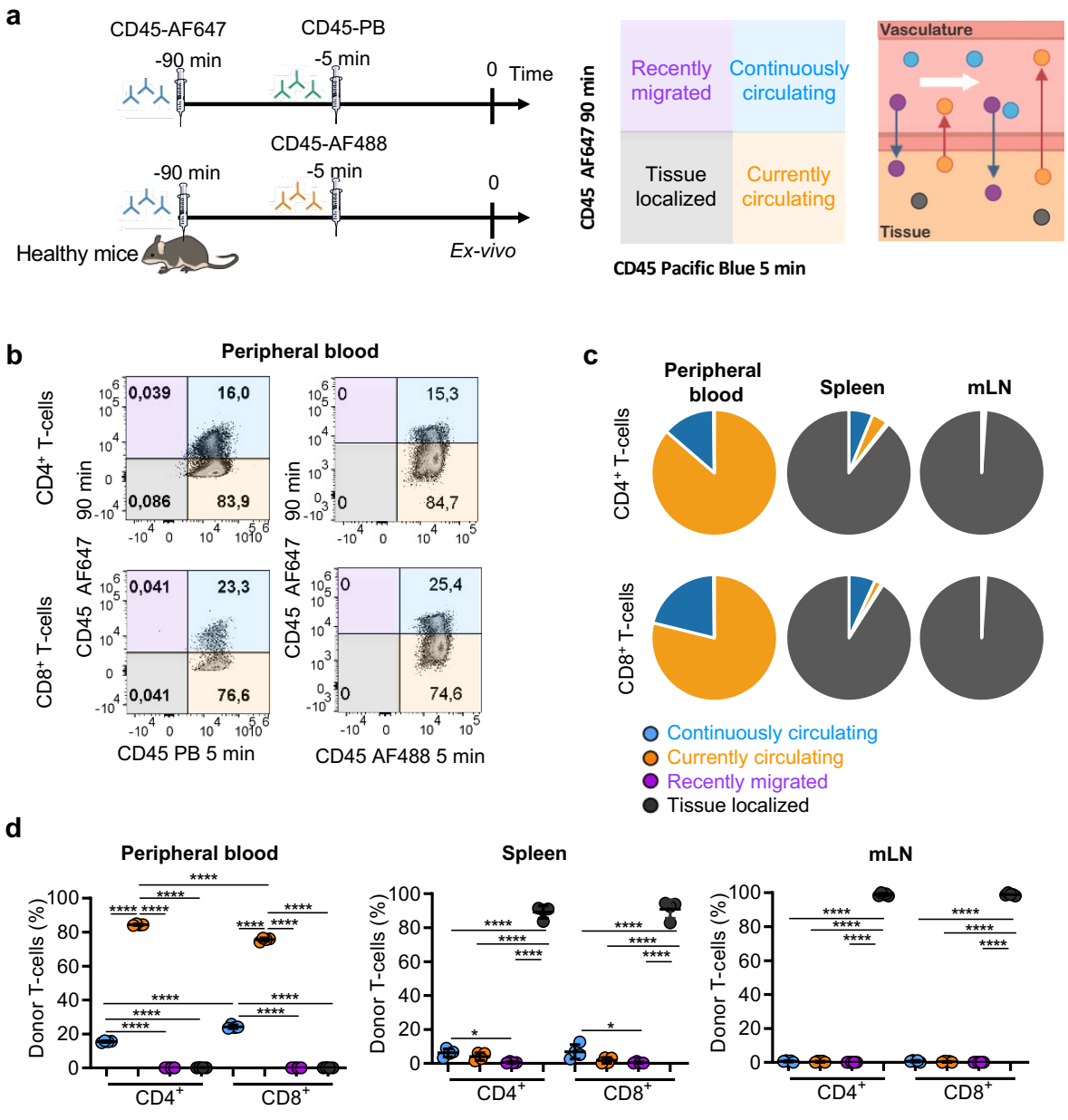

Fig. 4.3 Timed serial intravascular staining allowed us to differentiate cells that extravasated from the blood within a specific time window. We differentiated bloodborne cells that were extravasated from blood to different organs within a particular time window from tissue-localized lymphocytes using CD45 serial intravascular staining. **a.** Mice were intravenously injected with CD45 coupled to different fluorophores at defined time points before sacrificing the mice (90 min with CD45-AF647 and 5 min before necropsy with CD45-AF488 or CD45-PB). Lymphocytes were classified into four different compartments based on their spatiotemporal localization: continuously circulating (blue), currently circulating (orange), recently infiltrating (violet), and tissue localized (black). **b.** Flow cytometry dot plots of peripheral blood, pre-gated on live $CD45^+$ cells, show representative $CD4^+$ and $CD8^+$ T-cells. We used different antibody combinations as described in point a. **c.** The pie chart illustrates the spatiotemporal compartments of healthy mice in peripheral blood, spleen, and mLN (n = 4)**. d.** Graphs depicting the percentage of $CD4^+$ and $CD8^+$ T-cells in the different spatiotemporal compartments of healthy mice in peripheral blood, spleen, and mLN (n = 4). Statistical significance was determined with two-tailed unpaired Student t tests. Asterisks indicate statistical significance (* $p \leq 0{,}05$, ** $p \leq 0{,}01$, *** $p \leq 0{,}001$, and **** for $p \leq 0{,}0001$).

4.2.2. Photoconversion can be combined with serial intravascular staining to study the spatiotemporal localization of Peyer´s patches-derived T-cells

Next, we wanted to assess the spatiotemporal distribution of donor T-cells in mice developing aGvHD. Following allo-HCT, we used SIVS to examine the temporal compartmentalization of donor T-cells in specific organs. We divided lymphocytes into four different compartments based on their spatiotemporal localization: continuously circulating, currently circulating, recently infiltrating, and tissue localized.

To investigate the direct migration of PP-derived T-cells and their potential impact on the recruitment of specific T-cell populations and additional bloodborne lymphocytes, we employed photoconversion in conjunction with SIVS. By performing PP photoconversion, we could distinguish PP-derived T-cells from donor T-cells originating from other areas (**Fig. 4.4 a**). Initially, we confirmed the successful photoconversion of splenocytes and the detection of both unconverted and photoconverted T-cells through flow cytometry (**Fig. 4.4 b**). We transferred Dendra2 T-cells into haploidentical and unirradiated CB6F1 recipients. On day +3,5 after allo-HCT, we sacrificed a mouse immediately following photoconversion to verify the effective photoconversion of donor T-cells in PP after UV light exposure. At this time, unconverted T-cells were minimally detectable, ensuring the efficiency of photoconversion (**Fig. 4.4 c**).

We photoconverted Dendra2 T-cells in PPs on days +1,5; +3; and +3,5 after allo-HCT, irreversibly switching the Dendra2 fluorescence from green to red. To track

T-cells in the bloodstream and those migrating to GvHD target tissues, half a day later, we administered CD45 fluorescent labels 90 min (anti-CD45-AF647) and 5 min (anti-CD45-PB) before necropsy. According to their different spatiotemporal localization, lymphocytes were divided into four compartments, as shown in **Fig. 4.3**: continuously circulating, currently circulating, recently infiltrating, and tissue localized.

Most donor T-cells who localized to PP on day +4 after allo-HCT were photoconverted (81%), and tissue localized within the 90 min of intravascular staining (97% of $CD4^+$ and 78% of $CD8^+$) (**Fig. 4.4 d**). We also detected newly arrived (unconverted) donor T-cells in PP, most of these cells were tissue localized (89% of $CD4^+$ and 74% of $CD8^+$) within the 90 min of analysis. A higher proportion of $CD8^+$ donor T-cells were found to be continuously circulating compared to $CD4^+$ donor T-cells, regardless of whether the donor T-cells were converted or unconverted. This difference correlated with fewer tissue-localized $CD8^+$ T-cells compared to $CD4^+$ cells in converted and unconverted donor T-cells (**Fig. 4.4 f**). Furthermore, a greater proportion of converted donor $CD4^+$ T-cells were tissue-localized compared to their unconverted counterparts. This difference was associated with a reduction in the percentage of recently migrated and currently circulating cells. Nonetheless, the spatiotemporal compartmentalization between converted and unconverted $CD8^+$ T-cells did not differ.

On the other hand, we found that most peripheral blood donor T-cells on day +4 after allo-HCT (96%) were not PP-derived (unconverted) (**Fig. 4.4 e**). As anticipated, in peripheral blood, all donor T-cells in peripheral blood were stained with a 5-minute antibody infusion, resulting in a negligible percentage of donor T-cells classified as tissue-localized and recently migrated for both unconverted and converted donor T-cells (**Fig. 4.4 e**). The percentage of $CD8^+$ donor T-cells in continuous circulation exceeded that of $CD4^+$ for both converted and unconverted donor T cells, which is associated with a lower frequency of cells currently in circulation. These results align with findings from PPs (**Fig. 4.4 f**) and healthy mice under steady-state conditions, where there were more $CD8^+$ T-cells in continuous circulation compared to $CD4^+$ T-cells (**Fig. 4.3 d**). Moreover, the percentage of donor T-cells in continuous circulation was higher in converted than in unconverted T-cells, both for $CD4^+$ as for $CD8^+$ T-cells.

All in all, we concluded that combining photoconversion with SIVS can be a valuable technique to study the spatiotemporal localization of PP-derived donor T-cells.

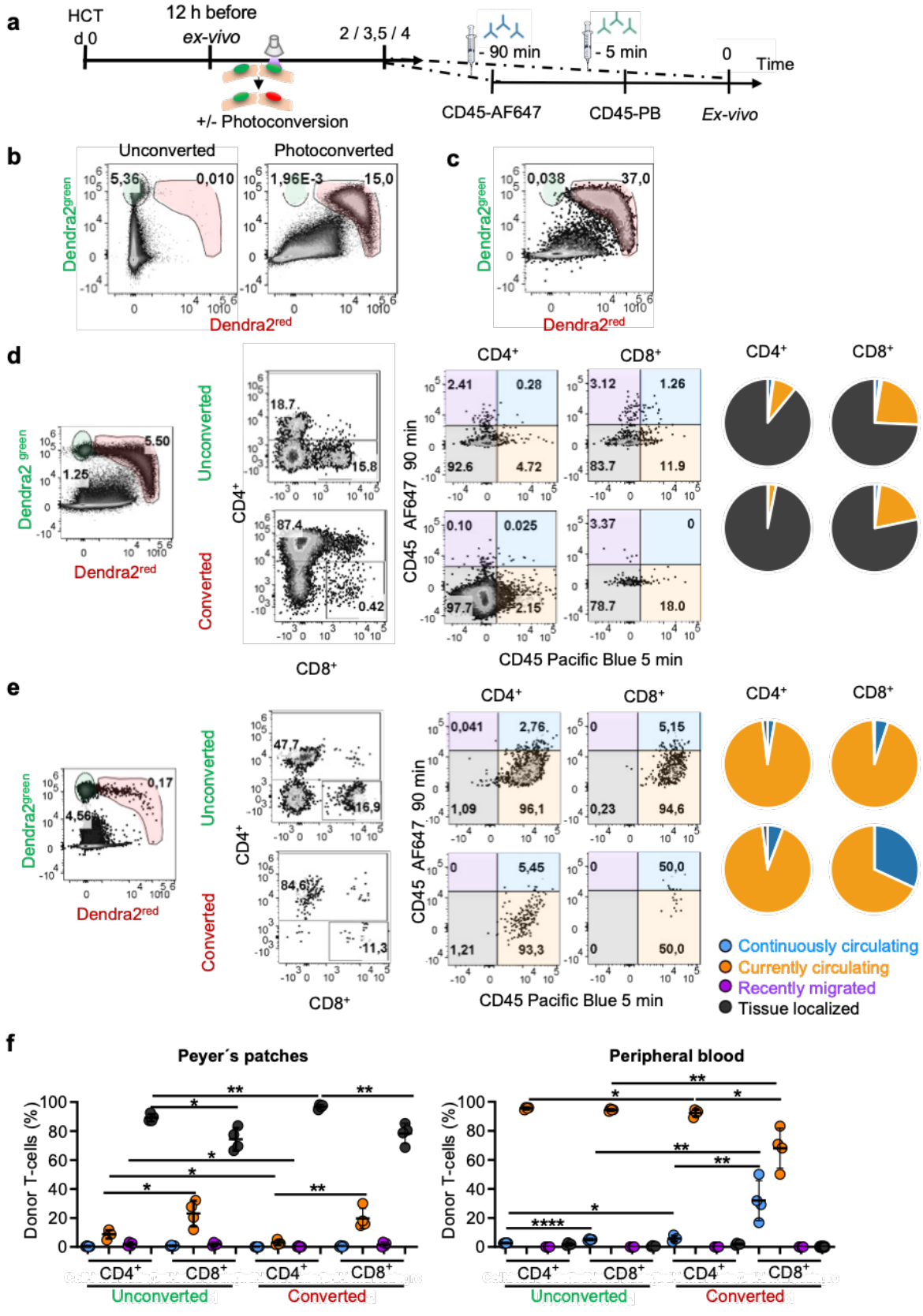

Fig. 4.4 Combining photoconversion with SIVS allowed us to study the spatiotemporal localization of Peyer's patches-derived T-cells. a. We transferred parental strain Dendra2 T-cells into haploidentical and unirradiated CB6F1 recipients. T-cells in PPs were photoconverted on days +1,5, +3, and +3,5 after allo-HCT, resulting in irreversible switches from green to red fluorescence. To track T-cells in the bloodstream and those migrating to GvHD target tissues, we administered CD45 fluorescent labels 90 min (anti-CD45-AF647) and 5 min (anti-CD45-PB) before necropsy. Lymphocytes were divided into four compartments based on their different spatiotemporal localization, as shown in Fig. 4.3: continuously circulating (blue), currently circulating (orange), recently infiltrating (violet), and tissue localized (black). **b.** Representative flow cytometry plots of unconverted and *in-vitro* converted Dendra2 splenocytes, gated in alive lymphocytes. **c.** Representative flow cytometry plot of PPs from a mouse euthanized directly after photoconversion on day +3,5 after allo-HCT, gated in alive lymphocytes. **d.** Representative flow cytometry plots and pie charts represent the spatiotemporal compartments of SIVS of PPs on day +4 after allo-HCT (n = 4). **e.** Representative flow cytometry plots and pie charts represent the spatiotemporal compartments of SIVS of peripheral blood on day +4 after allo-HCT (n = 4). **f.** Graphs depicting the percentage of $CD4^+$ and $CD8^+$ unconverted and converted donor T-cells in the different spatiotemporal compartments on day +3,5 after allo-HCT in PPs and peripheral blood (n = 4) Statistical significance was determined with two-tailed unpaired Student t tests. Asterisks indicate statistical significance (* $p \leq 0,05$, ** $p \leq 0,01$, *** $p \leq 0,001$, and **** for $p \leq 0,0001$).

4.2.3. Peyer´s patches-derived T-cells directly infiltrated the *lamina propria* before bloodborne T-cells

After concluding that photoconversion can be combined with SIVS to study the spatiotemporal localization of PP-derived donor T-cells, we wanted to assess the spatiotemporal distribution of donor T-cells that infiltrated intestinal *LP* in mice that developed aGvHD in different days after allo-HCT. In this experiment, we performed photoconversion of T-cells in PPs on different days following allo-HCT. To track the converted cells, we administered anti-CD45 fluorescent antibodies (anti-CD45-AF647 and anti-CD45-pacific blue) 90 and 5 min before the necropsy, respectively. Experimental details as described in **4.2.2**. Using SIVS, we classified directly migrating from PP and bloodborne donor-T-cells that infiltrated intestinal *LP* into four compartments based on their spatiotemporal localization: continuously circulating, currently circulating, recently infiltrating, and tissue localized (**Fig. 4.3**).

Donor T-cells infiltrating *LP* after allo-HCT are composed of directly migrating from PP (converted) and bloodborne-derived emigrants (unconverted). We found that the percentage of directly migrated T-cells infiltrating *LP* significantly dropped from 57% to 19% from day +2 to +4 after allo-HCT. Concomitantly, the percentage of bloodborne-derived donor T-cells infiltrating *LP* significantly increased (**Fig. 4.5 b-c**). In conclusion, the dominant presence of directly migrated T-cells in the early stages

following allo-HCT demonstrated that direct PP-to-*LP* T-cell migration led to faster recruitment of cells compared to the vasculature route (**Fig. 4.5 a**).

Additionally, we analyzed the percentage of $CD4^+$ and $CD8^+$ donor T-cells directly migrating from PP and bloodborne emigrants that infiltrated intestinal *LP*. We observed that most donor T-cells that migrated directly from *LP* were $CD4^+$ T-cells at the analyzed time points. Specifically, 90% on day +2, 85% on day +3,5, and 94% on day +4 after allo-HCT. On day +2 after allo-HCT, we observed a dominant proportion of $CD4^+$ T-cells extravasating from the blood, accounting for 80% of the total. However, $CD8^+$ donor T-cells infiltrated *LP* later, representing 37% on day +3,5 and 40% on day +4 after allo-HCT (**Fig. 4.5 d**).

The spatiotemporal compartmentalization of *LP*-infiltrated donor $CD4^+$ T-cells did not differ significantly between days +2 to +4 after allo-HCT for donor T-cells directly migrating from PPs and bloodborne-derived emigrants. At all analyzed time points, a higher percentage (97%) of converted $CD4^+$ T-cells in *LP* were categorized as tissue-localized, as opposed to those infiltrating from the bloodstream, which ranged from 89% to 92% (**Fig. 4.5 f**). Concomitantly, there was a reduction in the currently circulating donor T-cells in the $CD4^+$ T-cells in *LP* that originated directly from PPs. The tissue-localized T-cells in the *LP* that remained unconverted were likely derived from either unconverted PPs, partially converted PPs, or had infiltrated the *LP* before the 90-minute analysis with SIVS.

The spatiotemporal distribution of directly migrating from PPs $CD8^+$ T-cells that infiltrated the *LP* remained relatively stable between days +2, +3,5 and +4 after allo-HCT. Similarly to converted $CD4^+$ T-cells, the majority of converted $CD8^+$ T-cells were classified as tissue-localized (97, 96, and 93%, respectively). However, on day +4, a small drop in the percentage of tissue-localized $CD8^+$ T-cells (93%) was observed, accompanied by a corresponding increase in circulating $CD8^+$ T-cells (**Fig. 4.5 f**). This shift in distribution suggests a more advanced stage of the immune response.

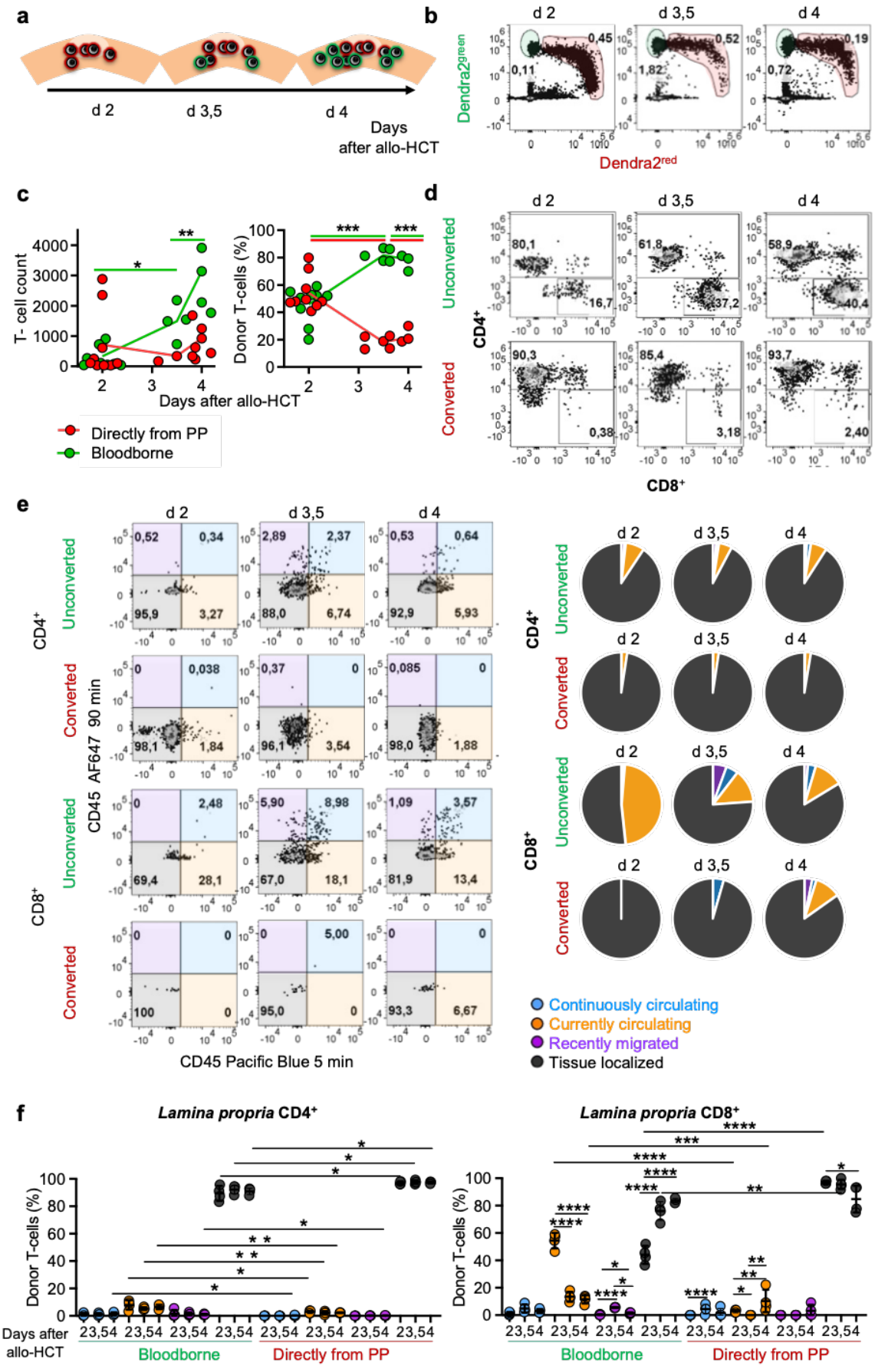

Fig. 4.5 PP-derived tissue-localized CD4⁺ T-cells actively migrated to the *lamina propria* earlier than the vascular route. The experimental scheme is described in Fig. 4.4. **a.** The illustration depicts

the localization in intestinal *LP* of PP-derived T-cells (converted) that directly migrate from PP and donor T-cells that come from the vasculature (unconverted) on different days after allo-HCT. **b.** Representative flow cytometry dot plots of unconverted and converted donor T-cells infiltrating intestinal *LP* on days +2 to 4 after allo-HCT, gated in alive lymphocytes ($CD45^+$). **c.** T-cell count of directly migrated and bloodborne T-cells into intestinal *LP* calculated from flow cytometry plots of unconverted and converted donor T-cells that infiltrated intestinal *LP* on days +2 to +4 after allo-HCT. We calculated the percentage of directly migrated and bloodborne T-cells in the intestinal *LP* by determining the proportion of converted and unconverted donor T-cells out of the total donor T-cell population. **d.** Representative flow cytometry dot plots of $CD4^+$ and $CD8^+$ donor T-cells that infiltrated intestinal *LP* on days +2 to 4, gated in alive unconverted or converted lymphocytes. **e.** Representative flow cytometry plots and pie charts represent the spatiotemporal compartments of SIVS of converted and unconverted donor T-cells that infiltrated intestinal *LP* on days +2 to 4 after allo-HCT ($n = 4$). According to their different spatiotemporal localization, lymphocytes can be divided into continuously circulating (blue), currently circulating (orange), recently infiltrating (violet), and tissue localized (black). **f.** Graphs depicting the percentage of $CD4^+$ and $CD8^+$ unconverted and converted donor T-cells in the different spatiotemporal compartments that infiltrated intestinal *LP* on days +2 to 4 after allo-HCT ($n = 4$). Statistical significance was determined with two-tailed unpaired Student t tests. Asterisks indicate statistical significance (* $p \leq 0,05$, ** $p \leq 0,01$, *** $p \leq 0,001$, and **** for $p \leq 0,0001$).

In contrast to the stable distribution of converted $CD8^+$ T-cells, the distribution of unconverted $CD8^+$ T-cells infiltrating the *LP* from the circulation exhibited significant variation over time. On day +2 after allo-HCT, a substantial proportion (47%) of unconverted $CD8^+$ T-cells in *LP* were still within the vasculature of the small intestine, indicating that they were actively extravasating from the bloodstream. This proportion of currently circulating unconverted T-cells decreased to 13% and 11% on days +3,5 and +4 after allo-HCT, respectively. Conversely, the percentage of unconverted $CD8^+$ T-cells that infiltrated the intestine and were classified as tissue-localized increased on days +3,5 and +4. This suggests that these cells may have originated from unconverted PPs, partially converted PPs, or most likely migrated into the *LP* before the 90-minutes of SIVS (**Fig. 4.5 f**). Additionally, we detected few unconverted donor T-cells that infiltrated the small intestine during the 90 min analysis (recently migrated) (**Fig. 4.5 e**).

Most importantly, we found that photoconverted $CD4^+$ and $CD8^+$ donor T-cells were not stained with the CD45 antibody infusion 90 min or 5 min before *ex-vivo*, allowing us to classify them as tissue localized. This finding provided further confirmation that these cells originated from PP and directly infiltrated *LP* rather than infiltrating through conventional blood extravasation (**Fig. 4.5 e**).

4.3. Phenotyping of alloreactive T-cells directly migrating from Peyer´s patches to *lamina propria*

4.3.1. Activated and proliferating alloreactive T-cells directly migrated from Peyer´s patches to *lamina propria*

We employed flow cytometry to determine the phenotypic profile and identify any unique characteristics of donor T-cells that directly migrate from PP into adjacent *LP*. First, we assessed the expression of proliferation ($Ki67^+$) and activation markers ($CD25^+$, $CD44^+$, $CD62\text{-}L^-$) on day +3 after allo-HCT. We observed that donor T-cells found in *LP* on day +3 after allo-HCT have a higher activation status than donor T-cells found in mLN. Donor T-cells from the small intestine exhibited significant increases in $CD25^+$ and $CD44^+$ expression, along with decreases in $CD62\text{-}L^+$ expression, compared to those from mLN. Furthermore, more donor $CD4^+$ T-cells in *LP* proliferated ($Ki67^+$) compared with donor T-cells in mLN (**Fig. 4.6 a**).

4.3.2. Alloreactive T-cells directly migrating from Peyer´s patches to *lamina propria* secreted TNF-α and IFN-γ and had a T_H1-like T_H17 cell phenotype.

Additionally, we examined the expression of lineage-specific markers, such as transcription factors, to gain insights into their differentiation status and potential functional capabilities. Flow cytometry analysis revealed that $CD4^+$ and $CD8^+$ donor T-cells that infiltrated intestinal *LP* on day +3 after allo-HCT expressed transcription factors $Tbet^+$ and $ROR\gamma t^+$ (**Fig. 4.6 b**).

To determine the cytokines expressed by donor T-cells directly migrating from PP into *LP*, we measured and quantified cytokine levels in *LP* at different distances from PP. On day +3 after allo-HCT, we segmented the small intestine into three regions: those adjacent to PPs (0-500 µm), intermediate distances (500-1500 µm), and regions further away (>1500 µm). We pooled segments from each distance group, lysed them, and performed a bead-based flow cytometry immunoassay to analyze cytokine levels. Our results revealed a significant increase in IFN-γ concentration in *LP* adjacent to PPs (0-500 µm) compared to *LP* located further away (>1500 µm) on day +3 after allo-HCT. However, concentrations of TNF-α in *LP* at different distances from PP remained unchanged (**Fig. 4.6 c**). These findings suggest a local expression of IFN-γ by donor T-cells that directly egress from PPs.

Moreover, we investigated the production of TNF-α and IFN-γ by $CD4^+$ and $CD8^+$ donor T-cells that infiltrated intestinal *LP* after allo-HCT. On day +3 after allo-HCT, we harvested lymphocytes from intestinal *LP* and stimulated them with PMA and ionomycin in the presence of brefeldin A. This stimulation allows cells to produce and accumulate cytokines intracellularly. To serve as controls, we employed stimulated and unstimulated splenocytes. The majority of stimulated splenocytes, including both $CD4^+$ and $CD8^+$ T-cell subsets, secreted IFN-γ and/or TNF-α. However, a notable 21% of donor T-cells in both $CD4^+$ and $CD8^+$ subsets did not express either of these cytokines. Among those expressing cytokines, a small fraction exclusively produced IFN-γ. $CD4^+$ T-cells showed a significant proportion (64%) expressing TNF-α without concurrent IFN-γ expression, while a smaller subset (15%) co-expressed both TNF-α and IFN-γ. Conversely, in $CD8^+$ T-cells, a lower percentage (30%) expressed TNF-α. Nevertheless, nearly half of $CD8^+$ T-cells (44%) co-expressed both TNF-α and IFN-γ , surpassing the corresponding percentage in $CD4^+$ T-cells. As anticipated, none of the unstimulated splenocytes expressed either of the cytokines (**Fig. 4.7**). Therefore, our assay effectively stimulated, detected, and measured cytokines produced by mouse T-cells, validating its appropriateness for the study.

On day +3 after allo-HCT, the majority of $CD4^+$ and $CD8^+$ T-cells in stimulated *LP* lymphocytes produced TNF-α and/or IFN-γ. Nonetheless, nearly a fifth of donor T-cells did not express either of these cytokines. $CD4^+$ (63%) and $CD8^+$ (60%) donor T-cells in *LP* both exhibited predominant TNF-α expression without concurrent IFN-γ. Moreover, co-expression of TNF-α and IFN-γ was substantially higher in $CD8^+$ T-cells (22%) compared to CD4+ T-cells (11%). Additionally, a small fraction exclusively produced IFN-γ (**Fig. 4.6 d**). All in all, flow cytometry measurements of stimulated *LP* lymphocytes on day +3 after allo-HCT revealed predominant TNF-α expression, with some T-cells also producing IFN-γ.

4.3.3. Alloreactive T-cells directly migrating from Peyer´s patches to *lamina propria* express α_4^+ α_E^+ and α_L^+ integrins, and CxCR3$^+$, CCR5$^+$, and CCR9$^+$ chemokine receptors

Additionally, we contrasted the expression levels of integrins on donor T-cells that infiltrated *LP* on day +3,5 after allo-HCT in 2 Gray irradiated CB6F1 mice with those in PPs (**Fig. 4.6 e**). We discovered that $CD4^+$ and $CD8^+$ donor T-cells in PP and *LP*

exhibited high levels of α_L integrin. The high expression of α_L integrin in PP and *LP* agreed with its role as a critical cell adhesion molecule in T-cell trafficking, migration, and interactions with other immune cells (**Fig. 4.6 e**). Furthermore, we found that 19% of donor $CD4^+$ and 56% of donor $CD8^+$ T-cells in *LP* expressed α_4 integrin. $CD4^+$ and $CD8^+$ T-cells express significantly more α_4 integrin in *LP* than in PP. Furthermore, we noticed that 15% of donor $CD4^+$ T-cells and 48% of donor $CD8^+$ T-cells expressed α_E integrin. However, in PP, we did not observe any expression of α_E integrin on $CD4^+$ T-cells, while 18% of $CD8^+$ T-cells expressed α_E integrin. T-cells in *LP* exhibit higher expression of α_4 integrin and α_E integrin than PP, indicating that these cells were better equipped to home to gut mucosa and other gut-associated tissues (**Fig. 4.6 e**).

We also compared the expression of chemokine-coupled receptors on donor T-cells that infiltrated *LP* in 2 Gray irradiated CB6F1 mice on day +3,5 after allo-HCT with expression levels in mLN. We discovered that a subset of T-cells in *LP* and mLN expressed CXCR3, a chemokine receptor essential for T-cell migration and homing to inflammatory sites. CXCR3 was expressed by 19% of $CD4^+$ T-cells and 25% of $CD8^+$ T-cells in *LP,* compared to 4% of $CD4^+$ and 8% of $CD8^+$ T-cells in mLN (**Fig. 4.6 e**).

We found that CCR5, a chemokine receptor involved in T-cell migration and recruitment to inflammatory sites, was expressed by a subset in both *LP* and mLN. We discovered that 6% of $CD4^+$ and 8% of $CD8^+$ T-cells in *LP* expressed CCR5. Similarly, in mLN, we found that 20% of $CD4^+$ T-cells and 26% of $CD8^+$ T-cells expressed CCR5. Furthermore, the higher expression of CCR5 in mLN compared to *LP* indicated a greater potential for T-cell recruitment and migration to mLN (**Fig. 4.6 e**).

We discovered that neither $CD4^+$ T-cells nor $CD8^+$ T-cells in mLN expressed CCR9 on day +3,5 after allo-HCT, a chemokine receptor essential for T-cell migration and homing to the gut mucosa, specifically the small intestine. Interestingly, in *LP,* we found a subset of T-cells that expressed CCR9 (**Fig. 4.6 e**). These results agreed with their activation status, suggesting that at day +3,5 after allo-HCT, donor T-cells in *LP* became more activated and differentiated compared to mLN (**Fig. 4.6 a**). Overall, our flow cytometry experimental approach provided valuable insights into phenotype and potential functional properties of T-cells migrating from PP to *LP* early after allo-HCT.

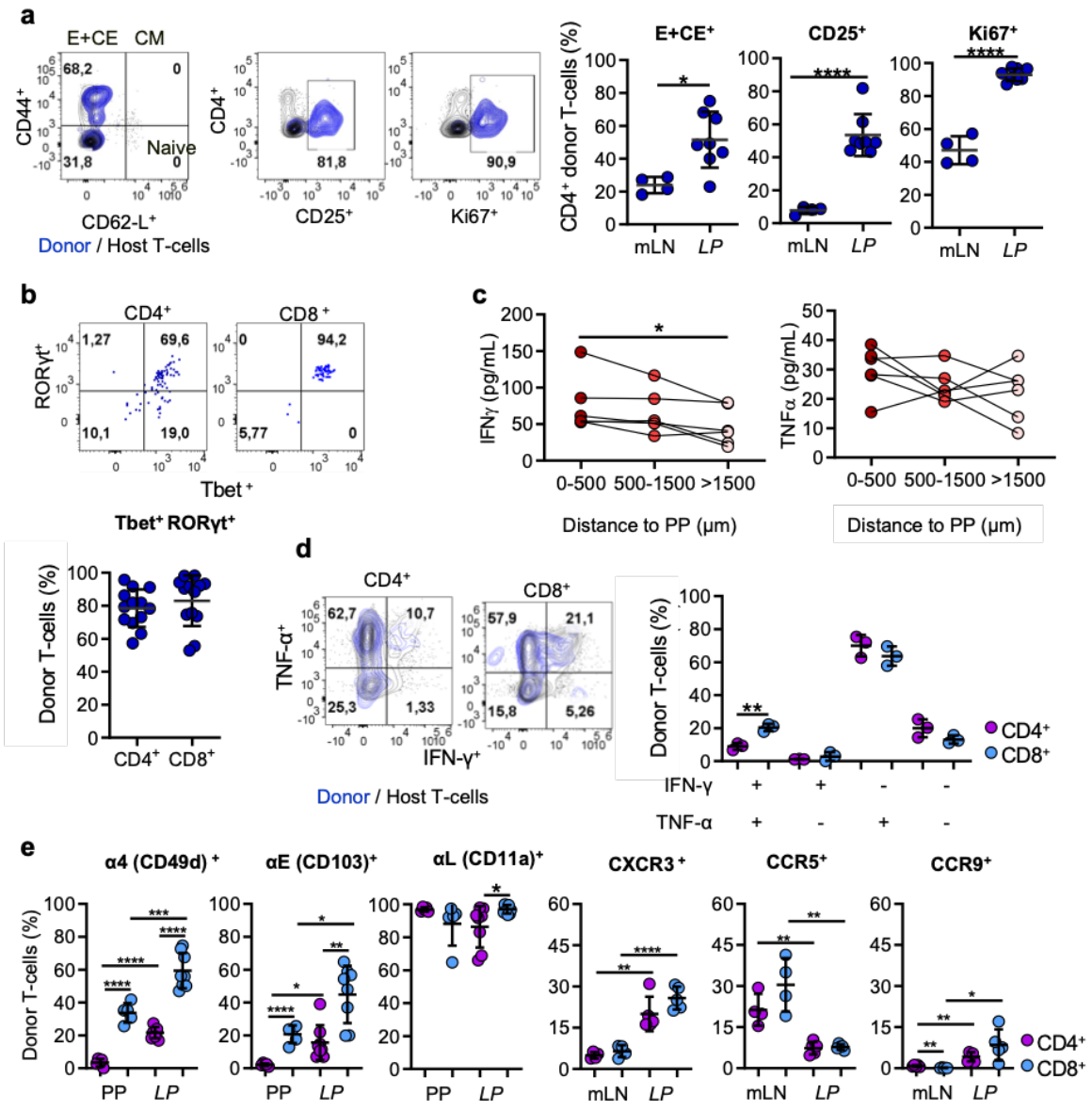

Fig. 4.6 Alloreactive-T-cells that directly migrate from Peyer's patches to *lamina propria* were activated, proliferated, secreted TNF-α and IFN-γ, and had a T_H1-like T_H17 cell phenotype. a-d We transferred parental strain T-cells into haploidentical and unirradiated CB6F1 recipients. **a.** Representative flow cytometry plots of proliferation ($Ki67^+$) and activation markers ($CD25^+$ and $CD44^+$) of donor T-cells that infiltrated intestinal *LP* on day +3 after allo-HCT. Graphs depicting the percentage of donor $CD4^+$ and $CD8^+$ T-cells expressing $CD25^+$ and $CD44^+$, and $Ki67^+$ on intestinal *LP* and mLN (*n* = 8). **b.** Representative flow cytometry plots of $Tbet^+$ and $ROR\gamma t^+$ expression by single alive donor $CD4^+$ and $CD8^+$ donor T-cells infiltrating intestinal *LP* on day +3 after allo-HCT (up). Graphs depicting the percentage of donor $CD4^+$ and $CD8^+$ T-cells expressing $Tbet^+$ and $ROR\gamma t^+$ (*n* = 13) (down). **c.** IFN-γ and TNF-α concentrations in *LP* at different distances to PPs on day +3 after allo-HCT (*n* = 6). **d.** Representative flow cytometry plots of TNF-α and IFN-γ expressed by single alive donor $CD4^+$ and $CD8^+$ donor T-cells that infiltrated intestinal *LP* on day +3 after allo-HCT. Graphical results (*n* = 3). **e.** Chemokine receptors $CxCR3^+$, $CCR5^+$, $CCR9^+$, and integrins α_4^+ α_E^+ and α_L^+ expressed by single alive $CD4^+$ and $CD8^+$ donor T-cells that infiltrated intestinal *LP* in 2 Gray irradiated CB6F1 mice on day +3,5 after allo-HCT (n = 6 to 8). Unpaired (a-b, d-e), or paired (c) two-sided Student's t-tests were conducted, considering *p* values under 0,05 as indicative of a significant difference. Asterisks indicate statistical significance (* $p \leq 0{,}05$, ** $p \leq 0{,}01$, *** $p \leq 0{,}001$, and **** for $p \leq 0{,}0001$).

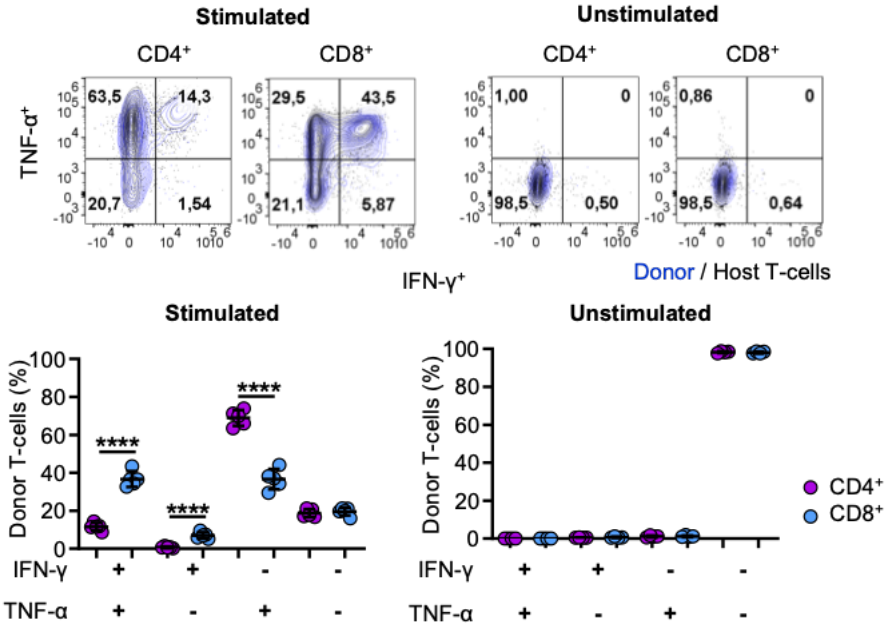

Fig. 4.7 TNF-α and IFN-γ expression by CD4⁺ and CD8⁺ donor T-cells in stimulated and unstimulated splenocytes. Representative flow cytometry plots of the expression of TNF-α and IFN-γ by CD4⁺ and CD8⁺ donor T-cells in both stimulated and unstimulated splenocytes on day +3 after allo-HCT. Graphical results (*n* = 4 to 5). Statistical significance was determined with two-tailed unpaired Student t tests. Asterisks indicate statistical significance (* $p \leq 0,05$, ** $p \leq 0,01$, *** $p \leq 0,001$, and **** for $p \leq 0,0001$).

4.4. Mechanism of direct T-cell migration from Peyer´s patch to *lamina propria*

4.4.1. Integrins or chemokines did not mediate direct T-cell migration from Peyer's patch to the *lamina propria*

We next examined whether chemokines or integrins control the direct migration of T-cells from PP to *LP*. Although T-cells migrate largely integrin-independent in a 3D tissue environment, T-cells may interact with other cell types and the ECM via integrins. Therefore, we examined whether integrins control the direct migration of T-cells from PP to *LP* using a cocktail of integrin-blocking antibodies. We investigated the role of chemokines in direct T-cell migration from PP to *LP* using pertussis toxin (PT_X), an inhibitor of chemokine receptor-dependent Gαi-type G protein signaling. PT_X inhibits the GTP-binding proteins Gi and Go, limiting chemokine-mediated cell migration regardless of the redundancy of chemokines and chemokine receptor systems. It also irreversibly disrupts signaling from other G protein-coupled receptors and chemokine receptors.

On day +2 after allo-HCT, we infused a mixture of integrin-blocking antibodies (α_4, α_E, and α_L) into GvHD-developing mice. On day +3,5 after allo-HCT, we evaluated surface saturation of the blocking monoclonal antibodies by counterstaining cells with fluorochrome-conjugated antibodies directed against the same integrins (identical clones), and we compared them to PBS-treated mice. Flow cytometry analysis revealed effective blocking of α_4, α_E, and α integrins in *LP*, PP, and mLN following the infusion of integrin-blocking antibodies (**Fig. 4.8 a**).

Moreover, we determined that PTx effectively blocked the migration of activated T-cells through chemotaxis assays towards CXCL11. In these assays, we observed that pre-treating activated T-cells with a PTx mutant induced directed migration towards CXCL11, while pre-treating T-cells with PTx did not promote directional migration. As a negative control, we examined the migration of activated T-cells in a medium without the addition of CXCL11, and we observed no directional migration of activated T-cells. (**Fig. 4.8 b**). In summary, we concluded that the mixture of integrin-blocking antibodies and PTx effectively blocked the integrins and chemokine-coupled receptors on activated T-cells, respectively.

We quantified donor T-cell densities around PP with LSFM in mice treated with integrin-blocking antibodies or PTx in relation to control mice that received PBS or a mutant version of PTx without catalytic activity. We transferred parental strain T-cells into haploidentical F1 recipients irradiated with 2 Gray. On day +2 after allo-HCT, we infused a mix of integrin-blocking antibodies into GvHD-developing mice. On day +3,5, we euthanized the mice and prepared tissue for LSFM acquisition (**Fig. 4.9 a**).

After blocking integrins and chemokine-coupled receptors, we discovered a gradient of donor T-cells on day +3,5 after allo-HCT, suggesting that direct T-cell migration from PP to *LP* was not dependent on integrins or chemokines. If chemokines or integrins were crucial in T-cell migration from PP to *LP*, a donor T-cell gradient around PP would not have been observed in mice treated with PTx or integrin-blocking antibodies, respectively (**Fig. 4.9 b**). Interestingly, PTx treatment increased donor T-cells in *LP* surrounding PP (**Fig. 4.9 b**). These results suggested that loss of chemokine sequestration, likely due to loss of detection of CCL19 and CCL21 chemokines,

increases direct PP-to-*LP* T-cell migration. We hypothesized that loss of CCR7 after T-cell priming could be one of the relevant mechanisms for direct PP-to-*LP* T-cell migration after allo-HCT.

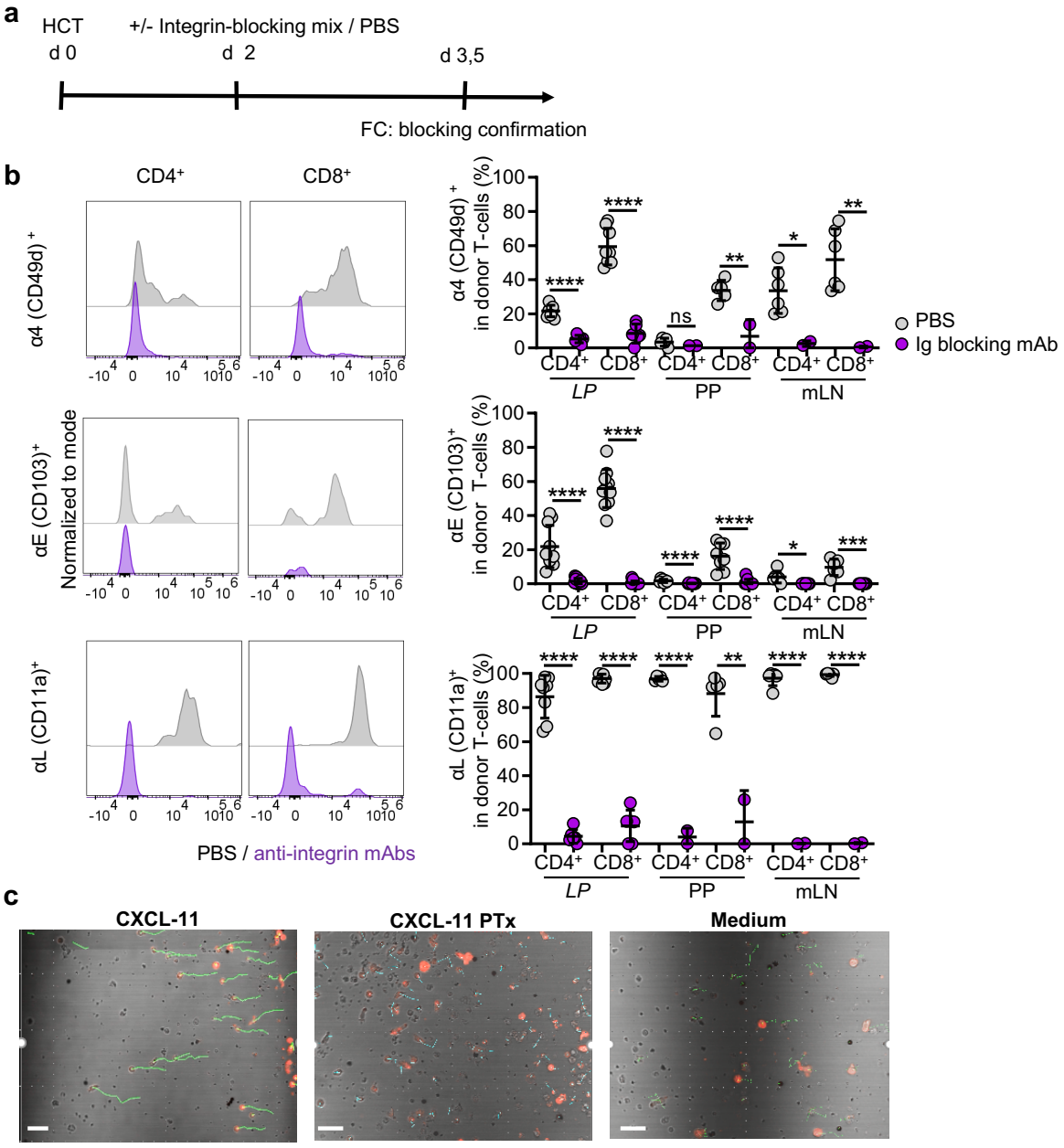

Fig. 4.8 Mixture of integrin-blocking antibodies and pertussis toxin effectively blocked integrins and chemokine-coupled receptors on activated T-cells, respectively. a. Parental strain T-cells were transferred into haploidentical F1 recipients irradiated 2 Gray. On day +2 after allo-HCT, a mix of integrin-blocking antibodies was infused into GvHD-developing mice (α4, αE, and αL). On day +3,5, after allo-HCT mice, surface saturation was evaluated by counterstaining with fluorochrome-conjugated antibodies directed against the same integrins (identical clones). Statistical significance was determined with two-tailed unpaired Student t tests. Asterisks indicate statistical significance (* $p \leq 0{,}05$, ** $p \leq 0{,}01$, *** $p \leq 0{,}001$, and **** for $p \leq 0{,}0001$). **b.** Representative plot of $CD4^+$ and $CD8^+$ donor T-cells in intestinal *LP*. Flow cytometry (n = 6 to 8). **c.** Pertussis toxin inhibits migration of *in-vitro* activated T-cells towards a CXCL11 gradient. Scale bar 30 µm.

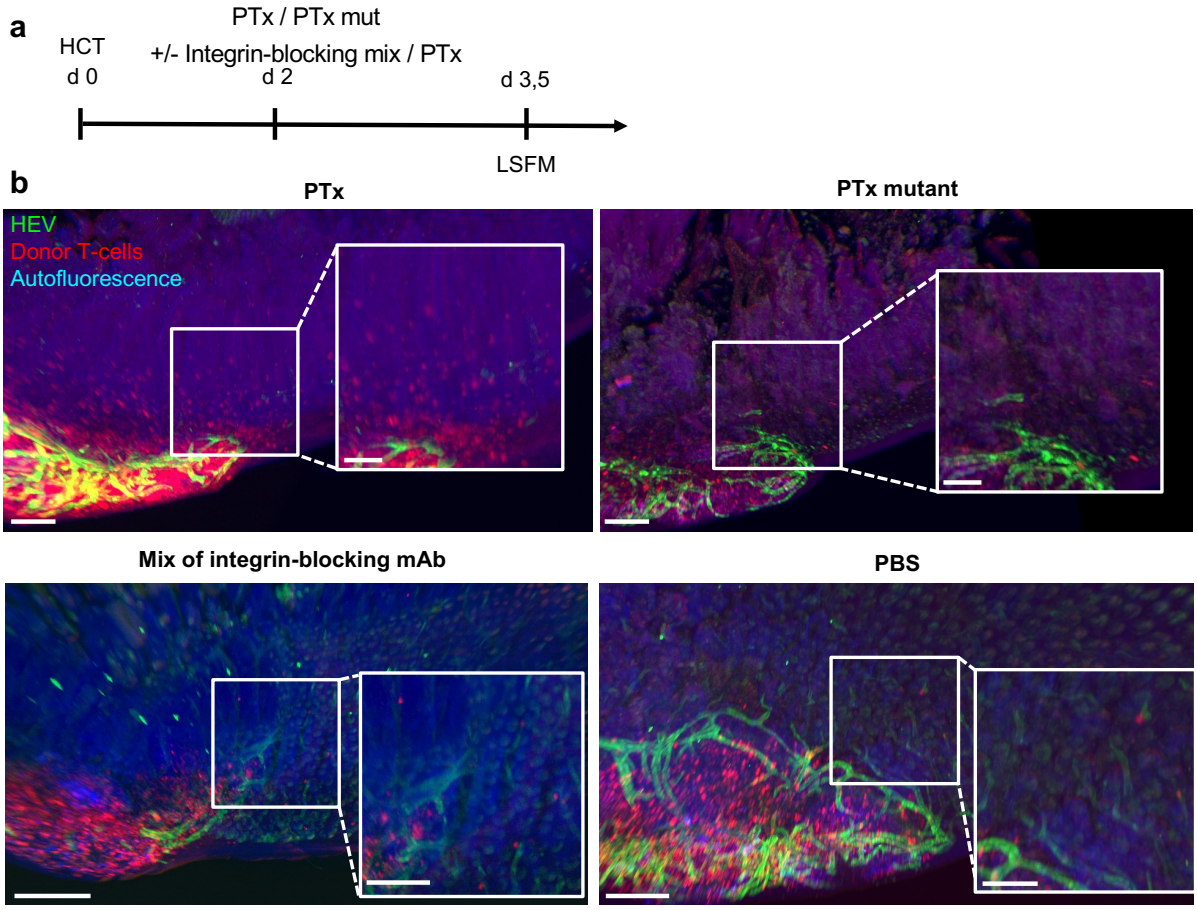

Fig. 4.9 Direct T-cell migration from Peyer's patches to the *lamina propria* does not require integrins or αi chemokines. a. We transferred parental strain T-cells into haploidentical F1 recipients irradiated with 2 Gray. On day +2 after allo-HCT, we infused a mix of integrin-blocking antibodies (α4, αE, and αL) (i.v), PBS (i.v), PTx (i.p), or an inactive mutant (i.p) into GvHD-developing mice. On day +3,5, we euthanized the mice and prepared the tissue for LSFM acquisition. **b.** Light sheet fluorescence 3D reconstruction of PPs and surrounding *LP* of the small intestine from mice treated with a PTx, a PTx inactive mutant, an integrin-blocking antibody mix, or PBS on day +3,5 after allo-HCT, which shows donor T-cells (CD45.1) in red, MAdCAM-1 in green. Scale bar 200 µm and 100 µm for inserts.

4.5. Directly migrated T-cells induce a secondary recruitment of additional bloodborne activated T-cells.

Next, we wanted to address whether directly migrating T-cells serve as seed cells to attract more circulating T-cells from blood to the site of early inflammation. We transferred B6.Dendra2 T-cells into haploidentical unirradiated F1 recipients. We photoconverted donor T-cells in PPs using UV light on day +2 after allo-HCT. On day +3, we embedded PPs and performed immunofluorescence microscopy to assess the co-localization of directly migrating from PP (converted) and bloodborne derived donor T-cells (unconverted) infiltrating *LP* after allo-HCT (**Fig. 4.10 a**). Immunofluorescence

microscopy confirmed the co-localization of bloodborne T-cells with PP-derived T-cells. In addition, we observed that converted donor T-cells were only present in regions adjacent to converted PPs (**Fig. 4.10 b**).

To further confirm vascular recruitment, we transferred B6.Dendra2 T-cells into haploidentical unirradiated F1 recipients. On day +2 after allo-HCT, we transferred 4 days of activated DsRed T-cells to the vasculature of mice developing GvHD. On day +4, we embedded PPs and performed immunofluorescence microscopy to assess the co-localization of directly migrating from PP (Dendra2) and bloodborne activated T-cells (DsRed) infiltrating *LP* after allo-HCT (**Fig. 4.10 c**). Immunofluorescence microscopy confirmed that directly migrating T-cells recruited activated T-cells to intestinal *LP* adjacent to PP (**Fig. 4.10 h**).

After 4 days of *in-vitro* stimulation, we performed flow cytometry to verify the success of our activation protocol. We specifically examined the expression levels of CD44 and CD62-L on the T-cells that were activated *in-vitro*. Our findings revealed that approximately 58% of the $CD4^+$ T-cells and 33% of the $CD8^+$ T-cells expressed CD62-L, indicating that these cells can access SLOs. Conversely, 40% of the $CD4^+$ T-cells and 61% of the CD8+ T-cells expressed CD44 and lacked CD62-L expression ($CD62\text{-}L^-$) (**Fig. 4.11 b**). This phenotype suggests a central effector and effector phenotype, which aligns with our experimental goals. Furthermore, we observed that naïve T-cells were minimally detectable in our samples, further supporting the effectiveness of our *in-vitro* activation protocol (**Fig. 4.11 b**). Overall, these results confirm the successful activation of T-cells *in-vitro* and the generation of a desired central effector and effector phenotype, with minimal presence of naïve T-cells.

In addition to PP and the small intestine, we embedded other SLOs such as the mLN, spleen, inguinal lymph nodes (iLN), and lung tissue allowing us to assess the distribution of the transferred activated T-cells throughout the mouse. Based on our flow cytometry analysis, we observed that approximately 58% of the activated $CD4^+$ T-cells and 33% of the activated $CD8^+$ T-cells expressed CD62-L, indicating their capability to access SLOs suggesting that a significant portion of the activated T-cells can migrate to these lymphoid organs. Immunofluorescence microscopy revealed many transferred activated T-cells localized in the mLN, spleen, and iLN (**Fig. 4.10 d-**

f). Interestingly, we observed more activated T-cells in the mLN than in the iLN, which might be attributed to including retinoic acid in our activation protocol. It is well known that retinoic acid improves T-cell homing into the small intestine.

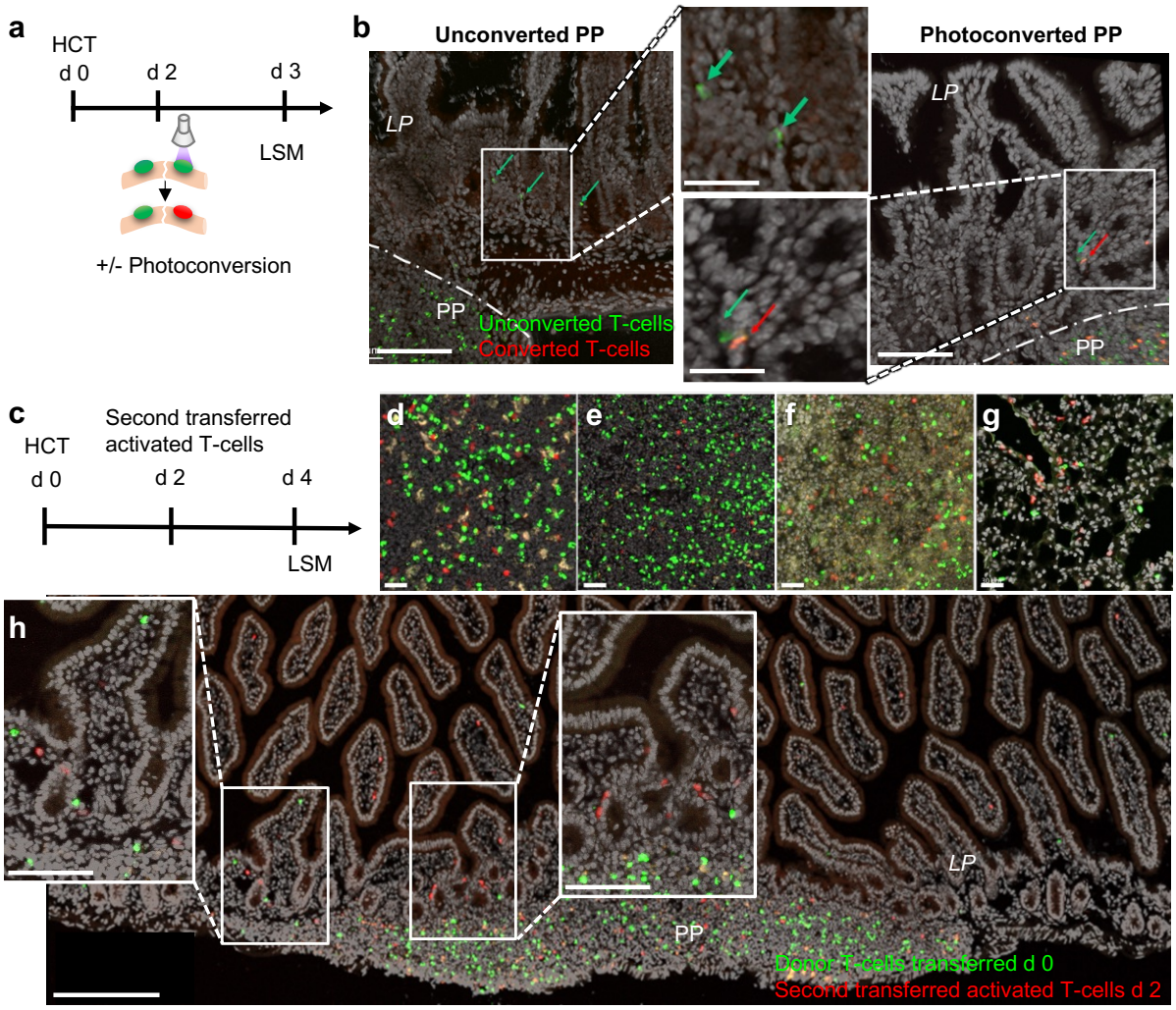

Fig. 4.10 Co-localization of directly migrating from Peyer's patches and bloodborne activated T-cells infiltrating *lamina propria* early after allogeneic hematopoietic cell transplantation. We transferred parental strain B6.Dendra2 T-cells into haploidentical unirradiated F1 recipients. **a.** We photoconverted donor T-cells in PPs on day +2 after allo-HCT. On day +3, we euthanized the mice and prepared the tissue for LSM acquisition. **b**. Representative Immunofluorescence microscopy images show the PP-derived donor T-cells in red (converted), bloodborne donor T-cells in green (unconverted), and cell nuclei stained with DAPI in grey. The scale bar is 100 µm, with inserts shown at 50 µm. **c.** On day +2 after allo-HCT, we transferred 20 x10^6 activated DsRed T-cells to GvHD-developing mice. On day +4 after allo-HCT, we euthanized the mice and prepared the tissue for LSM acquisition. **d-h.** Representative Immunofluorescence microscopy showing alloreactive T-cells transferred on day +0 in green, *in-vitro* activated DsRed T-cells transferred on day +2 in red, and cell nuclei stained by DAPI in grey. **d.** mLN, **e.** iLN, **f.** spleen, **g.** lung. **h.** small intestine. **d-g.** Scale bar 30 µm (*n* = 3)**. h.** Scale bar 200 µm and inserts 100 µm.

We embedded lung tissue to assess whether activated T-cells, following adoptive transfer, were "trapped" in pulmonary microcirculation due to factors such as

the smaller diameter of pulmonary capillaries or reduced deformability of activated T-cells. We performed immunofluorescence microscopy and observed that only a few transferred activated T-cells were present in the lung. However, they were not found in clusters or large numbers, suggesting that trapping activated T-cells in the lung was not a significant issue (**Fig. 4.10 g**).

To enhance certainty regarding vascular recruitment, we made the window between the transfer of activated T-cells and *ex-vivo* analysis smaller. Specifically, we tested whether the co-localization of directly migrating T-cells and bloodborne T-cells remained detectable by transferring the activated T-cells on day +3 after allo-HCT instead of day +2. This experiment aimed to determine if the transfer timing impacted the observed co-localization, thus providing further confirmation of vascular recruitment (**Fig. 4.11 a**). On day +4, we embedded PPs and performed immunofluorescence microscopy to assess the co-localization of directly migrating from PP (Dendra2) and bloodborne activated T-cells (DsRed) infiltrating *LP* after allo-HCT. Immunofluorescence microscopy confirmed that, in this case, directly migrating T-cells also recruited activated T-cells to intestinal *LP* adjacent to PP (**Fig. 4.11 c**).

To confirm the recruitment of activated T-cells by T-cells directly migrating from PPs, we incorporated a sham control group where healthy mice received the adoptive transfer of activated T-cells one day before *ex-vivo* analysis. Immunofluorescence microscopy of the small intestine confirmed that activated T-cells were only located in SLOs in sham control mice (**Fig. 4.11 c**). There was virtually no infiltration of activated T-cells into the intestinal mucosa. We determined the minimal distance between an activated T-cell and a directly migrated T-cell and observed that most of the activated T-cells were in close vicinity to directly migrating alloreactive T-cells. The number of activated T-cells found within less than 100 µm from a directly migrated T-cell was significantly higher compared to the number of T-cells found in the 100-200 µm and 200-300 µm intervals. Specifically, we found that 60% of the T-cells were located within less than 100 µm (**Fig. 4.11 d**).

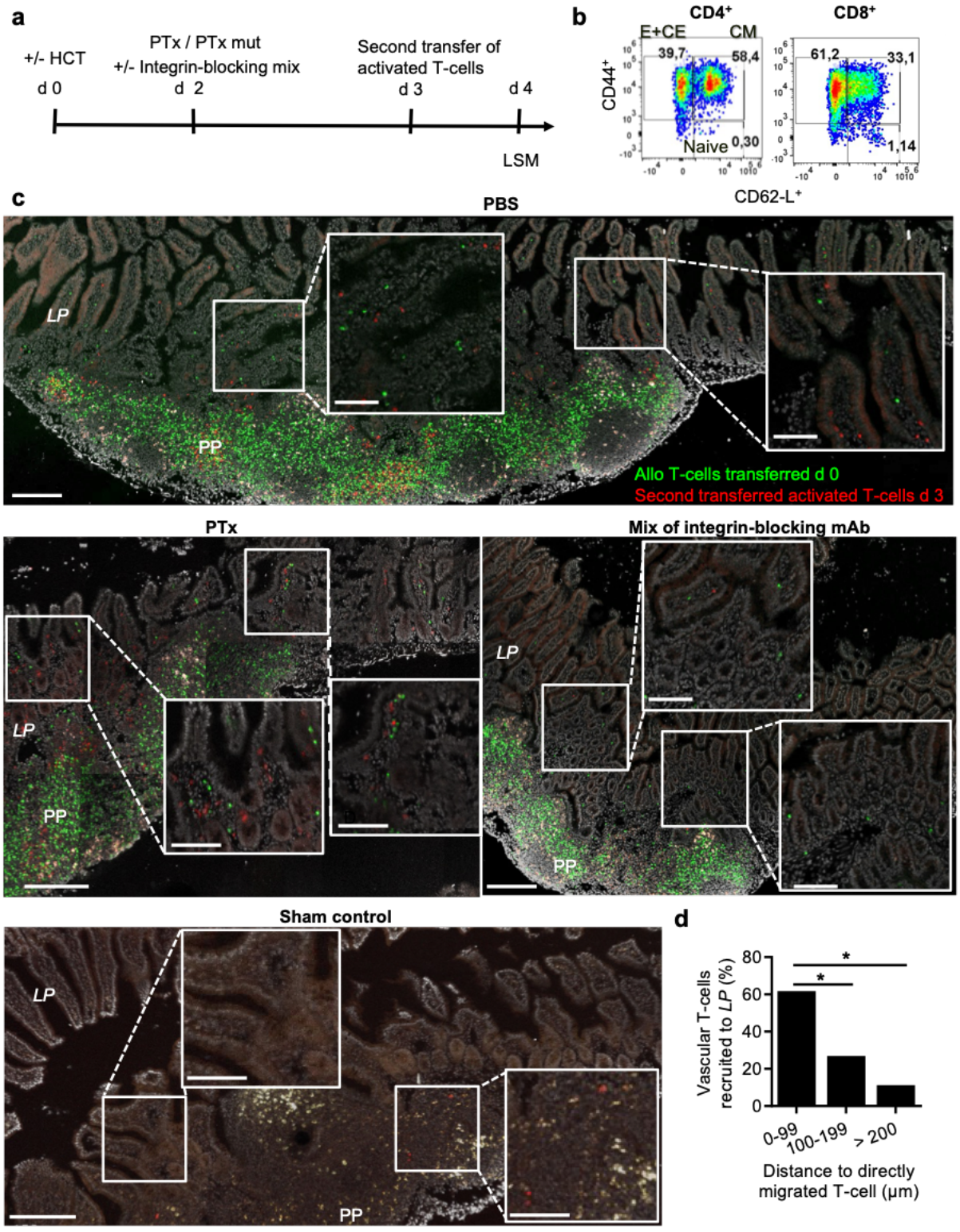

Fig. 4.11 Direct migration of alloreactive T-cells to the *lamina propria* and their co-localization with bloodborne activated T-cells occurred independently of chemokines. a. We transferred parental strain B6.Dendra2 T-cells into haploidentical unirradiated F1 recipients. On day +2 after allo-HCT, we infused a mix of integrin-blocking antibodies (α4, αE, and αL) (i.v), PBS (i.v), PTx (i.p), or an inactive mutant (i.p) into GvHD-developing mice. On day +3 after allo-HCT, we transferred 20 x10^6 activated DsRed T-cells to the GvHD-developing mice. On day +4, we euthanized the mice and prepared the tissue for LSM acquisition. **b.** Representative flow cytometry plots of activation markers ($CD44^+$, $CD62\text{-}L^-$) of DsRed T-cells activated *in-vitro* 4 days, gated on live $CD4^+$ and $CD8^+$ T-cells. **c.**

Representative Immunofluorescence microscopy of PPs and surrounding *LP* of the small intestine from mice treated with a PTx, an integrin-blocking antibody mix, or PBS on day +4 after allo-HCT, showing alloreactive T-cells transferred on day +0 in green, *in-vitro* activated DsRed T-cells transferred on day +2 in red, and cell nuclei stained by DAPI in grey. Scale bar 200 µm and inserts 100 µm. **d**. Graph depicting the percentage of vascular T-cells recruited to *LP* at increasing distances to directly migrated T-cells (n = 6). Statistical significance was determined with two-tailed paired Student t tests. Asterisks indicate statistical significance (* $p \leq 0{,}05$, ** $p \leq 0{,}01$, *** $p \leq 0{,}001$, and **** for $p \leq 0{,}0001$).

We conducted further experiments to investigate the potential involvement of chemokines and integrins in the vascular recruitment of activated T-cells by T-cells directly migrating from PP to *LP*. On day +2 after allo-HCT, we infused a mixture of integrin-blocking antibodies (specifically targeting α_4, α_E, and α_L integrins) or PTx into mice developing GvHD. We compared these treatments to mice that received PBS as a control. On day +3 after allo-HCT, we transferred activated DsRed T-cells to the GvHD-developing mice. Subsequently, on day +4, we embedded PP for histological analysis (**Fig. 4.11 a**). Immunofluorescence microscopy analysis of the small intestine revealed that activated T-cells could not extravasate from the bloodstream when integrins were blocked. This finding provided further evidence supporting the efficacy of our integrin-blocking antibodies in inhibiting the integrin function of T-cells, as demonstrated by the lack of T-cell migration across the endothelial barrier (**Fig. 4.11 c**). Interestingly, the recruitment of T-cells from circulation and direct migration of donor T-cells from PP to *LP* was not impaired by the inhibition of chemokine-coupled receptors, suggesting that chemokines may not be the primary mediators involved in these processes (**Fig. 4.11 c**).

5. Discussion

5.1. Direct alloreactive T-cells migration from Peyer´s patches to *lamina propria* regardless of pre-transplantation conditioning

Early after allo-HCT, a subset of alloreactive T-cells migrate directly from T-cell zones of PPs to nearby *LP* of the small intestine. This undiscovered migration route bypasses the normal lymphatic drainage and vascular trafficking pathways. Noteworthy, we observed direct PP-to-*LP* T-cell migration in mice that received total body irradiation as part of conditioning for cell transplantation (section **1.4.2**). Whether allogeneic T-cells can migrate directly from PP to adjacent *LP* in unirradiated GvHD models remained to be defined.

In conventional myeloablative conditioning regimens, higher doses of irradiation and/or chemotherapy are used to eliminate the recipient's bone marrow and suppress their immune system. The purpose of this approach is twofold: to minimize the risk of graft rejection and to create space for the transplanted cells to successfully engraft (Murphy and Weaver, 2022). However, irradiation also causes damage and inflammation in the recipient's healthy tissues.

Various cell types within the intestines are affected by ionizing irradiation, leading to damage and disruption of normal intestinal function. Irradiation damages a variety of intestinal cell types, making the gut one of the most irradiation-sensitive organs (**Fig. 1.1**). A significant impact of irradiation on the intestine is the compromise of tight junctions that disrupt the intestinal barrier and therefore increase intestinal permeability. Consequently, intestinal bacteria cross the intestinal barrier generating acute inflammation (Fredricks, 2019). Furthermore, irradiation can harm PPs' structural integrity. High irradiation dosages can directly damage cells within PPs, causing degeneration or malfunction. PP's typical structure and operation may be altered by persistent irradiation-induced inflammation, leading to fibrotic changes and a diminished capacity to sample intestinal antigens and mount effective immune responses (Gervaz et al., 2009).

Non-myeloablative or low-intensity conditioning regimens are designed to avoid toxicity and adverse side effects while suppressing the immune system of the patient

just enough to prevent rejection of the cell transplant. Whether allogeneic T-cells migrate directly from PP to *LP* after non-myeloablative conditioning remained to be elucidated. We postulated that irradiation could damage stromal cells lining the edge of PP, such as macrophages, FRCs, or other stromal cells, opening new migration pathways for allogeneic T-cells. To assess this, we evaluated whether donor T-cells can migrate from PP to the *LP* in the parent-into-F1 allo-HCT model (B6→ unirradiated F1, H-2^{b}→ H-2^{bxd}) without pre-transplantation irradiation (Ft et al., 1991; Fu et al., 2019; S et al., 2011; Shimoji et al., 2017; Y et al., 2012). Furthermore, the imaging of cellular contacts was made easier by the decreased frequency of donor T-cell infiltration in the unirradiated allo-HCT model and the lack of irradiation harm.

We observed the presence of donor T-cells in intestinal *LP* adjacent to PPs in both irradiated and unirradiated mice on day +3,5 after allo-HCT. Furthermore, on day +3,5 after allo-HCT, we identified a cell gradient from PPs to *LP* in both irradiated and unirradiated GvHD recipients. Additionally, using photoconversion we discovered PPs-derived donor T-cells in the intestinal *LP* of unirradiated recipients (**Fig. 4.1**). Our findings proved that irradiation is not a prerequisite for the direct migration of T-cells from PPs to intestinal *LP* in allo-HCT recipients and that irradiation damage to stromal cells lining the edge of PP was not a relevant mechanism for the observed direct T-cell migration.

5.2. Peyer´s patches-derived T-cells directly infiltrated the *lamina propria* before bloodborne T-cells

5.2.1. Serial intravascular staining tracks leukocyte trafficking kinetics in mice

Leukocyte trafficking is a complex process critical to immune function and overall health (**1.3.1**). James Gowans' groundbreaking research using cannulation and radioactive labeling of lymphocytes proved that lymphocytes cycle between the blood and the lymphatic system (Ford and Gowans, 1968). Although our knowledge of leukocyte trafficking has advanced, accurately tracking and monitoring leukocyte trafficking *in-vivo* still poses limitations.

Cannulation studies involve surgically inserting a cannula into lymphatic vessels to collect lymph fluid, which is then analyzed for its cellular composition using

flow cytometry and microscopy. In early studies of leukocyte trafficking, researchers isolated lymphocytes, labeled them, and reintroduced them into the body for tracking purposes. In older research, labeling cells with radioactive substances was common practice. Today, fluorescent markers are preferred. Limitations of these techniques include *ex-vivo* handling, distinguishing between circulating and tissue-resident cells, and specific cell subsets (Ford and Gowans, 1968; Ford and Simmonds, 1972; Reynolds et al., 1982; Smith and Ford, 1983).

Newer techniques such as adoptive transfer studies, photoconversion, and two-photon microscopy have accelerated our knowledge of leukocyte trafficking. **Adoptive transfer** experiments involve injecting donor cells into a different animal to study trafficking. Adoptively transferred cells, however, might not reflect naturally migrating cells. On the other hand, **photoconversion** utilizes light to induce irreversible fluorescence changes in cells expressing photoconvertible proteins. This innovative technique converts cells in one location and time and tracks the movement of converted cells to other body parts (Tomura et al., 2010b, 2010a).

Additionally, **two-photon microscopy** has become a successful technique for observing lymphocyte trafficking *in-vivo* (Mandl et al., 2012; Tomura et al., 2008). Fluorophore excitation in this technique relies on two-photon absorption and utilizes long-wavelength light. Two-photon microscopy enables deeper imaging with reduced scattering and minimal photodamage. However, it has limitations in analyzing dense tissues and multiple fluorescent signals (Hunter et al., 2016; Rainger and Mcgettrick, 2017).

Furthermore, integrating these techniques allows for a more comprehensive understanding of leukocyte trafficking. Adoptive transfer studies provide insights into cell behavior in controlled experiments, while photoconversion enables tracking specific cell populations. By complementing these techniques with intravital two-photon microscopy, researchers can achieve high-resolution imaging and quantification of lymphocyte trafficking in live animals. For instance, combining two-photon microscopy and fluorescent convertible mice has made it possible to observe and follow recruited lymphocytes as they move across tissues (Hunter et al., 2016; Jarick et al., 2018; Rainger and Mcgettrick, 2017).

In a recent study, researchers led by Mario Roederer introduced a novel technique called **SIVS** to quantify leukocyte trafficking in non-human primates. In Potter et al., 2021 work, the researchers examined leukocyte trafficking kinetics in healthy and *M. tuberculosis*-infected non-human primates using SIVS. To do this, they injected variously labeled antibodies at various times, essentially "barcoding" circulating leukocytes according to where they were at the time of each infusion. Next, we utilized flow cytometry analysis to monitor the changes in cellular location over time for various leukocyte populations. The data analysis allowed us to determine leukocyte trafficking kinetics and learn more about how the migration patterns of healthy and sick animals differed. Similarly, Tkachev et al., 2021 applied SIVS to study the trafficking of donor T-cells in non-human primates with GvHD. By using SIVS, they could track the movement of labeled donor T-cells during GvHD development.

Unlike traditional approaches that involve *ex-vivo* cell processing, SIVS enables *in-vivo* tracking of leukocyte migration. However, SIVS has its limitations. The antibodies used imposed restrictions on experiment duration and can trigger anti-antibody responses. SIVS primarily focuses on cellular influx into tissues and does not comprehensively analyze cellular emigration or the return of cells to the bloodstream. Additionally, SIVS assumes an equilibrium state that may not accurately reflect dynamics under diseased conditions or specific drug treatments.

In this thesis, we present to our knowledge the first report on utilizing SIVS in mice models of GvHD and demonstrate the potential for its combination with photoconversion to enhance our understanding of leukocyte trafficking. To permit staining by repeated infusions in SIVS, subsaturating dosages of monoclonal antibodies are required. In our titration experiments of αCD45 in mice for SIVS, we opted for doses of 0,5 to 0,8 µg for 20 g mice (**Fig. 4.2**). In titrations of αCD45 in non-human primates for SIVS, doses ranging from 30 to 100 µg/kg (Potter et al., 2021). To translate these doses for mice, we calculated equivalent doses based on body weight to be 0,6 to 2 µg for a 20 g mouse. Our doses are comparable to results obtained in titration experiments conducted in non-human primates.

We found that in a healthy mouse, ~ 15% of $CD4^+$ and 25% of $CD8^+$ T-cells remain in circulation over 90 min (**Fig. 4.3 b**). In the absence of an active immunological response, most circulating T-cells remain naïve. Naïve T-cells recirculate between blood and LNs every 12 to 24 h (Punt, 2013). Only a small fraction, around one in 10^5 to 10^6, react to a specific antigen. In a mouse with 2×10^8, this would mean that only 200 to 2000 T-cells are antigen-specific (Jenkins and Moon, 2012). Therefore, lymphocytes recirculate through SLOs, boosting their chances of encountering their cognate antigen.

According to Smith and Ford's study on lymphocyte recirculation in rats, within 4 to 16 h after intravenous injection, injected cells returned to the thoracic duct. Their calculations revealed that, with an average residence duration of 25 min, 1% to 3% of the transplanted cells stayed in circulation at a steady state (Smith and Ford, 1983). This suggests that most naïve T-cells dedicate their time to exploring SLOs, searching for specific antigens (Lee et al., 2012). Naïve T-cells had long been believed to only travel between SLOs via lymph and blood. Recent data, however, suggests this viewpoint could be oversimplified. Naïve T-cells, albeit in lesser numbers, also move across non-lymphoid tissues (Cose et al., 2006).

Our findings indicated longer transit times for $CD8^+$ T-cells in blood compared to $CD4^+$ T-cells. This observation was surprising, considering previous studies showing $CD4^+$ T-cells have faster transit times through LN than $CD8^+$ T-cells (Tomura et al., 2008). Higher residence times of $CD8^+$ T-cells in the spleen or non-lymphoid organs can potentially explain these differences.

5.2.2. Photoconversion can be combined with serial intravascular staining to study the spatiotemporal localization of Peyer´s patches-derived T-cells

In this thesis, we present an application of SIVS in mouse models, which has allowed us to gain valuable insights into leukocyte trafficking. Additionally, we demonstrated the advantages of combining SIVS with photoconversion, which enhanced our understanding of this process. This approach allows for the investigation of leukocyte migration in both healthy mice and during GvHD development.

Through SIVS, we categorized T-cells directly migrating from PP and bloodborne donor T-cells infiltrating intestinal *LP* into four distinct compartments based on their spatiotemporal localization: continuously circulating, currently circulating, recently infiltrating, and tissue localized (**Fig. 4.3**). By integrating photoconversion, we could track and analyze the movement of PP-derived donor T-cells, providing valuable insights into the dynamics of leukocyte trafficking in these contexts. Moreover, we successfully distinguished between PP-derived donor T-cells (converted) and bloodborne T-cells (unconverted) that infiltrated *LP*. This novel combination holds promise for advancing our knowledge of immune cell behavior and its role in health and disease.

5.2.3. Peyer's patches-derived T-cells directly infiltrated the *lamina propria* before bloodborne T-cells

We used SIVS and photoconversion to study the direct migration of donor T-cells from PP to *LP* and its impact on bloodborne T-cell recruitment. Flow cytometry analysis revealed a decrease in the proportion of directly migrated T-cells in *LP* from 57% to 19% between day +2 and +4 after allo-HCT. Concomitantly, the percentage of bloodborne-derived donor T-cells infiltrating *LP* increased (**Fig. 4.5 b-c**). Directly migrated T-cells were the dominant population early after allo-HCT, implying that direct PP-to-*LP* T-cell migration led to faster recruitment of donor T-cells than the vasculature route. We hypothesize that direct T-cell migration from PP to *LP* is a general mechanism in mucosal immunity not restricted to the allo-setting. In this regard, the faster recruitment of cells to the *LP* implies that intruders can be effectively halted from spreading to distant body sites. Consequently, direct PP-to-*LP* T-cell migration can prevent pathogen spread to other organs or individuals and efficiently contain and combat infections within the mucosal tissues.

Ex-vivo two-photon quantifications conducted on day +3,5 after allo-HCT in a myeloablative irradiated model showed that close to PPs, around 50% of the donor T-cells originated directly from PP, while the other half entered tissue from circulation (**Fig. 1.6 d**). These results suggested that there may be differences in kinetics between the two models. Alternatively, there could be a bias due to *ex-vivo* two-photon quantifications focused exclusively on the region adjacent to PP, while flow cytometry analysis considered the entire *LP* after removing PPs.

Additionally, we observed that most donor T-cells migrating directly from PP to *LP* were $CD4^+$ T-cells at the analyzed time points. Consequently, our findings aligned with our expectation of predominantly observing $CD4^+$ T-cells around PP early after allo-HCT and are consistent with the role of $CD4^+$ T-cells as cytokine producers, attracting T-cells from circulation (**Fig. 4.10**).

On the other hand, bloodborne T-cells infiltrating *LP* exhibited a sequential infiltration pattern, with $CD4^+$ T-cells preceding the infiltration of $CD8^+$ T-cells (**Fig. 4.5 d**). In our observations, 47% of the unconverted T-cells detected in *LP* on day +2 after allo-HCT showed positive staining with the CD45 antibody infusion administered 5 min before *ex-vivo* analysis. We hypothesized that these donor T-cells in the perivascular compartment of the small intestine were not actively trafficking but rather in the process of extravasation from the bloodstream (**Fig. 4.5 e**).

Importantly, we observed that photoconverted $CD4^+$ and $CD8^+$ donor T-cells, which originated from PP and directly infiltrated *LP*, were not stained with the CD45 antibody infusion performed 90 or 5 min before *ex-vivo.* This finding provided additional confirmation that these T-cells were localized within the tissue and did not infiltrate through the conventional process of blood extravasation (**Fig. 4.5 e**).

5.3. Phenotyping of alloreactive T-cells directly migrating from Peyer´s patches to intestinal *lamina propria*

5.3.1. Alloreactive T-cells directly migrating from Peyer´s patches to *lamina propria* were activated, proliferated, secreted TNF-α and IFN-γ and had a T_H1-like T_H17 cell phenotype

We used flow cytometry to characterize the donor T-cells migrating from PP to adjacent *LP*. We observed that donor T-cells infiltrating *LP* on day +3 after allo-HCT exhibited activation markers ($CD25^+$, $CD44^+$, $CD62\text{-}L^+$) and proliferation marker ($Ki67^+$), indicating their alloreactivity (**Fig. 4.6 a**). Given that aGvHD is primarily driven by T_H1 and T_H17 alloreactive T-cells infiltrating target organs (Ferrara et al., 2009), we investigated the transcription factors, namely Tbet and RORγt, as well as the cytokine production associated with these T-cell subsets, by donor T-cells isolated from the

intestinal *LP* early after allo-HCT. The role of IFN-γ during aGvHD progression has been widely known and discussed. Early after allo-HCT, T-cells are polarized into a T_H1 phenotype, producing IL-2 and IFN-γ, establishing a positive feedback cycle and hyperinflammation. IFN-γ production by alloreactive T-cells plays a significant role in the apoptosis of intestinal stem cells and intestinal damage (Takashima et al., 2019). Additionally, IFN-γ induces expression of CXCL9-11, which attracts $CXCR3^+$ alloreactive T-cells to target organs (Bouazzaoui et al., 2009).

Flow cytometry analysis revealed that donor T-cells infiltrating intestinal *LP* on day +3 after allo-HCT co-expressed transcription factors $Tbet^+$ and $ROR\gamma t^+$ (**Fig. 4.6 b**), indicating that this early infiltrating donor T-cells that directly migrate from PP to *LP* have a T_H1-like T_H17 phenotype. This cytokine profile shift is highly pathogenic in preclinical models of GvHD (Gartlan et al., 2017), and is associated with increased pathogenicity in various diseases, including colitis (Lee et al., 2009), Crohn's disease (Annunziato et al., 2007), arthritis (Nistala et al., 2010), diabetes (Bending et al., 2009), experimental autoimmune encephalomyelitis (Hirota et al., 2011), and multiple sclerosis (Kebir et al., 2009). Our analysis revealed that infiltrating donor T-cells in the *LP* produced T_H1-associated cytokines, including TNF-α and IFN-γ (**Fig. 4.6 d**). Furthermore, the concentration of IFN-γ was found to be higher in the *LP* near PP compared to the *LP* further away on day +3 after allo-HCT, suggesting that donor T-cells directly migrating from PP to *LP* were responsible for local IFN-γ production (**Fig. 4.6 c**). However, the detection of T_H17-associated cytokines IL-17A and GM-CSF was not observed, possibly due to the transient nature of IL-17 secretion by T_H17 cells. Future studies using fate-reporter-based systems might provide better tracking of T_H17 cells (Hirota et al., 2011).

In summary, we provided evidence that activated and proliferating donor T-cells migrated from PPs to adjacent *LP* early after allo-HCT. These results were expected, considering that naïve T-cells are not typically found in the peripheral tissues. Supporting the notion that the donor T-cells directly migrating to the *LP* were previously activated in the PPs. Surprisingly, donor T-cells directly migrating from PP to *LP* had a T_H1-like T_H17 phenotype, this correlates with higher cytokine coexpression, and therefore, a more proinflammatory phenotype. These observations make the donor T-cells migrating from PP to *LP* an attractive target for blocking or preventing gut GvHD.

Furthermore, targeting the proinflammatory phenotype of these migrating T-cells could also be beneficial. Modulating the expression or activity of cytokines or other molecules associated with the T_H1-like T_H17 phenotype may help mitigate the inflammatory response in the intestines and decrease GvHD severity.

5.3.2. Alloreactive T-cells directly migrating from Peyer´s patches *to lamina propria* expressed α_4^+ α_E^+ and α_L^+ integrins, and CxCR3$^+$, CCR5$^+$, CCR9$^+$ chemokines receptors

Additionally, we compared the expression of integrins and chemokine-coupled receptors on donor T-cells that invaded *LP* mice with those located in PPs and mLN, respectively. We observed high expression of α_L integrin in PPs and *LP*, consistent with its role as a critical cell adhesion molecule in T-cell trafficking, migration, and interactions with other immune cells (**Fig. 4.6 e**). α_L integrin (CD11a), forms a heterodimer with β2 integrin (CD18), forming the adhesion molecule LFA-1 (CD11a/CD18). LFA-1 is primarily expressed in leukocytes, including T-cells, and binds to ICAM-1, ICAM-2, and ICAM-3 (Fu et al., 2016).

Furthermore, we observed a higher percentage of donor T-cells in *LP* expressing α_4 integrin and α_E integrin than PPs. Specifically, 19% of donor CD4$^+$ T-cells and 56% of donor CD8$^+$ T-cells in *LP* expressed α_4 integrin, while 15% of donor CD4$^+$ T-cells and 48% of donor CD8$^+$ T-cells in *LP* expressed α_E integrin (**Fig. 4.6 e**). These findings suggest that T-cells in *LP* are better equipped for homing to gut mucosa and other gut-associated tissues. Expression of α_E integrin allows binding to E-cadherin on intestinal epithelial cells, enabling T-cell localization and interaction with gut epithelium (Cheroutre et al., 2011). α_4 integrin forms heterodimers with β1 integrin (VLA-4) and β7 integrin (lymphocyte PP adhesion molecule or (LPAM). $\alpha_4\beta_1$ integrin binds to collagen and laminin in the extracellular matrix and VCAM-1 on endothelial cells. In contrast, $\alpha_4\beta_7$ integrin binds to MAdCAM-1, VCAM-1, and fibronectin promoting T-cell adhesion and migration within the gut mucosa (Beilhack et al., 2008; Hammerschmidt et al., 2008). During GvHD, donor T-cells that infiltrate the gut epithelium express $\alpha_E\beta_7$ (Zhou et al., 2008) and $\alpha_4\beta_7$ (Beilhack et al., 2008; Iwata et al., 2004) integrins. Studies have demonstrated that blocking or deleting $\alpha_4\beta_7$ (Gorfu et al., 2009; Schreder et al., 2015) or CD103 in donor T-cells can improve GvHD outcomes. Overall, the higher expression of α_4 and α_E integrin in donor T-cells in *LP* compared to PPs was consistent

with the high activation state of T-cells in *LP*, suggesting that these cells may have a higher capacity to migrate and interact with intestinal tissue.

In addition, we found that neither $CD4^+$ T-cells nor $CD8^+$ donor T-cells in mLN expressed CCR9, a chemokine receptor crucial for T-cell migration and homing to gut mucosa (Iwata et al., 2004). Nevertheless, we discovered a subpopulation of donor T-cells in *LP* that expressed CCR9 (**Fig. 4.6 e**). These findings were consistent with their activation status and indicate that donor T-cells in *LP* became more activated and differentiated than those in mLN on day +3,5 after allo-HCT (**Fig. 4.6 a**).

T_H1 cells express specific chemokine receptors that regulate their migration into inflammatory tissues and play relevant roles in aGvHD. These include CXCR3, which recognizes CXCL9-11, and CCR5, which recognizes CCL3-5 (Bouazzaoui et al., 2009; Fu et al., 2016; Moy et al., 2017). Our study examined the expression of CXCR3 and CCR5 in donor T-cells migrating directly from PP to *LP* after allo-HCT. We found that a subset of T-cells in both *LP* and mLN expressed CXCR3, with higher expression observed in *LP* compared to mLN (**Fig. 4.6 e**). On the other hand, we observed higher expression of CCR5 in mLN compared to *LP*.

These findings indicate that T-cells involved in GvHD pathogenesis exhibit distinct patterns of chemokine receptor expression that contribute to their migration and recruitment to inflammatory sites. Flow cytometry provided valuable insights into the phenotype and functional properties of T-cells migrating from PP to *LP* early after allo-HCT. These molecules play a crucial role in GvHD pathogenesis, and the process of T-cell infiltration into the tissue through extravasation. However, the specific involvement of integrins and chemokine-coupled receptors in the direct migration of T-cells from PP to *LP* remains to be fully understood. To address this, our subsequent investigations aimed to mechanistically explore the relevance of integrins and chemokine receptors in facilitating direct PP-to-*LP* T-cell migration.

5.4. Integrins or chemokines did not mediate direct T-cell migration from Peyer's patch to *lamina propria*

Previously, we confirmed that S1PR1 or topographical features of macrophages did not mediate egress from PPs to *LP* (**1.4.3** and **1.4.4)**. However, the potential role of other lipid chemoattractants in directing PP-to-*LP* T-cell migration requires further investigation. Highly diffusible lipid chemoattractants can be generated quickly and exert control over T-cell migration. For example, leukotrienes such as leukotriene B4 (LTB4) act as potent leukocyte chemoattractants in inflammation. LTB4, acts through two G protein-coupled receptors: BLT1 (high-affinity receptor) and BLT2 (low-affinity receptor). Both receptors primarily couple to PTx-sensitive Gi-like G proteins and play a significant role in inducing cell migration (Yokomizo, 2015).The upregulation of the high-affinity LTB4 receptor (BLT1) in effector T-cells mediates their early recruitment to inflamed tissues (Sadik and Luster, 2012).

Other molecular candidates that we hypothesized might be facilitating this process were integrins and chemokines. We investigated the role of integrins and chemokines in T-cell migration from PP to *LP.* Using LSFM, we quantified the density of donor T-cells around PP in mice treated with integrin-blocking antibodies or PTx, compared to control mice receiving PBS or a mutant version of PTx (**Fig. 4.9 a**). Surprisingly, even after blocking integrins, LTB4 receptors and chemokine-coupled receptors, we observed a gradient of donor T-cells on day +3,5 post-transplant. This showed that T-cells required neither integrins nor chemokines or LTB4 to migrate directly from PP to *LP*. If chemokines LTB4, or integrins were essential for this migration, we would not have observed a gradient of donor T-cells around PP in mice treated with PTx or integrin-blocking antibodies (**Fig. 4.9 b**). These results align with our previous findings from intravital two-photon microscopy, which demonstrated that T-cells directly exiting PPs migrated randomly, suggesting that they were not following a chemoattractant gradient (**Fig. 1.6 e-f**).

Intriguingly, PTx treatment enhanced the number of donor T-cells in the *LP* region surrounding PP compared to mice treated with the mutant version of PTx (**Fig. 4.9 b**). These findings suggested that direct PP-to-*LP* T-cell migration is increased by chemokine sequestration loss, most likely because of decreased CCL19 and CCL21 chemokine detection after CCR7 downregulation. To investigate this hypothesis, we

can perform experiments using donor T-cells that overexpress CCR7. If the loss of chemokine sequestration is the mechanism involved, CCR7-overexpressing T-cells would remain retained in the PPs rather than migrating to the *LP*. Furthermore, we can assess the presence of a T-cell gradient from PPs to *LP* in a healthy mouse by inhibiting PTx or blocking antibodies against CCL19 or CCL21.

We used laser-capture microdissection of intestinal tissue to isolate *LP* close to PPs (0-500 m) and regions further distant (>1500 m) to identify additional molecular candidates involved in the attraction of T-cells to the *LP*. Among the 143 differentially expressed genes, we observed the upregulation of several transcripts encoding proteins involved in cytoskeletal dynamics and cell motility in the *LP* adjacent to PP. These included Dock2, Coro1-α, Parvin-γ, and Rac2 (unpublished data medical thesis of Lukas Scheller). Additionally, we confirmed the expression of Coro1-α and Parvin-γ in donor T-cells that directly migrated from PP using immunofluorescence microscopy. Based on these findings, we propose that mediators involved in cytoskeleton reorganization may play a role in direct PP-to-*LP* T-cell migration. To further investigate this hypothesis, we plan to compare knockout donor T-cells lacking Coro1a, Dock2, or Cdc42 genes with wild-type mice. By doing so, we aim to analyze whether the knockout T-cells can still leave PP and migrate into *LP.*

5.5. Directly migrated T-cells appear to induce secondary recruitment of additional bloodborne activated T-cells

We hypothesized that the presence of directly migrating T-cells in *LP* adjacent to PPs might create a local inflammatory microenvironment that attracts circulating T-cells. We conducted two experiments to investigate the potential role of directly migrating T-cells in attracting additional T-cells from the bloodstream.

In the first experiment, we transferred photoconvertible T-cells into haploidentical unirradiated F1 recipients and photoconverted them in PPs on day +2 after allo-HCT (**Fig. 4.10 a**). Through immunofluorescence microscopy, we were able to confirm the colocalization of bloodborne T-cells (unconverted) with PP-derived T-cells (converted) infiltrating *LP* early after allo-HCT (**Fig. 4.10 b**). However, we decided to pursue alternative experiments to address any concerns regarding the possibility of unconverted T-cells originating from partially converted PPs.

In the second set of experiments, we directly transferred activated T-cells into the vasculature of mice developing GvHD. Specifically, we transferred 4 days of *in-vitro*-activated DsRed T-cells into the vasculature of mice developing GvHD on day +2 or +3 after allo-HCT. On day +4, we embedded PPs and employed immunofluorescence microscopy to evaluate the colocalization between T-cells directly migrating from PP (Dendra2) and bloodborne activated T-cells (DsRed) infiltrating *LP* after allo-HCT (**Fig. 4.10 c** and **Fig. 4.11 a**). The findings from immunofluorescence microscopy confirmed that directly migrating T-cells recruited activated T-cells to the intestinal *LP*, particularly in regions adjacent to PPs (**Fig. 4.10 h** and **Fig. 4.11 a**).

We determined the minimal distance between an activated T-cell and a directly migrated T-cell and observed that most of the activated T-cells were in close vicinity to directly migrating alloreactive T-cells, confirming their recruitment (**Fig. 4.11 d**). To further ensure the recruitment of activated T-cells by T-cells migrating directly from PP, we conducted a sham control experiment in healthy mice that got the adoptive transfer of activated T-cells one day before *ex-vivo*. Through immunofluorescence microscopy, we observed that activated T-cells are exclusively located in SLOs, with no infiltration of the intestinal mucosa (**Fig. 4.11 c**). Overall, these observations support the idea that the directly migrating T-cells act as seed cells, attracting and recruiting additional activated T-cells from the bloodstream to the site of inflammation.

Based on our previous results, which involved *in-vitro* polyclonal activation of T-cells using CD3 and CD28 antibodies, we observed that directly migrating T-cells serve as "seed cells" capable of attracting activated T-cells from the bloodstream, regardless of T-cell specificity (**Fig. 4.10 h** and **Fig. 4.11 a**). To further investigate this phenomenon, we conducted pilot experiments where we transferred *in-vitro*-activated antigen non-specific OT-1 or OT-2 T-cells into mice developing GvHD. Remarkably, we observed colocalization between directly migrating T-cells and bloodborne T-cells in *LP* adjacent to PPs (data not shown). These findings strongly suggest that vascular recruitment of activated T-cells to *LP*, adjacent to directly migrating T-cells, can occur irrespective of their antigen specificity. This indicates the presence of antigen-non-specific mechanisms contributing to the vascular recruitment process.

To investigate the role of chemokines and integrins in the vascular recruitment of activated T-cells by T-cells migrating from PP to *LP*, we performed similar experiments adding the administrating of either integrin-blocking antibodies or PTx on day +2 after allo-HCT (**Fig. 4.11 a**). We selected this timing to precede the transfer of activated T-cells on the subsequent day. Immunofluorescence microscopy analysis of the small intestine showed that activated T-cells were unable to extravasate from the bloodstream when integrins were blocked, indicating the efficacy of our integrin-blocking antibodies in inhibiting T-cell migration across the endothelial barrier (Ley et al., 2007) (**Fig. 4.11 c**). Interestingly, inhibition of chemokine-coupled receptors did not impair the recruitment of T-cells from circulation or direct migration of donor T-cells from PP to *LP*, suggesting that chemokines may not be the primary mediators involved in these processes (**Fig. 4.11 c**).

Based on our results, which demonstrated that blocking chemokine-coupled receptors did not affect the recruitment of T-cells from the vasculature, we hypothesize that cytokines released by directly migrating donor T-cells may be involved in their vascular recruitment. To test this hypothesis, we will transfer knockout T-cells deficient in producing cytokines such as IFN-γ, IL-18, GM-CSF, GM-CSF/IL7R, and TNF-α into recipient animals. On day +3 after allo-HCT, we will transfer in-vitro-activated T-cells and evaluate their vascular recruitment. By comparing the recruitment of the transferred activated T-cells by directly migrating T-cells in the presence and absence of specific cytokines, we aim to elucidate the role of cytokines produced by directly migrating T-cells in the vascular recruitment process.

We postulate that direct migration of antigen-specific T-cells from PPs to *LP* allows the immune system to concentrate its response in areas where pathogens and antigens are more likely to be encountered. This targeted response allows for more efficient and effective immune surveillance of the intestinal environment. Additionally, the recruitment of circulating activated T-cells to *LP* further amplifies the immune response in this specific region, ensuring a robust defense against potential threats. Alongside resident immune cells and rapid recruitment of neutrophils, the egress of highly specific T-cells from PPs to *LP*, in conjunction with the associated vascular recruitment of activated T-cells, directs systemic immune attention to those areas.

6. Conclusion

Our findings reveal a new route of T-cell entry into the small intestine, independent of vascular extravasation. A subset of alloreactive T-cells migrates directly from PPs to *LP* of the intestine. Therefore, this alternative route should be considered in future therapeutic approaches for treating gastrointestinal GvHD, as blocking extravasation alone will not effectively prevent alloreactive T-cell infiltration.

The significance of antigen-specific T-cells entering *LP* through direct migration is still being investigated, but we propose that it is a general mechanism in intestinal immunity. T-cells entering *LP* via direct migration could have dual effects: protecting against invading pathogens or contributing to harmful reactions against commensal bacteria or intestinal antigens. Therefore, we could leverage the direct PP-to-*LP* T-cell migration pathway to develop targeted vaccination strategies. By directing antigens to PPs, it may be possible to induce local T-cell memory near the site of pathogen entry, thereby enhancing the effectiveness of the immune response. Moreover, we hypothesize that Tregs generated in response to food proteins in PPs can migrate directly to *LP*, contributing to oral tolerance to food proteins. Other cell types, such as B-cells, may also directly exit PPs and migrate into *LP*.

The discovery of direct T-cell migration to intestinal *LP* might have implications for understanding intestinal infections, inflammatory bowel diseases, oral tolerance, and potential vaccination strategies.

7. References

Abbas, A.K., Lichtman, A.H., Pillai, S., 2017. Cellular and Molecular Immunology. Elsevier Health Sciences.

Abdelsamed, H.A., Lakkis, F.G., 2021. The role of self-peptides in direct T cell allorecognition. J. Clin. Invest. 131. https://doi.org/10.1172/JCI154096

Abram, C.L., Lowell, C.A., 2009. The Ins and Outs of Leukocyte Integrin Signaling. Annu. Rev. Immunol. 27, 339–362. https://doi.org/10.1146/annurev.immunol.021908.132554

Anderson, K.G., Mayer-Barber, K., Sung, H., Beura, L., James, B.R., Taylor, J.J., Qunaj, L., Griffith, T.S., Vezys, V., Barber, D.L., Masopust, D., 2014. Intravascular staining for discrimination of vascular and tissue leukocytes. Nat. Protoc. 9, 209–222. https://doi.org/10.1038/nprot.2014.005

Annunziato, F., Cosmi, L., Santarlasci, V., Maggi, L., Liotta, F., Mazzinghi, B., Parente, E., Filì, L., Ferri, S., Frosali, F., Giudici, F., Romagnani, P., Parronchi, P., Tonelli, F., Maggi, E., Romagnani, S., 2007. Phenotypic and functional features of human Th17 cells. J. Exp. Med. 204, 1849–1861. https://doi.org/10.1084/jem.20070663

Asavaroengchai, W., Wang, H., Wang, S., Wang, L., Bronson, R., Sykes, M., Yang, Y.-G., 2007. An Essential Role for IFN-γ in Regulation of Alloreactive CD8 T Cells Following Allogeneic Hematopoietic Cell Transplantation. Biol. Blood Marrow Transplant. J. Am. Soc. Blood Marrow Transplant. 13, 46–55. https://doi.org/10.1016/j.bbmt.2006.09.014

Azarov, I., Peskov, K., Helmlinger, G., Kosinsky, Y., 2019. Role of T Cell-To-Dendritic Cell Chemoattraction in T Cell Priming Initiation in the Lymph Node: An Agent-Based Modeling Study. Front. Immunol. 10.

Bader, P., Kuçi, Z., Bakhtiar, S., Basu, O., Bug, G., Dennis, M., Greil, J., Barta, A., Kállay, K.M., Lang, P., Lucchini, G., Pol, R., Schulz, A., Sykora, K.-W., Luettichau, I. von, Herter-Sprie, G., Uddin, M.A., Jenkin, P., Alsultan, A., Buechner, J., Stein, J., Kelemen, A., Jarisch, A., Soerensen, J., Salzmann-Manrique, E., Hutter, M., Schäfer, R., Seifried, E., Klingebiel, T., Bonig, H., Kuçi, S., 2018. Effective treatment of steroid and therapy-refractory acute graft-versus-host disease with a novel mesenchymal stromal cell product (MSC-FFM). Bone Marrow Transplant. 1. https://doi.org/10.1038/s41409-018-0102-z

Bajénoff, M., Egen, J.G., Koo, L.Y., Laugier, J.P., Brau, F., Glaichenhaus, N., Germain, R.N., 2006. Stromal cell networks regulate lymphocyte entry, migration, and territoriality in lymph nodes. Immunity 25, 989–1001. https://doi.org/10.1016/j.immuni.2006.10.011

Beilhack, A., Schulz, S., Baker, J., Beilhack, G.F., Nishimura, R., Baker, E.M., Landan, G., Herman, E.I., Butcher, E.C., Contag, C.H., Negrin, R.S., 2008. Prevention of acute graft-versus-host disease by blocking T-cell entry to secondary lymphoid organs. Blood 111, 2919–2928. https://doi.org/10.1182/blood-2007-09-112789

Beilhack, A., Schulz, S., Baker, J., Beilhack, G.F., Wieland, C.B., Herman, E.I., Baker, E.M., Cao, Y.-A., Contag, C.H., Negrin, R.S., 2005. In vivo analyses of early events in acute graft-versus-host disease reveal sequential infiltration of T-cell subsets. Blood 106, 1113–1122. https://doi.org/10.1182/blood-2005-02-0509

Bekkum, D.W. van, Roodenburg, J., Heidt, P.J., Waaij, D. van der, 1974. Mitigation of Secondary Disease of Allogeneic Mouse Radiation Chimeras by Modification of the Intestinal Microflora. JNCI J. Natl. Cancer Inst. 52, 401–404. https://doi.org/10.1093/jnci/52.2.401

Beltman, J.B., Marée, A.F.M., Lynch, J.N., Miller, M.J., de Boer, R.J., 2007. Lymph node topology dictates T cell migration behavior. J. Exp. Med. 204, 771–780. https://doi.org/10.1084/jem.20061278

Benichou, G., Thomson, A.W., 2009. Direct versus Indirect Allorecognition Pathways: On the Right Track. Am. J. Transplant. Off. J. Am. Soc. Transplant. Am. Soc. Transpl. Surg. 9, 655–656. https://doi.org/10.1111/j.1600-6143.2009.02572.x

Bensussen, A., Santana, M.A., Rodríguez-Jorge, O., 2022. Metabolic alterations impair differentiation and effector functions of CD8+ T cells. Front. Immunol. 13.

Bergert, M., Erzberger, A., Desai, R.A., Aspalter, I.M., Oates, A.C., Charras, G., Salbreux, G., Paluch, E.K., 2015. Force transmission during adhesion-independent migration. Nat. Cell Biol. 17, 524–529. https://doi.org/10.1038/ncb3134

Boissonnas, A., Fetler, L., Zeelenberg, I.S., Hugues, S., Amigorena, S., 2007. In vivo imaging of cytotoxic T cell infiltration and elimination of a solid tumor. J. Exp. Med. 204, 345–356. https://doi.org/10.1084/jem.20061890

Bouazzaoui, A., Spacenko, E., Mueller, G., Miklos, S., Huber, E., Holler, E., Andreesen, R., Hildebrandt, G.C., 2009. Chemokine and chemokine receptor expression analysis in target organs of acute graft-versus-host disease. Genes Immun. 10, 687–701. https://doi.org/10.1038/gene.2009.49

Bousso, P., Robey, E., 2003. Dynamics of CD8+ T cell priming by dendritic cells in intact lymph nodes. Nat. Immunol. 4, 579–585. https://doi.org/10.1038/ni928

Breedveld, A., van Egmond, M., 2019. IgA and FcαRI: Pathological Roles and Therapeutic Opportunities. Front. Immunol. 10,

553. https://doi.org/10.3389/fimmu.2019.00553

Browse, N.L., Doig, R.L., Sizeland, D., 1984. The resistance of a lymph node to lymph flow. Br. J. Surg. 71, 192–196. https://doi.org/10.1002/bjs.1800710308

Castellino, F., Huang, A.Y., Altan-Bonnet, G., Stoll, S., Scheinecker, C., Germain, R.N., 2006. Chemokines enhance immunity by guiding naive CD8+ T cells to sites of CD4+ T cell-dendritic cell interaction. Nature 440, 890–895. https://doi.org/10.1038/nature04651

Cheroutre, H., Lambolez, F., Mucida, D., 2011. The light and dark sides of intestinal intraepithelial lymphocytes. Nat. Rev. Immunol. 11, 445–456. https://doi.org/10.1038/nri3007

Cherrier, M., Sawa, S., Eberl, G., 2012. Notch, Id2, and RORγt sequentially orchestrate the fetal development of lymphoid tissue inducer cells. J. Exp. Med. 209, 729–740. https://doi.org/10.1084/jem.20111594

Coelho, F.M., Natale, D., Soriano, S.F., Hons, M., Swoger, J., Mayer, J., Danuser, R., Scandella, E., Pieczyk, M., Zerwes, H.-G., Junt, T., Sailer, A.W., Ludewig, B., Sharpe, J., Figge, M.T., Stein, J.V., 2013. Naive B-cell trafficking is shaped by local chemokine availability and LFA-1-independent stromal interactions. Blood 121, 4101–4109. https://doi.org/10.1182/blood-2012-10-465336

Commins, S.P., 2015. Mechanisms of Oral Tolerance. Pediatr. Clin. North Am. 62, 1523–1529. https://doi.org/10.1016/j.pcl.2015.07.013

Cook, D.N., Smithies, O., Strieter, R.M., Frelinger, J.A., Serody, J.S., 1999. CD8+ T cells are a biologically relevant source of macrophage inflammatory protein-1 alpha in vivo. J. Immunol. Baltim. Md 1950 162, 5423–5428.

Cornes, J.S., 1965. Number, size, and distribution of Peyer's patches in the human small intestine: Part I The development of Peyer's patches. Gut 6, 225–229. https://doi.org/10.1136/gut.6.3.225

Cose, S., Brammer, C., Khanna, K.M., Masopust, D., Lefrançois, L., 2006. Evidence that a significant number of naive T cells enter non-lymphoid organs as part of a normal migratory pathway. Eur. J. Immunol. 36, 1423–1433. https://doi.org/10.1002/eji.200535539

Crees, Z.D., Rettig, M.P., Jayasinghe, R.G., Stockerl-Goldstein, K., Larson, S.M., Arpad, I., Milone, G.A., Martino, M., Stiff, P., Sborov, D., Pereira, D., Micallef, I., Moreno-Jiménez, G., Mikala, G., Coronel, M.L.P., Holtick, U., Hiemenz, J., Qazilbash, M.H., Hardy, N., Latif, T., García-Cadenas, I., Vainstein-Haras, A., Sorani, E., Gliko-Kabir, I., Goldstein, I., Ickowicz, D., Shemesh-Darvish, L., Kadosh, S., Gao, F., Schroeder, M.A., Vij, R., DiPersio, J.F., 2023. Motixafortide and G-CSF to mobilize hematopoietic stem cells for autologous transplantation in multiple myeloma: a randomized phase 3 trial. Nat. Med. 29, 869–879. https://doi.org/10.1038/s41591-023-02273-z

Cyster, J.G., Schwab, S.R., 2012. Sphingosine-1-phosphate and lymphocyte egress from lymphoid organs. Annu. Rev. Immunol. 30, 69–94. https://doi.org/10.1146/annurev-immunol-020711-075011

Dean, D., Sroussi, H., 2022. Oral Chronic Graft-Versus-Host Disease. Front. Oral Health 3.

DeSimone, D.W., Horwitz, A.R., 2014. Cell Biology. Many modes of motility. Science 345, 1002–1003. https://doi.org/10.1126/science.1259176

Diaz, M.A., Gasior, M., Molina, B., Pérez-Martínez, A., González-Vicent, M., 2021. "Ex-vivo" T-cell depletion in allogeneic hematopoietic stem cell transplantation: New clinical approaches for old challenges. Eur. J. Haematol. 107, 38–47. https://doi.org/10.1111/ejh.13636

D'Souza, A., Fretham, C., Lee, S.J., Arora, M., Brunner, J., Chhabra, S., Devine, S., Eapen, M., Hamadani, M., Hari, P., Pasquini, M.C., Perez, W., Phelan, R.A., Riches, M.L., Rizzo, J.D., Saber, W., Shaw, B.E., Spellman, S.R., Steinert, P., Weisdorf, D.J., Horowitz, M.M., 2020. Current Use of and Trends in Hematopoietic Cell Transplantation in the United States. Biol. Blood Marrow Transplant. 26, e177–e182. https://doi.org/10.1016/j.bbmt.2020.04.013

Egen, J.G., Rothfuchs, A.G., Feng, C.G., Horwitz, M.A., Sher, A., Germain, R.N., 2011. Intravital imaging reveals limited antigen presentation and T cell effector function in mycobacterial granulomas. Immunity 34, 807–819. https://doi.org/10.1016/j.immuni.2011.03.022

Eickhoff, S., Brewitz, A., Gerner, M.Y., Klauschen, F., Komander, K., Hemmi, H., Garbi, N., Kaisho, T., Germain, R.N., Kastenmüller, W., 2015. Robust Anti-viral Immunity Requires Multiple Distinct T Cell-Dendritic Cell Interactions. Cell 162, 1322–1337. https://doi.org/10.1016/j.cell.2015.08.004

Fang, V., Chaluvadi, V.S., Ramos-Perez, W.D., Mendoza, A., Baeyens, A., Rivera, R., Chun, J., Cammer, M., Schwab, S.R., 2017. Gradients of the signaling lipid S1P in lymph nodes position natural killer cells and regulate their interferon-γ response. Nat. Immunol. 18, 15–25. https://doi.org/10.1038/ni.3619

Ferrara, J.L.M., Levine, J.E., Reddy, P., Holler, E., 2009. Graft-versus-Host Disease. Lancet 373, 1550–1561. https://doi.org/10.1016/S0140-6736(09)60237-3

Ferrara, J.L.M., Smith, C.M., Sheets, J., Reddy, P., Serody, J.S., 2017. Altered homeostatic regulation of innate and adaptive

immunity in lower gastrointestinal tract GVHD pathogenesis. J. Clin. Invest. 127, 2441–2451. https://doi.org/10.1172/JCI90592

Ford, W.L., Gowans, J.L., 1968. [Lymphocyte circulation in the rat]. Nouv. Rev. Fr. Hematol. 8, 509–518.

Ford, W.L., Simmonds, S.J., 1972. The tempo of lymphocyte recirculation from blood to lymph in the rat. Cell Tissue Kinet. 5, 175–189. https://doi.org/10.1111/j.1365-2184.1972.tb01014.x

Fredricks, D.N., 2019. The gut microbiota and graft-versus-host disease. J. Clin. Invest. 129, 1808–1817. https://doi.org/10.1172/JCI125797

Ft, H., So, S., S, P., Gm, S., 1991. Repopulation of host lymphohematopoietic systems by donor cells during graft-versus-host reaction in unirradiated adult F1 mice injected with parental lymphocytes. J. Immunol. Baltim. Md 1950 146.

Fu, H., Ward, E.J., Marelli-Berg, F.M., 2016. Mechanisms of T cell organotropism. Cell. Mol. Life Sci. 73, 3009–3033. https://doi.org/10.1007/s00018-016-2211-4

Fu, Y.-Y., Egorova, A., Sobieski, C., Kuttiyara, J., Calafiore, M., Takashima, S., Clevers, H., Hanash, A.M., 2019. T Cell Recruitment to the Intestinal Stem Cell Compartment Drives Immune-Mediated Intestinal Damage after Allogeneic Transplantation. Immunity 51, 90-103.e3. https://doi.org/10.1016/j.immuni.2019.06.003

García-Cuesta, E.M., Rodríguez-Frade, J.M., Gardeta, S.R., D'Agostino, G., Martínez, P., Soler Palacios, B., Cascio, G., Wolf, T., Mateos, N., Ayala-Bueno, R., Santiago, C.A., Lucas, P., Llorente, L., Allende, L.M., González-Granado, L.I., Martín-Cófreces, N., Roda-Navarro, P., Sallusto, F., Sánchez-Madrid, F., García-Parajo, M.F., Martínez-Muñoz, L., Mellado, M., 2022. Altered CXCR4 dynamics at the cell membrane impairs directed cell migration in WHIM syndrome patients. Proc. Natl. Acad. Sci. 119, e2119483119. https://doi.org/10.1073/pnas.2119483119

Gartlan, K.H., Markey, K.A., Varelias, A., Bunting, M.D., Koyama, M., Kuns, R.D., Raffelt, N.C., Olver, S.D., Lineburg, K.E., Cheong, M., Teal, B.E., Lor, M., Comerford, I., Teng, M.W.L., Smyth, M.J., McCluskey, J., Rossjohn, J., Stockinger, B., Boyle, G.M., Lane, S.W., Clouston, A.D., McColl, S.R., MacDonald, K.P.A., Hill, G.R., 2015. Tc17 cells are a proinflammatory, plastic lineage of pathogenic CD8+ T cells that induce GVHD without antileukemic effects. Blood 126, 1609–1620. https://doi.org/10.1182/blood-2015-01-622662

Gartlan, K.H., Varelias, A., Koyama, M., Robb, R.J., Markey, K.A., Chang, K., Wilkinson, A.N., Smith, D., Ullah, M.A., Kuns, R.D., Raffelt, N.C., Olver, S.D., Lineburg, K.E., Teal, B.E., Cheong, M., Teng, M.W.L., Smyth, M.J., Tey, S.-K., MacDonald, K.P.A., Hill, G.R., 2017. Th17 plasticity and transition toward a pathogenic cytokine signature are regulated by cyclosporine after allogeneic SCT. Blood Adv. 1, 341–351. https://doi.org/10.1182/bloodadvances.2016002980

Gervaz, P., Morel, P., Vozenin-Brotons, M.-C., 2009. Molecular aspects of intestinal radiation-induced fibrosis. Curr. Mol. Med. 9, 273–280. https://doi.org/10.2174/156652409787847164

Glucksberg, H., Storb, R., Fefer, A., Buckner, C.D., Neiman, P.E., Clift, R.A., Lerner, K.G., Thomas, E.D., 1974. Clinical manifestations of graft-versus-host disease in human recipients of marrow from HL-A-matched sibling donors. Transplantation 18, 295–304.

Gommerman, J.L., 2020. Intestinal protection without T cell help. Nat. Rev. Immunol. 20, 275–275. https://doi.org/10.1038/s41577-020-0280-y

Gooley, T.A., Chien, J.W., Pergam, S.A., Hingorani, S., Sorror, M.L., Boeckh, M., Martin, P.J., Sandmaier, B.M., Marr, K.A., Appelbaum, F.R., Storb, R., McDonald, G.B., 2010. Reduced mortality after allogeneic hematopoietic cell transplantation. N. Engl. J. Med. 363, 2091–2101. https://doi.org/10.1056/NEJMoa1004383

Gorfu, G., Rivera-Nieves, J., Ley, K., 2009. Role of β7 integrins in intestinal lymphocyte homing and retention. Curr. Mol. Med. 9, 836–850.

Graham, G.J., Handel, T.M., Proudfoot, A.E.I., 2019. Leukocyte Adhesion: Reconceptualizing Chemokine Presentation by Glycosaminoglycans. Trends Immunol. 40, 472–481. https://doi.org/10.1016/j.it.2019.03.009

Habtezion, A., Nguyen, L.P., Hadeiba, H., Butcher, E.C., 2016. Leukocyte Trafficking to the Small Intestine and Colon. Gastroenterology 150, 340–354. https://doi.org/10.1053/j.gastro.2015.10.046

Hammerschmidt, S.I., Ahrendt, M., Bode, U., Wahl, B., Kremmer, E., Förster, R., Pabst, O., 2008. Stromal mesenteric lymph node cells are essential for the generation of gut-homing T cells in vivo. J. Exp. Med. 205, 2483–2490. https://doi.org/10.1084/jem.20080039

Hanash, A.M., Dudakov, J.A., Hua, G., O'Connor, M.H., Young, L.F., Singer, N.V., West, M.L., Jenq, R.R., Holland, A.M., Kappel, L.W., Ghosh, A., Tsai, J.J., Rao, U.K., Yim, N.L., Smith, O.M., Velardi, E., Hawryluk, E.B., Murphy, G.F., Liu, C., Fouser, L.A., Kolesnick, R., Blazar, B.R., van den Brink, M.R.M., 2012. Interleukin-22 protects intestinal stem cells from immune-mediated tissue damage and regulates sensitivity to graft versus host disease. Immunity 37, 339–350. https://doi.org/10.1016/j.immuni.2012.05.028

Harris, T.H., Banigan, E.J., Christian, D.A., Konradt, C., Tait Wojno, E.D., Norose, K., Wilson, E.H., John, B., Weninger, W.,

Luster, A.D., Liu, A.J., Hunter, C.A., 2012. Generalized Lévy walks and the role of chemokines in migration of effector CD8+ T cells. Nature 486, 545–548. https://doi.org/10.1038/nature11098

Hashimoto, D., Chow, A., Greter, M., Saenger, Y., Kwan, W.-H., Leboeuf, M., Ginhoux, F., Ochando, J.C., Kunisaki, Y., van Rooijen, N., Liu, C., Teshima, T., Heeger, P.S., Stanley, E.R., Frenette, P.S., Merad, M., 2011. Pretransplant CSF-1 therapy expands recipient macrophages and ameliorates GVHD after allogeneic hematopoietic cell transplantation. J. Exp. Med. 208, 1069–1082. https://doi.org/10.1084/jem.20101709

Heidegger, S., van den Brink, M.R.M., Haas, T., Poeck, H., 2014. The Role of Pattern-Recognition Receptors in Graft-Versus-Host Disease and Graft-Versus-Leukemia after Allogeneic Stem Cell Transplantation. Front. Immunol. 5.

Helander, H.F., Fändriks, L., 2014. Surface area of the digestive tract - revisited. Scand. J. Gastroenterol. 49, 681–689. https://doi.org/10.3109/00365521.2014.898326

Hill, G.R., Betts, B.C., Tkachev, V., Kean, L.S., Blazar, B.R., 2021. Current Concepts and Advances in Graft-Versus-Host Disease Immunology. Annu. Rev. Immunol. 39, 19–49. https://doi.org/10.1146/annurev-immunol-102119-073227

Hill, G.R., Ferrara, J.L.M., 2000. The primacy of the gastrointestinal tract as a target organ of acute graft-versus-host disease: rationale for the use of cytokine shields in allogeneic bone marrow transplantation. Blood 95, 2754–2759. https://doi.org/10.1182/blood.V95.9.2754.009k25_2754_2759

Hill, L., Alousi, A., Kebriaei, P., Mehta, R., Rezvani, K., Shpall, E., 2018. New and emerging therapies for acute and chronic graft versus host disease. Ther. Adv. Hematol. 9, 21–46. https://doi.org/10.1177/2040620717741860

Hirota, K., Duarte, J.H., Veldhoen, M., Hornsby, E., Li, Y., Cua, D.J., Ahlfors, H., Wilhelm, C., Tolaini, M., Menzel, U., Garefalaki, A., Potocnik, A.J., Stockinger, B., 2011. Fate mapping of IL-17-producing T cells in inflammatory responses. Nat. Immunol. 12, 255–263. https://doi.org/10.1038/ni.1993

Holler, E., Greinix, H., Zeiser, R., 2019. Acute Graft-Versus-Host Disease, in: Carreras, E., Dufour, C., Mohty, M., Kröger, N. (Eds.), The EBMT Handbook: Hematopoietic Stem Cell Transplantation and Cellular Therapies. Springer International Publishing, Cham, pp. 323–330. https://doi.org/10.1007/978-3-030-02278-5_43

Holtan, S.G., Yu, J., Paranagama, D., Tang, J., Choe, H.K., Naim, A., Joachim Deeg, H., Galvin, J., 2022. Disease progression, hospital readmissions, and clinical outcomes for patients with steroid-refractory acute graft-versus-host disease: A multicenter, retrospective study. Bone Marrow Transplant. 57, 1399–1404. https://doi.org/10.1038/s41409-022-01736-0

Hong, W., Yang, B., He, Q., Wang, J., Weng, Q., 2022. New Insights of CCR7 Signaling in Dendritic Cell Migration and Inflammatory Diseases. Front. Pharmacol. 13, 841687. https://doi.org/10.3389/fphar.2022.841687

Hons, M., Kopf, A., Hauschild, R., Leithner, A., Gaertner, F., Abe, J., Renkawitz, J., Stein, J.V., Sixt, M., 2018. Chemokines and integrins independently tune actin flow and substrate friction during intranodal migration of T cells. Nat. Immunol. 19, 606–616. https://doi.org/10.1038/s41590-018-0109-z

Hunter, M.C., Teijeira, A., Halin, C., 2016. T Cell Trafficking through Lymphatic Vessels. Front. Immunol. 7, 613. https://doi.org/10.3389/fimmu.2016.00613

Iwata, M., Hirakiyama, A., Eshima, Y., Kagechika, H., Kato, C., Song, S.-Y., 2004. Retinoic Acid Imprints Gut-Homing Specificity on T Cells. Immunity 21, 527–538. https://doi.org/10.1016/j.immuni.2004.08.011

Iweala, O.I., Nagler, C.R., 2019. The Microbiome and Food Allergy. Annu. Rev. Immunol. 37, 377–403. https://doi.org/10.1146/annurev-immunol-042718-041621

Jagasia, M.H., Greinix, H.T., Arora, M., Williams, K.M., Wolff, D., Cowen, E.W., Palmer, J., Weisdorf, D., Treister, N.S., Cheng, G.-S., Kerr, H., Stratton, P., Duarte, R.F., McDonald, G.B., Inamoto, Y., Vigorito, A., Arai, S., Datiles, M.B., Jacobsohn, D., Heller, T., Kitko, C.L., Mitchell, S.A., Martin, P.J., Shulman, H., Wu, R.S., Cutler, C.S., Vogelsang, G.B., Lee, S.J., Pavletic, S.Z., Flowers, M.E.D., 2015. National Institutes of Health Consensus Development Project on Criteria for Clinical Trials in Chronic Graft-versus-Host Disease: I. The 2014 Diagnosis and Staging Working Group report. Biol. Blood Marrow Transplant. J. Am. Soc. Blood Marrow Transplant. 21, 389-401.e1. https://doi.org/10.1016/j.bbmt.2014.12.001

Jankowiak, G., Peurichard, D., Reversat, A., Schmeiser, C., Sixt, M., 2020. Modelling adhesion-independent cell migration. Math. Models Methods Appl. Sci. 30, 513–537. https://doi.org/10.1142/S021820252050013X

Jansen, S.A., Nieuwenhuis, E.E.S., Hanash, A.M., Lindemans, C.A., 2022. Challenges and opportunities targeting mechanisms of epithelial injury and recovery in acute intestinal graft-versus-host disease. Mucosal Immunol. 15, 605–619. https://doi.org/10.1038/s41385-022-00527-6

Jarick, K., 2020. Migration of allogenic T cells in intestinal lymphoid structures during acute Graft-versus-Host Disease. Universität Würzburg. https://doi.org/10.25972/OPUS-17875

Jarick, K.J., Mokhtari, Z., Scheller, L., Hartweg, J., Thusek, S., Le, D.-D., Ranecky, M., Shaikh, H., Qureischi, M., Heinze, K.G., Beilhack, A., 2018. Photoconversion of Alloreactive T Cells in Murine Peyer's Patches During Acute Graft-Versus-Host Disease:

Tracking the Homing Route of Highly Proliferative Cells In Vivo. Front. Immunol. 9. https://doi.org/10.3389/fimmu.2018.01468

Jenkins, M.K., Moon, J.J., 2012. The Role of Naive T Cell Precursor Frequency and Recruitment in Dictating Immune Response Magnitude. J. Immunol. 188, 4135–4140. https://doi.org/10.4049/jimmunol.1102661

Jenq, R.R., Taur, Y., Devlin, S.M., Ponce, D.M., Goldberg, J.D., Ahr, K.F., Littmann, E.R., Ling, L., Gobourne, A.C., Miller, L.C., Docampo, M.D., Peled, J.U., Arpaia, N., Cross, J.R., Peets, T.K., Lumish, M.A., Shono, Y., Dudakov, J.A., Poeck, H., Hanash, A.M., Barker, J.N., Perales, M.-A., Giralt, S.A., Pamer, E.G., Brink, M.R.M. van den, 2015. Intestinal Blautia Is Associated with Reduced Death from Graft-versus-Host Disease. Biol. Blood Marrow Transplant. 21, 1373–1383. https://doi.org/10.1016/j.bbmt.2015.04.016

Jenq, R.R., Ubeda, C., Taur, Y., Menezes, C.C., Khanin, R., Dudakov, J.A., Liu, C., West, M.L., Singer, N.V., Equinda, M.J., Gobourne, A., Lipuma, L., Young, L.F., Smith, O.M., Ghosh, A., Hanash, A.M., Goldberg, J.D., Aoyama, K., Blazar, B.R., Pamer, E.G., van den Brink, M.R.M., 2012. Regulation of intestinal inflammation by microbiota following allogeneic bone marrow transplantation. J. Exp. Med. 209, 903–911. https://doi.org/10.1084/jem.20112408

Kappel, L.W., Goldberg, G.L., King, C.G., Suh, D.Y., Smith, O.M., Ligh, C., Holland, A.M., Grubin, J., Mark, N.M., Liu, C., Iwakura, Y., Heller, G., van den Brink, M.R.M., 2009. IL-17 contributes to CD4-mediated graft-versus-host disease. Blood 113, 945–952. https://doi.org/10.1182/blood-2008-08-172155

Kastenmüller, W., Brandes, M., Wang, Z., Herz, J., Egen, J.G., Germain, R.N., 2013. Peripheral pre-positioning and local CXCL9 chemokine-mediated guidance orchestrate rapid memory CD8+ T cell responses in the lymph node. Immunity 38, 502–513. https://doi.org/10.1016/j.immuni.2012.11.012

Katakai, T., Habiro, K., Kinashi, T., 2013. Dendritic cells regulate high-speed interstitial T cell migration in the lymph node via LFA-1/ICAM-1. J. Immunol. Baltim. Md 191, 1188–1199. https://doi.org/10.4049/jimmunol.1300739

Katakai, T., Hara, T., Lee, J.-H., Gonda, H., Sugai, M., Shimizu, A., 2004. A novel reticular stromal structure in lymph node cortex: an immuno-platform for interactions among dendritic cells, T cells and B cells. Int. Immunol. 16, 1133–1142. https://doi.org/10.1093/intimm/dxh113

Katakai, T., Kinashi, T., 2016. Microenvironmental Control of High-Speed Interstitial T Cell Migration in the Lymph Node. Front. Immunol. 7, 194. https://doi.org/10.3389/fimmu.2016.00194

Kebir, H., Ifergan, I., Alvarez, J.I., Bernard, M., Poirier, J., Arbour, N., Duquette, P., Prat, A., 2009. Preferential recruitment of interferon-γ–expressing TH17 cells in multiple sclerosis. Ann. Neurol. 66, 390–402. https://doi.org/10.1002/ana.21748

Knochelmann, H.M., Dwyer, C.J., Bailey, S.R., Amaya, S.M., Elston, D.M., Mazza-McCrann, J.M., Paulos, C.M., 2018. When worlds collide: Th17 and Treg cells in cancer and autoimmunity. Cell. Mol. Immunol. 15, 458–469. https://doi.org/10.1038/s41423-018-0004-4

Koyama, M., Hill, G.R., 2019. The primacy of gastrointestinal tract antigen-presenting cells in lethal graft-versus-host disease. Blood 134, 2139–2148. https://doi.org/10.1182/blood.2019000823

Koyama, M., Kuns, R.D., Olver, S.D., Raffelt, N.C., Wilson, Y.A., Don, A.L.J., Lineburg, K.E., Cheong, M., Robb, R.J., Markey, K.A., Varelias, A., Malissen, B., Hämmerling, G.J., Clouston, A.D., Engwerda, C.R., Bhat, P., MacDonald, K.P.A., Hill, G.R., 2011. Recipient nonhematopoietic antigen-presenting cells are sufficient to induce lethal acute graft-versus-host disease. Nat. Med. 18, 135–142. https://doi.org/10.1038/nm.2597

Krummel, M.F., Bartumeus, F., Gérard, A., 2016. T cell migration, search strategies and mechanisms. Nat. Rev. Immunol. 16, 193–201. https://doi.org/10.1038/nri.2015.16

Lämmermann, T., Bader, B.L., Monkley, S.J., Worbs, T., Wedlich-Söldner, R., Hirsch, K., Keller, M., Förster, R., Critchley, D.R., Fässler, R., Sixt, M., 2008. Rapid leukocyte migration by integrin-independent flowing and squeezing. Nature 453, 51–55. https://doi.org/10.1038/nature06887

Lämmermann, T., Germain, R.N., 2014. The multiple faces of leukocyte interstitial migration. Semin. Immunopathol. 36, 227–251. https://doi.org/10.1007/s00281-014-0418-8

Lämmermann, T., Kastenmüller, W., 2019. Concepts of GPCR-controlled navigation in the immune system. Immunol. Rev. 289, 205–231. https://doi.org/10.1111/imr.12752

Lämmermann, T., Sixt, M., 2009. Mechanical modes of “amoeboid” cell migration. Curr. Opin. Cell Biol. 21, 636–644. https://doi.org/10.1016/j.ceb.2009.05.003

Lee, M., Mandl, J.N., Germain, R.N., Yates, A.J., 2012. The race for the prize: T-cell trafficking strategies for optimal surveillance. Blood 120, 1432–1438. https://doi.org/10.1182/blood-2012-04-424655

Lee, Y.K., Turner, H., Maynard, C.L., Oliver, J.R., Chen, D., Elson, C.O., Weaver, C.T., 2009. Late developmental plasticity in the T helper 17 lineage. Immunity 30, 92–107. https://doi.org/10.1016/j.immuni.2008.11.005

Levin, D., Osman, M.S., Durand, C., Kim, H., Hemmati, I., Jamani, K., Howlett, J.G., Johannson, K.A., Weatherald, J., Woo, M.,

Lee, J., Storek, J., 2022. Hematopoietic Cell Transplantation for Systemic Sclerosis—A Review. Cells 11, 3912. https://doi.org/10.3390/cells11233912

Ley, K., Laudanna, C., Cybulsky, M.I., Nourshargh, S., 2007. Getting to the site of inflammation: the leukocyte adhesion cascade updated. Nat. Rev. Immunol. 7, 678–689. https://doi.org/10.1038/nri2156

Li, H., Demetris, A.J., McNiff, J., Matte-Martone, C., Tan, H.S., Rothstein, D.M., Lakkis, F.G., Shlomchik, W.D., 2012. Profound depletion of host conventional dendritic cells, plasmacytoid dendritic cells, and B cells does not prevent graft-versus-host disease induction. J. Immunol. Baltim. Md 1950 188, 3804–3811. https://doi.org/10.4049/jimmunol.1102795

Li, H., Kaplan, D.H., Matte-Martone, C., Tan, H.S., Venkatesan, S., Johnson, K., Demetris, A.J., McNiff, J., Shlomchik, M.J., Shlomchik, W.D., 2011. Langerhans cells are not required for graft-versus-host disease. Blood 117, 697–707. https://doi.org/10.1182/blood-2010-07-299073

Lim, F.Y., Koon, Y.L., Chiam, K.-H., 2013. A computational model of amoeboid cell migration. Comput. Methods Biomech. Biomed. Engin. 16, 1085–1095. https://doi.org/10.1080/10255842.2012.757598

Lindquist, R.L., Shakhar, G., Dudziak, D., Wardemann, H., Eisenreich, T., Dustin, M.L., Nussenzweig, M.C., 2004. Visualizing dendritic cell networks in vivo. Nat. Immunol. 5, 1243–1250. https://doi.org/10.1038/ni1139

Liu, Y.-J., Le Berre, M., Lautenschlaeger, F., Maiuri, P., Callan-Jones, A., Heuzé, M., Takaki, T., Voituriez, R., Piel, M., 2015. Confinement and low adhesion induce fast amoeboid migration of slow mesenchymal cells. Cell 160, 659–672. https://doi.org/10.1016/j.cell.2015.01.007

Lo, C.M., Wang, H.B., Dembo, M., Wang, Y.L., 2000. Cell movement is guided by the rigidity of the substrate. Biophys. J. 79, 144–152.

MacDonald, K.P.A., Palmer, J.S., Cronau, S., Seppanen, E., Olver, S., Raffelt, N.C., Kuns, R., Pettit, A.R., Clouston, A., Wainwright, B., Branstetter, D., Smith, J., Paxton, R.J., Cerretti, D.P., Bonham, L., Hill, G.R., Hume, D.A., 2010. An antibody against the colony-stimulating factor 1 receptor depletes the resident subset of monocytes and tissue- and tumor-associated macrophages but does not inhibit inflammation. Blood 116, 3955–3963. https://doi.org/10.1182/blood-2010-02-266296

Machado, A.M.N., Rodrigues, M., Malvezzi, H., de Azevedo Piccinato, C., Hamerschlak, N., Podgaec, S., 2022. Graft-versus-host disease in the female genital tract: a prospective cohort study. Arch. Gynecol. Obstet. 305, 1551–1558. https://doi.org/10.1007/s00404-021-06330-1

Majumdar, R., Sixt, M., Parent, C.A., 2014. New paradigms in the establishment and maintenance of gradients during directed cell migration. Curr. Opin. Cell Biol. 30, 33–40. https://doi.org/10.1016/j.ceb.2014.05.010

Malard, F., Holler, E., Sandmaier, B.M., Huang, H., Mohty, M., 2023. Acute graft-versus-host disease. Nat. Rev. Dis. Primer 9, 1–18. https://doi.org/10.1038/s41572-023-00438-1

Mandl, J.N., Liou, R., Klauschen, F., Vrisekoop, N., Monteiro, J.P., Yates, A.J., Huang, A.Y., Germain, R.N., 2012. Quantification of lymph node transit times reveals differences in antigen surveillance strategies of naive CD4+ and CD8+ T cells. Proc. Natl. Acad. Sci. U. S. A. 109, 18036–18041. https://doi.org/10.1073/pnas.1211717109

Martin, P.J., McDonald, G.B., Sanders, J.E., Anasetti, C., Appelbaum, F.R., Deeg, H.J., Nash, R.A., Petersdorf, E.W., Hansen, J.A., Storb, R., 2004. Increasingly frequent diagnosis of acute gastrointestinal graft-versus-host disease after allogeneic hematopoietic cell transplantation. Biol. Blood Marrow Transplant. J. Am. Soc. Blood Marrow Transplant. 10, 320–327. https://doi.org/10.1016/j.bbmt.2003.12.304

Masopust, D., Choo, D., Vezys, V., Wherry, E.J., Duraiswamy, J., Akondy, R., Wang, J., Casey, K.A., Barber, D.L., Kawamura, K.S., Fraser, K.A., Webby, R.J., Brinkmann, V., Butcher, E.C., Newell, K.A., Ahmed, R., 2010. Dynamic T cell migration program provides resident memory within intestinal epithelium. J. Exp. Med. 207, 553–564. https://doi.org/10.1084/jem.20090858

Mathewson, N.D., Jenq, R., Mathew, A.V., Koenigsknecht, M., Hanash, A., Toubai, T., Oravecz-Wilson, K., Wu, S.-R., Sun, Y., Rossi, C., Fujiwara, H., Byun, J., Shono, Y., Lindemans, C., Calafiore, M., Schmidt, T.M., Honda, K., Young, V.B., Pennathur, S., van den Brink, M., Reddy, P., 2016. Gut microbiome-derived metabolites modulate intestinal epithelial cell damage and mitigate graft-versus-host disease. Nat. Immunol. 17, 505–513. https://doi.org/10.1038/ni.3400

Matloubian, M., Lo, C.G., Cinamon, G., Lesneski, M.J., Xu, Y., Brinkmann, V., Allende, M.L., Proia, R.L., Cyster, J.G., 2004. Lymphocyte egress from thymus and peripheral lymphoid organs is dependent on S1P receptor 1. Nature 427, 355–360. https://doi.org/10.1038/nature02284

Matte-Martone, C., Wang, X., Anderson, B., Jain, D., Demetris, A.J., McNiff, J., Shlomchik, M.J., Shlomchik, W.D., 2010. Recipient B cells are not required for graft-versus-host disease induction. Biol. Blood Marrow Transplant. J. Am. Soc. Blood Marrow Transplant. 16, 1222–1230. https://doi.org/10.1016/j.bbmt.2010.03.015

McEver, R.P., 2015. Selectins: initiators of leucocyte adhesion and signalling at the vascular wall. Cardiovasc. Res. 107, 331–339. https://doi.org/10.1093/cvr/cvv154

Miller, M.J., Hejazi, A.S., Wei, S.H., Cahalan, M.D., Parker, I., 2004a. T cell repertoire scanning is promoted by dynamic dendritic cell behavior and random T cell motility in the lymph node. Proc. Natl. Acad. Sci. U. S. A. 101, 998–1003. https://doi.org/10.1073/pnas.0306407101

Miller, M.J., Safrina, O., Parker, I., Cahalan, M.D., 2004b. Imaging the single cell dynamics of CD4+ T cell activation by dendritic cells in lymph nodes. J. Exp. Med. 200, 847–856. https://doi.org/10.1084/jem.20041236

Misra, A., Shahiwala, A., 2020. Novel Drug Delivery Technologies: Innovative Strategies for Drug Re-positioning. Springer Nature.

Moser, B., Wolf, M., Walz, A., Loetscher, P., 2004. Chemokines: multiple levels of leukocyte migration control. Trends Immunol. 25, 75–84. https://doi.org/10.1016/j.it.2003.12.005

Mowat, A.M., Agace, W.W., 2014. Regional specialization within the intestinal immune system. Nat. Rev. Immunol. 14, 667–685. https://doi.org/10.1038/nri3738

Moy, R.H., Huffman, A.P., Richman, L.P., Crisalli, L., Wang, X.K., Hoxie, J.A., Mick, R., Emerson, S.G., Zhang, Y., Vonderheide, R.H., Porter, D.L., Reshef, R., 2017. Clinical and immunologic impact of CCR5 blockade in graft-versus-host disease prophylaxis. Blood 129, 906–916. https://doi.org/10.1182/blood-2016-08-735076

Murai, M., Yoneyama, H., Ezaki, T., Suematsu, M., Terashima, Y., Harada, A., Hamada, H., Asakura, H., Ishikawa, H., Matsushima, K., 2003. Peyer's patch is the essential site in initiating murine acute and lethal graft-versus-host reaction. Nat. Immunol. 4, 154–160. https://doi.org/10.1038/ni879

Murphy, K., Weaver, C., 2022. Janeway's Immunobiology, 10th Edition. Garland Science.

Nicolas-Boluda, A., Donnadieu, E., 2019. Obstacles to T cell migration in the tumor microenvironment. Comp. Immunol. Microbiol. Infect. Dis. 63, 22–30. https://doi.org/10.1016/j.cimid.2018.12.006

Ohno, H., 2016. Intestinal M cells. J. Biochem. (Tokyo) 159, 151–160. https://doi.org/10.1093/jb/mvv121

Overstreet, M.G., Gaylo, A., Angermann, B.R., Hughson, A., Hyun, Y.-M., Lambert, K., Acharya, M., Billroth-Maclurg, A.C., Rosenberg, A.F., Topham, D.J., Yagita, H., Kim, M., Lacy-Hulbert, A., Meier-Schellersheim, M., Fowell, D.J., 2013. Inflammation-induced interstitial migration of effector $CD4^+$ T cells is dependent on integrin αV. Nat. Immunol. 14, 949–958. https://doi.org/10.1038/ni.2682

Paluch, E.K., Aspalter, I.M., Sixt, M., 2016. Focal Adhesion-Independent Cell Migration. Annu. Rev. Cell Dev. Biol. 32, 469–490. https://doi.org/10.1146/annurev-cellbio-111315-125341

Pang, X., He, X., Qiu, Z., Zhang, H., Xie, R., Liu, Z., Gu, Y., Zhao, N., Xiang, Q., Cui, Y., 2023. Targeting integrin pathways: mechanisms and advances in therapy. Signal Transduct. Target. Ther. 8, 1–42. https://doi.org/10.1038/s41392-022-01259-6

Park, J.-Y., Chung, H., DiPalma, D.T., Tai, X., Park, J.-H., 2018. Immune quiescence in the oral mucosa is maintained by a uniquely large population of highly activated Foxp3 + regulatory T cells. Mucosal Immunol. 11, 1092–1102. https://doi.org/10.1038/s41385-018-0027-2

Patel, D.A., Schroeder, M.A., Choi, J., DiPersio, J.F., 2022. Chapter 3 - Mouse models of graft-versus-host disease, in: Montrose, D.C. (Ed.), Methods in Cell Biology, Experimental Models of Infection, Inflammation and Injury. Academic Press, pp. 41–66. https://doi.org/10.1016/bs.mcb.2021.12.008

Petersen, F.B., Buckner, C.D., Clift, R.A., Nelson, N., Counts, G.W., Meyers, J.D., Thomas, E.D., 1987. Infectious complications in patients undergoing marrow transplantation: a prospective randomized study of the additional effect of decontamination and laminar air flow isolation among patients receiving prophylactic systemic antibiotics. Scand. J. Infect. Dis. 19, 559–567. https://doi.org/10.3109/00365548709032423

Pham, T.H.M., Okada, T., Matloubian, M., Lo, C.G., Cyster, J.G., 2008. S1P1 receptor signaling overrides retention mediated by G alpha i-coupled receptors to promote T cell egress. Immunity 28, 122–133. https://doi.org/10.1016/j.immuni.2007.11.017

Potter, E.L., Gideon, H.P., Tkachev, V., Fabozzi, G., Chassiakos, A., Petrovas, C., Darrah, P.A., Lin, P.L., Foulds, K.E., Kean, L.S., Flynn, J.L., Roederer, M., 2021. Measurement of leukocyte trafficking kinetics in macaques by serial intravascular staining. Sci. Transl. Med. 13, eabb4582. https://doi.org/10.1126/scitranslmed.abb4582

Przepiorka, D., Weisdorf, D., Martin, P., Klingemann, H.G., Beatty, P., Hows, J., Thomas, E.D., 1995. 1994 Consensus Conference on Acute GVHD Grading. Bone Marrow Transplant. 15, 825–828.

Punt, J., 2013. Chapter 4 - Adaptive Immunity: T Cells and Cytokines, in: Prendergast, G.C., Jaffee, E.M. (Eds.), Cancer Immunotherapy (Second Edition). Academic Press, San Diego, pp. 41–53. https://doi.org/10.1016/B978-0-12-394296-8.00004-X

Rainger, G.E., Mcgettrick, H.M. (Eds.), 2017. T-Cell Trafficking: Methods and Protocols, Methods in Molecular Biology. Springer, New York, NY. https://doi.org/10.1007/978-1-4939-6931-9

Reboldi, A., Arnon, T.I., Rodda, L.B., Atakilit, A., Sheppard, D., Cyster, J.G., 2016. IgA production requires B cell interaction with subepithelial dendritic cells in Peyer's patches. Science 352, aaf4822. https://doi.org/10.1126/science.aaf4822

Reboldi, A., Cyster, J.G., 2016. Peyer's patches: Organizing B cell responses at the intestinal frontier. Immunol. Rev. 271, 230–

245. https://doi.org/10.1111/imr.12400

Renkawitz, J., Kopf, A., Stopp, J., de Vries, I., Driscoll, M.K., Merrin, J., Hauschild, R., Welf, E.S., Danuser, G., Fiolka, R., Sixt, M., 2019. Nuclear positioning facilitates amoeboid migration along the path of least resistance. Nature 568, 546–550. https://doi.org/10.1038/s41586-019-1087-5

Renkawitz, J., Schumann, K., Weber, M., Lämmermann, T., Pflicke, H., Piel, M., Polleux, J., Spatz, J.P., Sixt, M., 2009. Adaptive force transmission in amoeboid cell migration. Nat. Cell Biol. 11, 1438–1443. https://doi.org/10.1038/ncb1992

Reversat, A., Gaertner, F., Merrin, J., Stopp, J., Tasciyan, S., Aguilera, J., de Vries, I., Hauschild, R., Hons, M., Piel, M., Callan-Jones, A., Voituriez, R., Sixt, M., 2020. Cellular locomotion using environmental topography. Nature 582, 582–585. https://doi.org/10.1038/s41586-020-2283-z

Reynolds, J., Heron, I., Dudler, L., Trnka, Z., 1982. T-cell recirculation in the sheep: migratory properties of cells from lymph nodes. Immunology 47, 415–421.

Rich, R.R., Fleisher, T.A., Shearer, W.T., Jr, H.W.S., Frew, A.J., Weyand, C.M., 2012. Clinical Immunology E-Book: Principles and Practice. Elsevier Health Sciences.

Rowlings, P.A., Przepiorka, D., Klein, J.P., Gale, R.P., Passweg, J.R., Henslee-Downey, P.J., Cahn, J.Y., Calderwood, S., Gratwohl, A., Socié, G., Abecasis, M.M., Sobocinski, K.A., Zhang, M.J., Horowitz, M.M., 1997. IBMTR Severity Index for grading acute graft-versus-host disease: retrospective comparison with Glucksberg grade. Br. J. Haematol. 97, 855–864.

Russell, J.A., Chaudhry, A., Booth, K., Brown, C., Woodman, R.C., Valentine, K., Stewart, D., Ruether, J.D., Ruether, B.A., Jones, A.R., Coppes, M.J., Bowen, T., Anderson, R., Bouchard, M., Rallison, L., Stotts, M., Poon, M.C., 2000. Early outcomes after allogeneic stem cell transplantation for leukemia and myelodysplasia without protective isolation: a 10-year experience. Biol. Blood Marrow Transplant. J. Am. Soc. Blood Marrow Transplant. 6, 109–114. https://doi.org/10.1016/s1083-8791(00)70073-5

S, T., M, Kadowaki, K, Aoyama, M, Koyama, T, O., K, T., K, Akashi, T, T., 2011. The Wnt agonist R-spondin1 regulates systemic graft-versus-host disease by protecting intestinal stem cells. J. Exp. Med. 208. https://doi.org/10.1084/jem.20101559

Sadik, C.D., Luster, A.D., 2012. Lipid-cytokine-chemokine cascades orchestrate leukocyte recruitment in inflammation. J. Leukoc. Biol. 91, 207–215. https://doi.org/10.1189/jlb.0811402

Sage, P.T., Carman, C.V., 2009. Settings and mechanisms for trans-cellular diapedesis. Front. Biosci. J. Virtual Libr. 14, 5066–5083.

Sarris, M., Sixt, M., 2015. Navigating in tissue mazes: chemoattractant interpretation in complex environments. Curr. Opin. Cell Biol. 36, 93–102. https://doi.org/10.1016/j.ceb.2015.08.001

Schmidt, T.H., Bannard, O., Gray, E.E., Cyster, J.G., 2013. CXCR4 promotes B cell egress from Peyer's patches. J. Exp. Med. 210, 1099–1107. https://doi.org/10.1084/jem.20122574

Schreder, A., Moschovakis, G.L., Halle, S., Schlue, J., Lee, C.-W., Schippers, A., David, S., Bernhardt, G., Ganser, A., Pabst, O., Förster, R., Koenecke, C., 2015. Differential Effects of Gut-Homing Molecules CC Chemokine Receptor 9 and Integrin-β7 during Acute Graft-versus-Host Disease of the Liver. Biol. Blood Marrow Transplant. 21, 2069–2078. https://doi.org/10.1016/j.bbmt.2015.08.038

Schumann, K., Lämmermann, T., Bruckner, M., Legler, D.F., Polleux, J., Spatz, J.P., Schuler, G., Förster, R., Lutz, M.B., Sorokin, L., Sixt, M., 2010. Immobilized chemokine fields and soluble chemokine gradients cooperatively shape migration patterns of dendritic cells. Immunity 32, 703–713. https://doi.org/10.1016/j.immuni.2010.04.017

Schwarz, J., Bierbaum, V., Vaahtomeri, K., Hauschild, R., Brown, M., de Vries, I., Leithner, A., Reversat, A., Merrin, J., Tarrant, T., Bollenbach, T., Sixt, M., 2017. Dendritic Cells Interpret Haptotactic Chemokine Gradients in a Manner Governed by Signal-to-Noise Ratio and Dependent on GRK6. Curr. Biol. CB 27, 1314–1325. https://doi.org/10.1016/j.cub.2017.04.004

Serody, J.S., Burkett, S.E., Panoskaltsis-Mortari, A., Ng-Cashin, J., McMahon, E., Matsushima, G.K., Lira, S.A., Cook, D.N., Blazar, B.R., 2000. T-lymphocyte production of macrophage inflammatory protein-1alpha is critical to the recruitment of CD8(+) T cells to the liver, lung, and spleen during graft-versus-host disease. Blood 96, 2973–2980.

Shakhar, G., Lindquist, R.L., Skokos, D., Dudziak, D., Huang, J.H., Nussenzweig, M.C., Dustin, M.L., 2005. Stable T cell-dendritic cell interactions precede the development of both tolerance and immunity in vivo. Nat. Immunol. 6, 707–714. https://doi.org/10.1038/ni1210

Shimoji, S., Hashimoto, D., Tsujigiwa, H., Miyawaki, K., Kato, K., Takahashi, S., Ogasawara, R., Jiromaru, T., Iwasaki, H., Miyamoto, T., Akashi, K., Teshima, T., 2017. Graft-versus-host disease targets ovary and causes female infertility in mice. Blood 129, 1216–1225. https://doi.org/10.1182/blood-2016-07-728337

Shiow, L.R., Rosen, D.B., Brdicková, N., Xu, Y., An, J., Lanier, L.L., Cyster, J.G., Matloubian, M., 2006. CD69 acts downstream of interferon-alpha/beta to inhibit S1P1 and lymphocyte egress from lymphoid organs. Nature 440, 540–544. https://doi.org/10.1038/nature04606

Shono, Y., Docampo, M.D., Peled, J.U., Perobelli, S.M., Velardi, E., Tsai, J.J., Slingerland, A.E., Smith, O.M., Young, L.F., Gupta, J., Lieberman, S.R., Jay, H.V., Ahr, K.F., Porosnicu Rodriguez, K.A., Xu, K., Calarfiore, M., Poeck, H., Caballero, S., Devlin, S.M., Rapaport, F., Dudakov, J.A., Hanash, A.M., Gyurkocza, B., Murphy, G.F., Gomes, C., Liu, C., Moss, E.L., Falconer, S.B., Bhatt, A.S., Taur, Y., Pamer, E.G., van den Brink, M.R.M., Jenq, R.R., 2016. Increased GVHD-related mortality with broad-spectrum antibiotic use after allogeneic hematopoietic stem cell transplantation in human patients and mice. Sci. Transl. Med. 8, 339ra71. https://doi.org/10.1126/scitranslmed.aaf2311

Shulman, Z., Cohen, S.J., Roediger, B., Kalchenko, V., Jain, R., Grabovsky, V., Klein, E., Shinder, V., Stoler-Barak, L., Feigelson, S.W., Meshel, T., Nurmi, S.M., Goldstein, I., Hartley, O., Gahmberg, C.G., Etzioni, A., Weninger, W., Ben-Baruch, A., Alon, R., 2011. Transendothelial migration of lymphocytes mediated by intraendothelial vesicle stores rather than by extracellular chemokine depots. Nat. Immunol. 13, 67–76. https://doi.org/10.1038/ni.2173

Singh, A.K., McGuirk, J.P., 2016. Allogeneic Stem Cell Transplantation: A Historical and Scientific Overview. Cancer Res. 76, 6445–6451. https://doi.org/10.1158/0008-5472.CAN-16-1311

Sixt, M., Kanazawa, N., Selg, M., Samson, T., Roos, G., Reinhardt, D.P., Pabst, R., Lutz, M.B., Sorokin, L., 2005. The conduit system transports soluble antigens from the afferent lymph to resident dendritic cells in the T cell area of the lymph node. Immunity 22, 19–29. https://doi.org/10.1016/j.immuni.2004.11.013

Smith, M.E., Ford, W.L., 1983. The recirculating lymphocyte pool of the rat: a systematic description of the migratory behaviour of recirculating lymphocytes. Immunology 49, 83–94.

Snowden, J.A., Sánchez-Ortega, I., Corbacioglu, S., Basak, G.W., Chabannon, C., de la Camara, R., Dolstra, H., Duarte, R.F., Glass, B., Greco, R., Lankester, A.C., Mohty, M., Neven, B., de Latour, R.P., Pedrazzoli, P., Peric, Z., Yakoub-Agha, I., Sureda, A., Kröger, N., 2022. Indications for haematopoietic cell transplantation for haematological diseases, solid tumours and immune disorders: current practice in Europe, 2022. Bone Marrow Transplant. 57, 1217–1239. https://doi.org/10.1038/s41409-022-01691-w

Socie, G., Michonneau, D., 2022. Milestones in acute GVHD pathophysiology. Front. Immunol. 13, 1079708. https://doi.org/10.3389/fimmu.2022.1079708

Son, E.T., Faridi, P., Paul-Heng, M., Leong, M.L., English, K., Ramarathinam, S.H., Braun, A., Dudek, N.L., Alexander, I.E., Lisowski, L., Bertolino, P., Bowen, D.G., Purcell, A.W., Mifsud, N.A., Sharland, A.F., 2021. The self-peptide repertoire plays a critical role in transplant tolerance induction. J. Clin. Invest. 131, e146771. https://doi.org/10.1172/JCI146771

Song, Q., Wang, X., Wu, X., Qin, H., Li, Y., Riggs, A.D., Martin, P.J., Chen, Y.-Z., Zeng, D., 2021. Tolerogenic anti-IL-2 mAb prevents graft-versus-host disease while preserving strong graft-versus-leukemia activity. Blood 137, 2243–2255. https://doi.org/10.1182/blood.2020006345

Sorokin, L., 2010. The impact of the extracellular matrix on inflammation. Nat. Rev. Immunol. 10, 712–723. https://doi.org/10.1038/nri2852

Spindelboeck, W., Schulz, E., Uhl, B., Kashofer, K., Aigelsreiter, A., Zinke-Cerwenka, W., Mulabecirovic, A., Kump, P.K., Halwachs, B., Gorkiewicz, G., Sill, H., Greinix, H., Högenauer, C., Neumeister, P., 2017. Repeated fecal microbiota transplantations attenuate diarrhea and lead to sustained changes in the fecal microbiota in acute, refractory gastrointestinal graft-versus-host-disease. Haematologica 102, e210–e213. https://doi.org/10.3324/haematol.2016.154351

Sporrer, D., Gessner, A., Hehlgans, T., Oefner, P.J., Holler, E., 2015. The Microbiome and Allogeneic Stem Cell Transplantation. Curr. Stem Cell Rep. 1, 53–59. https://doi.org/10.1007/s40778-014-0006-9

Stegner, D., vanEeuwijk, J.M.M., Angay, O., Gorelashvili, M.G., Semeniak, D., Pinnecker, J., Schmithausen, P., Meyer, I., Friedrich, M., Dütting, S., Brede, C., Beilhack, A., Schulze, H., Nieswandt, B., Heinze, K.G., 2017. Thrombopoiesis is spatially regulated by the bone marrow vasculature. Nat. Commun. 8, 127. https://doi.org/10.1038/s41467-017-00201-7

Stolp, B., Thelen, F., Ficht, X., Altenburger, L.M., Ruef, N., Inavalli, V.V.G.K., Germann, P., Page, N., Moalli, F., Raimondi, A., Keyser, K.A., Seyed Jafari, S.M., Barone, F., Dettmer, M.S., Merkler, D., Iannacone, M., Sharpe, J., Schlapbach, C., Fackler, O.T., Nägerl, U.V., Stein, J.V., 2020. Salivary gland macrophages and tissue-resident CD8+ T cells cooperate for homeostatic organ surveillance. Sci. Immunol. 5, eaaz4371. https://doi.org/10.1126/sciimmunol.aaz4371

Storb, R., Prentice, R.L., Buckner, C.D., Clift, R.A., Appelbaum, F., Deeg, J., Doney, K., Hansen, J.A., Mason, M., Sanders, J.E., Singer, J., Sullivan, K.M., Witherspoon, R.P., Thomas, E.D., 1983. Graft-versus-host disease and survival in patients with aplastic anemia treated by marrow grafts from HLA-identical siblings. Beneficial effect of a protective environment. N. Engl. J. Med. 308, 302–307. https://doi.org/10.1056/NEJM198302103080602

Sun, Z., Costell, M., Fässler, R., 2019. Integrin activation by talin, kindlin and mechanical forces. Nat. Cell Biol. 21, 25–31. https://doi.org/10.1038/s41556-018-0234-9

Suzuki, K., Maruya, M., Kawamoto, S., Sitnik, K., Kitamura, H., Agace, W.W., Fagarasan, S., 2010. The sensing of environmental

stimuli by follicular dendritic cells promotes immunoglobulin A generation in the gut. Immunity 33, 71–83. https://doi.org/10.1016/j.immuni.2010.07.003

Tak W, M., Mary E., S., Jett, Bradley D., 2014. Chapter 17 - Transplantation, in: Primer to the Immune Response (Second Edition). Academic Cell, Boston, pp. 457–486. https://doi.org/10.1016/B978-0-12-385245-8.00017-0

Takashima, S., Martin, M.L., Jansen, S.A., Fu, Y., Bos, J., Chandra, D., O'Connor, M.H., Mertelsmann, A.M., Vinci, P., Kuttiyara, J., Devlin, S.M., Middendorp, S., Calafiore, M., Egorova, A., Kleppe, M., Lo, Y., Shroyer, N.F., Cheng, E.H., Levine, R.L., Liu, C., Kolesnick, R., Lindemans, C.A., Hanash, A.M., 2019. T cell-derived interferon-γ programs stem cell death in immune-mediated intestinal damage. Sci. Immunol. 4, eaay8556. https://doi.org/10.1126/sciimmunol.aay8556

TAKEDA, A., SASAKI, N., MIYASAKA, M., 2017. The molecular cues regulating immune cell trafficking. Proc. Jpn. Acad. Ser. B Phys. Biol. Sci. 93, 183–195. https://doi.org/10.2183/pjab.93.012

Taur, Y., Coyte, K., Schluter, J., Robilotti, E., Figueroa, C., Gjonbalaj, M., Littmann, E.R., Ling, L., Miller, L., Gyaltshen, Y., Fontana, E., Morjaria, S., Gyurkocza, B., Perales, M.-A., Castro-Malaspina, H., Tamari, R., Ponce, D., Koehne, G., Barker, J., Jakubowski, A., Papadopoulos, E., Dahi, P., Sauter, C., Shaffer, B., Young, J.W., Peled, J., Meagher, R.C., Jenq, R.R., van den Brink, M.R.M., Giralt, S.A., Pamer, E.G., Xavier, J.B., 2018. Reconstitution of the gut microbiota of antibiotic-treated patients by autologous fecal microbiota transplant. Sci. Transl. Med. 10, eaap9489. https://doi.org/10.1126/scitranslmed.aap9489

Thompson, S., Martínez-Burgo, B., Sepuru, K.M., Rajarathnam, K., Kirby, J.A., Sheerin, N.S., Ali, S., 2017. Regulation of Chemokine Function: The Roles of GAG-Binding and Post-Translational Nitration. Int. J. Mol. Sci. 18, 1692. https://doi.org/10.3390/ijms18081692

Tiercy, J.-M., 2016. How to select the best available related or unrelated donor of hematopoietic stem cells? Haematologica 101, 680–687. https://doi.org/10.3324/haematol.2015.141119

Tkachev, V., Kaminski, J., Potter, E.L., Furlan, S.N., Yu, A., Hunt, D.J., McGuckin, C., Zheng, H., Colonna, L., Gerdemann, U., Carlson, J., Hoffman, M., Olvera, J., English, C., Baldessari, A., Panoskaltsis-Mortari, A., Watkins, B., Qayed, M., Suessmuth, Y., Betz, K., Bratrude, B., Langston, A., Horan, J.T., Ordovas-Montanes, J., Shalek, A.K., Blazar, B.R., Roederer, M., Kean, L.S., 2021. Spatiotemporal single-cell profiling reveals that invasive and tissue-resident memory donor CD8+ T cells drive gastrointestinal acute graft-versus-host disease. Sci. Transl. Med. 13, eabc0227. https://doi.org/10.1126/scitranslmed.abc0227

Tomura, M., Honda, T., Tanizaki, H., Otsuka, A., Egawa, G., Tokura, Y., Waldmann, H., Hori, S., Cyster, J.G., Watanabe, T., Miyachi, Y., Kanagawa, O., Kabashima, K., 2010a. Activated regulatory T cells are the major T cell type emigrating from the skin during a cutaneous immune response in mice. J. Clin. Invest. 120, 883–893. https://doi.org/10.1172/JCI40926

Tomura, M., Itoh, K., Kanagawa, O., 2010b. Naive CD4+ T Lymphocytes Circulate through Lymphoid Organs To Interact with Endogenous Antigens and Upregulate Their Function. J. Immunol. 184, 4646–4653. https://doi.org/10.4049/jimmunol.0903946

Tomura, M., Yoshida, N., Tanaka, J., Karasawa, S., Miwa, Y., Miyawaki, A., Kanagawa, O., 2008. Monitoring cellular movement in vivo with photoconvertible fluorescence protein "Kaede" transgenic mice. Proc. Natl. Acad. Sci. U. S. A. 105, 10871–10876. https://doi.org/10.1073/pnas.0802278105

Trichet, L., Le Digabel, J., Hawkins, R.J., Vedula, S.R.K., Gupta, M., Ribrault, C., Hersen, P., Voituriez, R., Ladoux, B., 2012. Evidence of a large-scale mechanosensing mechanism for cellular adaptation to substrate stiffness. Proc. Natl. Acad. Sci. U. S. A. 109, 6933–6938. https://doi.org/10.1073/pnas.1117810109

Tsuji, M., Suzuki, K., Kitamura, H., Maruya, M., Kinoshita, K., Ivanov, I.I., Itoh, K., Littman, D.R., Fagarasan, S., 2008. Requirement for lymphoid tissue-inducer cells in isolated follicle formation and T cell-independent immunoglobulin A generation in the gut. Immunity 29, 261–271. https://doi.org/10.1016/j.immuni.2008.05.014

van Helvert, S., Storm, C., Friedl, P., 2018. Mechanoreciprocity in cell migration. Nat. Cell Biol. 20, 8–20. https://doi.org/10.1038/s41556-017-0012-0

Van Kruiningen, H.J., West, A.B., Freda, B.J., Holmes, K.A., 2002. Distribution of Peyer's patches in the distal ileum. Inflamm. Bowel Dis. 8, 180–185. https://doi.org/10.1097/00054725-200205000-00004

Vanheule, V., Metzemaekers, M., Janssens, R., Struyf, S., Proost, P., 2018. How post-translational modifications influence the biological activity of chemokines. Cytokine 109, 29–51. https://doi.org/10.1016/j.cyto.2018.02.026

Veldhoen, M., Ferreira, C., 2015. Influence of nutrient-derived metabolites on lymphocyte immunity. Nat. Med. 21, 709–718. https://doi.org/10.1038/nm.3894

Vossen, J.M., Heidt, P.J., van den Berg, H., Gerritsen, E.J., Hermans, J., Dooren, L.J., 1990. Prevention of infection and graft-versus-host disease by suppression of intestinal microflora in children treated with allogeneic bone marrow transplantation. Eur. J. Clin. Microbiol. Infect. Dis. Off. Publ. Eur. Soc. Clin. Microbiol. 9, 14–23. https://doi.org/10.1007/BF01969527

Wang, D.-R., Wu, X.-L., Sun, Y.-L., 2022. Therapeutic targets and biomarkers of tumor immunotherapy: response versus non-response. Signal Transduct. Target. Ther. 7, 1–27. https://doi.org/10.1038/s41392-022-01136-2

Wang, H., Yang, Y.-G., 2014. The complex and central role of interferon-γ in graft-versus-host disease and graft-versus-tumor activity. Immunol. Rev. 258, 30–44. https://doi.org/10.1111/imr.12151

Weiner, H.L., da Cunha, A.P., Quintana, F., Wu, H., 2011. Oral tolerance. Immunol. Rev. 241, 241–259. https://doi.org/10.1111/j.1600-065X.2011.01017.x

Wendt, E., Keshav, S., 2015. CCR9 antagonism: potential in the treatment of Inflammatory Bowel Disease. Clin. Exp. Gastroenterol. 8, 119–130. https://doi.org/10.2147/CEG.S48305

Wilson, E.H., Harris, T.H., Mrass, P., John, B., Tait, E.D., Wu, G.F., Pepper, M., Wherry, E.J., Dzierzinski, F., Roos, D., Haydon, P.G., Laufer, T.M., Weninger, W., Hunter, C.A., 2009. Behavior of parasite-specific effector CD8+ T cells in the brain and visualization of a kinesis-associated system of reticular fibers. Immunity 30, 300–311. https://doi.org/10.1016/j.immuni.2008.12.013

Woolf, E., Grigorova, I., Sagiv, A., Grabovsky, V., Feigelson, S.W., Shulman, Z., Hartmann, T., Sixt, M., Cyster, J.G., Alon, R., 2007. Lymph node chemokines promote sustained T lymphocyte motility without triggering stable integrin adhesiveness in the absence of shear forces. Nat. Immunol. 8, 1076–1085. https://doi.org/10.1038/ni1499

Y, E., S, T., H, O., S, Shimoji, K, N., H, U., S, Shimoda, H, I., N, S., T, A., K, A., T, T., 2012. Graft-versus-host disease disrupts intestinal microbial ecology by inhibiting Paneth cell production of α-defensins. Blood 120. https://doi.org/10.1182/blood-2011-12-401166

Yabe, H., Tanaka, A., Chinen, Y., Kato, S., Sawamoto, K., Yasuda, E., Shintaku, H., Suzuki, Y., Orii, T., Tomatsu, S., 2016. Hematopoietic stem cell transplantation for Morquio A syndrome. Mol. Genet. Metab. 117, 84–94. https://doi.org/10.1016/j.ymgme.2015.09.011

Yamada, K.M., Sixt, M., 2019. Mechanisms of 3D cell migration. Nat. Rev. Mol. Cell Biol. 20, 738–752. https://doi.org/10.1038/s41580-019-0172-9

Yokomizo, T., 2015. Two distinct leukotriene B4 receptors, BLT1 and BLT2. J. Biochem. (Tokyo) 157, 65–71. https://doi.org/10.1093/jb/mvu078

Zeiser, R., Blazar, B.R., 2017. Acute Graft-versus-Host Disease - Biologic Process, Prevention, and Therapy. N. Engl. J. Med. 377, 2167–2179. https://doi.org/10.1056/NEJMra1609337

Zeiser, R., Socié, G., Blazar, B.R., 2016. Pathogenesis of acute graft-versus-host disease: from intestinal microbiota alterations to donor T cell activation. Br. J. Haematol. 175, 191–207. https://doi.org/10.1111/bjh.14295

Zeiser, R., von Bubnoff, N., Butler, J., Mohty, M., Niederwieser, D., Or, R., Szer, J., Wagner, E.M., Zuckerman, T., Mahuzier, B., Xu, J., Wilke, C., Gandhi, K.K., Socié, G., REACH2 Trial Group, 2020. Ruxolitinib for Glucocorticoid-Refractory Acute Graft-versus-Host Disease. N. Engl. J. Med. 382, 1800–1810. https://doi.org/10.1056/NEJMoa1917635

Zheng, X., Tian, Z., 2021. Which is better, HLA-matched sibling or haploidentical transplantation? Cell. Mol. Immunol. 18, 1347–1347. https://doi.org/10.1038/s41423-021-00640-9

Zhou, S., Ueta, H., Xu, X.-D., Shi, C., Matsuno, K., 2008. Predominant donor CD103+CD8+ T cell infiltration into the gut epithelium during acute GvHD: a role of gut lymph nodes. Int. Immunol. 20, 385–394. https://doi.org/10.1093/intimm/dxm153

Zhu, C., Chen, W., Lou, J., Rittase, W., Li, K., 2019. Mechanosensing through immunoreceptors. Nat. Immunol. 20, 1269–1278. https://doi.org/10.1038/s41590-019-0491-1

8. Acknowledgments

Completing my Ph.D. thesis was only possible with the help of several people. I would like to take this chance to acknowledge each and every one of them.

I want to start by thanking Prof. Andreas Beilhack for letting me conduct my doctoral thesis project in his lab and offering me an exciting project to work on.

I want to express my gratitude to the members of my thesis committee, Professors Manfred Lutz, Wolfgang Kastenmüller, and Dirk Bumann. I greatly valued their scientific counsel, which helped me formulate the project's goals and research questions.

I thank Prof. Georg Gasteiger for chairing my thesis committee.

Thanks to the GSLS and Dr. Stephan Schröder-Köhne for accepting me in the fast-track international master program FOKUS in Life Sciences and allowing me an early start on my Ph.D. project.

I want to thank all the GvHD team members for the lively discussions and their help during the planning and execution of experiments. Further, thanks to all AG Beilhack lab members for their help and for the pleasant moments we shared. Last, I would like to thank my family and friends. Without their support, I will not be here.

9. List of publications

Josefina Peña Mosca, Katja J. Jarick, Lukas Scheller, Zeinab Mokhtari, Estibaliz Arellano Viera, Juan Gamboa Vargas, Caroline Graf, Michael Kern, Duc-Dung Le, Haroon Shaikh, Hermann Einsele, Andreas Beilhack (2023). A novel shortcut for T-cell infiltration into the small intestine: from Peyer´s patches directly into *lamina propria*. *Nature Immunology* (in preparation).

Rhonda L. McFleder, Anastasiia Makhotkina, Janos Groh, Ursula Keber, Fabian Imdahl, **Josefina Peña Mosca**, Alina Peteranderl, Jingjing Wu, Sawako Tabuchi, Jan Hoffmann, Ann-Kathrin Karl, Axel Pagenstecher, Jörg Vogel, Andreas Beilhack, James B. Koprich, Jonathan M. Brotchie, Antoine-Emmanuel Saliba, Jens Volkmann & Chi Wang Ip (2023). $CD11c^{+}$ cell-mediated trafficking of alpha-Synuclein from the brain to the gut in a mouse model of Parkinson's Disease. *Nature Communications 14: 7529.*

Haroon Shaikh, Jörn Pezoldt, Zeinab Mokhtari, Juan Gamboa Vargas, Duc-Dung Le, **Josefina Peña Mosca**, Estibaliz Arellano Viera, Michael Kern, Caroline Graf, Niklas Beyersdorf, Manfred B Lutz, Angela Riedel, Maike Büttner-Herold, Alma Zernecke, Hermann Einsele, Antoine-Emmanuel Saliba, Burkhard Ludewig, Jochen Hühn and Andreas Beilhack (2022). Fibroblastic reticular cells mitigate acute graft-versus-host disease via MHCII-dependent maintenance of regulatory T-cells. *JCI Insight 7(22): e154250.g*

Juan Gamboa Vargas, Jennifer Wagner, Haroon Shaikh, Isabell Lang, Juliane Medler, Mohamed Anany, Tim Steinfatt, **Josefina Peña Mosca**, Stephanie Haack, Julia Dahlhoff, Maike Büttner-Herold, Carolin Graf, Estibaliz Arellano Viera, Hermann Einsele, Harald Wajant, and Andreas Beilhack (2022). TNFR2-specific TNF fusion protein with improved *in-vivo* activity. *Frontiers in Immunology 13: 888274.*

Haroon Shaikh, Juan Gamboa Vargas, Zeinab Mokhtari, Katja J. Jarick, Maria Ulbrich, **Josefina Peña Mosca**, Estibaliz Arellano Viera, Caroline Graf, Duc-Dung Le, Katrin G. Heinze, Maike Büttner-Herold, Andreas Rosenwald, Jörn Pezoldt, Jochen Hühn, and Andreas Beilhack (2021). Mesenteric lymph node transplantation in mice to study immune responses of the gastrointestinal tract. *Frontiers in Immunology*, 12: 689896.

María Josefina Peña Mosca

10. Affidavit / Eidensstattliche Erklarung

I hereby confirm that my thesis entitled ‘Local regulation of T-cell Immunity in the intestinal mucosa.’ is the result of my work. I do not receive any help or support from commercial consultants. All sources and/ or materials applied are listed and specified in the thesis.

Furthermore, I confirm that this thesis has not yet been submitted as part of another examination process, neither in an identical nor in a similar form.

Place, date
Signature

Hiermit erkläre ich an Eides statt, die Dissertation „Lokale Regulation von T-Zellen Immunität in der Darmschleimhaut“ eigenständig, d.h. insbesondere selbständig und ohne Hilfe eines kommerziellen Promotionsberaters, angefertigt und keine anderen als die von mir angegebenen Quellen und Hilfsmittel verwendet zu haben.

Ich erkläre außerdem, dass die Dissertation weder in gleicher noch in ähnlicher Form bereits in einem anderen Prüfungsverfahren vorgelegen hat.

Ort, Datum
Unterschrift